Norwegian University
of Life Sciences

Master's Thesis 2021 30 ECTS
Faculty of Science and Technology

Advanced Method of Seismic Design of 2D Concrete Structure

Sarah Mostafa Edris
Structural Engineering and Architecture

ABSTRACT

Recent worldwide devastating earthquakes have highlighted the risk of many existing concrete structures of a total collapse or seismic damage because of their inadequate mechanisms of resisting the lateral forces. In order to decrease the destruction and economic losses, existing structures can be renovated. The rehabilitation of existing buildings can limit the damage that affects public safety and the building's function ability after this catastrophe.

The retrofit design is a multi-parametric field; the seismic capacity insufficiencies of the vulnerable building must be examined with regard to the materials, techniques, and analysis methods to develop a good upgrading approach. Many techniques, such as shear walls, jacketing, steel bracing, etc..., were and continue to be in use. Most of them put the building out of service for long periods. However, others provide benefits in terms of costs and simplicity of implementation and may affect the facade. Many researchers are working on helpful studies to include CLT in the existing buildings' retrofitting process. CLT has very effective sides regarding its environmental impact, weight, implementation, and shear resistance as a structural material.

This thesis introduces an advanced seismic design method by evaluating the resulting seismic performance of an existing reinforced concrete building retrofitted by CLT panels. The suggested retrofitting solutions vary by CLT panels thickness and the connector locations. Convenient finite element models of the two-dimensional reinforced concrete frames, the bare and retrofitted frames, were performed using SAP2000. The Response Spectrum analysis as a linear dynamic analysis was conducted to design and evaluate the seismic behavior according to Eurocodes criteria. Then, a nonlinear static analysis using Pushover was executed to observe the damage state of the models using the Capacity Spectrum Method. The analysis has shown that using CLT panels enhances the seismic performance of the existing building; the determination of CLT panels' thickness, and the connectors' location affect the deformation capacity, the ductility, and the stiffness of the structure.

ACKNOWLEDGEMENT

First of all, there is no sufficient expression of my deep gratitude for this precious opportunity. It is an honor to be a student at NMBU.

This work would not have been possible without the valuable comments and remarks of supervisor Dr. Abdelghani Meslem. I am especially indebted for his significant efforts and plentiful knowledge.

Great thanks extend to co-supervisor Dr. Roberto Tomasi for introducing me to the topic, as well as his treasured support and ample experience.

A sincere appreciation goes to eng. Muhammad Idrees, eng. Marmar Idrees, and Mr. John Slade for sharing their precious time and ideas.

Last but not least, pursuing this step would not have been possible without my Father*, sibs, and little family, a very profound thanks for unfailing support and continuous encouragement.*

Figures

Tables

Symbols

RC	*Reinforced Concrete*
CLT	*Cross-Laminated Timber*
2D	*Two dimensional*
EC8	*EN 1998 Eurocode 8: Design of structures for earthquake resistance*
RSA	*Response Spectrum analysis*
POA	*Pushover Analysis*
THA	*Time History Analysis*
DCL (LOW)	*Structural Ductility Class: Low dissipative structural behaviour.*
IDR	*The Interstorey Drift Ratio*
d_r	*the design Interstorey Drift*
v	*The reduction factor*
q	*The behaviour factor*
q_d	*The displacement behaviour factor*
P	*Axial Force*
M	*Bending Moment*
A_0	*The suggested existing RC Building*
FEM	*Finite Element Model*
A_{ret}	*The suggested retrofitted Solution.*
A_{ret_1}	*The First suggested retrofitted Solution.*
A_{ret_2}	*The Second suggested retrofitted Solution.*
A_{ret_3}	*The Third suggested retrofitted Solution.*
A_{ret_4}	*The Fourth suggested retrofitted Solution.*
B	*The Reference RC Building.*
PGA	*Peak Ground Acceleration.*
g	*Acceleration of Gravity.*
B	*Ground Type.*
S	*Soil Factor.*
T_b	*The Lower limit of the period.*
T_c	*The Upper limit of the period.*
T_d	*Defining the beginning of the constant displacement.*
β	*Lower Bound Factor, Beta.*

C(i)	*Column i=[1,2,3,4,5,6,7,8].*
B(i)	*Beam i=[1,2,3].*
H	*Storey Height.*
Δx	*Lateral Dispalcement, Axial X.*
d_{si}	*The displacement of a point of the structural system induced by the seismic action.*
F_X	*Base Force on X Direction, Base Shear.*
F_Z	*Base Force on Z Direction.*
M_Y	*Base Moment on Y Direction.*
FEMA	*FEDERAL EMERGENCY MANAGEMENT AGENCY.*
ASCE	*American Society of Civil Engineers.*
CSM	*Capacity Spectrum Method.*
ATC	*Applied Technology Council.*
B	*Yielding State.*
IO	*Immediate Occupancy State.*
LS	*Life Safety State.*
CP	*Collapse Prevention State.*

Contents

CHAPTER 1

1.1. Background

The influence of lateral forces caused by wind, earthquake, blast loads, Etc., is becoming extremely relevant. Several structures were severely damaged in recent catastrophic earthquakes worldwide, resulting in enormous social and economic consequences. Existing reinforced concrete structures not constructed to seismic codes with ductile details may experience significant damage during earthquake ground motion [1]. In seismic zones, the design process depending on experience may often be a challenge, if not incorrect, because many parameters might affect the structure's performance [2]. Seismic analysis is a method to estimate structural responses in the design of earthquake-resistant and/or rehabilitation structures in vulnerability. The challenge, in principle, is complex because of the dynamic, nonlinear, and unpredictable structural reaction to severe earthquakes. In structure engineering, the three features are uncommon, and most problems are static, linear, or predictable, at least adequately estimated [3].

Building retrofitting has been a more cost-effective and practical, urgent safe solution than reconstruction [1]. Many seismic design codes can be found, but codes with general criteria for evaluating, upgrading, rehabilitation/ retrofitting/strengthening, and structural repair are missed. Relatively, for many structural engineers, buildings' seismic retrofitting remains a recent activity [4]. In recent decades, a significant study has been carried out on the optimization of seismically excited constructions. However, fewer studies concern concrete or composite structures [2]. Retrofitting a structure demands that the existing structure be technically, economically, and socially estimated [5]. The most widely used retrofitting technique is adding a shear wall to existing structures rather than a column jacket, while the least commonly used option is adding Steel bracing and reinforcing beams [6]. As a potential material for retrofitting, Timber is available and workable. Steel and Concrete's stiffness and mass density lead to a more reliable seismic performance [7] . In addition, Timber, which comes from trees that sequester carbon, thus have much lower emissions, recapturing a growing market share in building materials [8]. Moreover, Timber is serviceable for facade aesthetics, ease of implementation, location difficulties, and evacuation because of the external execution.

1.2. Aim

This Master's thesis evaluates the resulting seismic performance of the 2-dimensional reinforced Concrete frame of an existing building retrofitted by CLT panels, adopting the capability of the advanced study of CLT as a shear wall proposed by [(Awad, V., et al. (2017))] [9].

1.3. Description

- CHAPTER 1: An introduction as a brief background about Seismic analysis, upgrading the existing RC structures seismically and CLT as a retrofitting material, flows first, followed by description of the thesis chapters.

- CHAPTER 2: A literature review comprises a short bibliography of retrofitting strategies and techniques, assessed by different researchers, subsidized by concise examples of Jacketing, Shear wall, and Steel bracing, displays first, accompanied by an introduction of CLT concept and features. The chapter ends with a comparison of Steel, Concrete, and CLT as retrofitting materials.

- CHAPTER 3: A summarized content about the seismic analysis followed by a section considering the Response Spectrum analysis method displays the selected case study with the characteristics of the used materials. Three submitted models as:

  Building A_0: The existing RC building designed for PGA = 0.15g, modelled as 2D RC frame, plays the base model of seismic performance that will be assessed for PGA = 0.35 after retrofitting by CLT panels. The structural, geometrical characteristics, and FEM are illustrated.

  - Building A_{ret}: Investigating the seismic performance of the 2D RC Frame A_0 retrofitted by CLT panels for PGA = 0.35g. Four 2D RC models are considered. The first three models are retrofitted by three layered, five layered, and three and five layered CLT panels connected to the beams. Fourth one is retrofitted by three layered CLT connected to the columns. The

details of the structural and geometrical characteristics, CLT panels, connectors, and FEM are illustrated.

- Building B: The reference Building designed for PGA = 0.35g, modelled as 2D RC frame designed for PGA = 0.35g, to be seismically a reference to evaluate the seismic performance of the retrofitted models. The structural, geometric, and FEM features are described.

This Chapter stops with a section about the Pushover analysis, presenting the case study with the modelling presumptions, FEM, and Capacity Spectrum Method.

❋ CHAPTER 4: this chapter displays the result of :

- RSA: Results of each model of the case study, and comparison discuss the effectivity of CLT panels on the seismic performance of the model A_{ret}, examining the records of displacement, Interstorey drift, base reaction, and the periods and frequencies, compared to the reference B.

- POA: Results of each model of the case study, with a comparison that discusses the effectivity of CLT panels on the seismic performance of the model A_{ret}, by examining the records of Capacity Curve, Capacity Spectrum, and the Performance Point compared to the reference B.

❋ CHAPTER 5 concludes a review concerning the contribution of CLT panels as a retrofitting option and their impact on seismic performance.

CHAPTER 2

A literature review comprises a short bibliography of retrofitting strategies and techniques, assessed by different researchers, subsidized by concise examples of Jacketing, Shear wall, and Steel bracing, displays first, accompanied by an introduction of CLT concept and features. The chapter ends with a comparison of Steel, Concrete, and CLT as retrofitting materials.

2.1. Bibliography

Earthquake is a hazard with severe long-term consequences in civil structures varying from direct and indirect financial losses resulting from repair or reconstruction, to social effects like injuries, death or homelessness and relocation because of damage or disruption in structural potentialities. For example, the 2010 Haiti earthquake was the most catastrophic natural disaster in history, with over 3% of the national population dead. The absence of historical seismic design in areas of low seismicity has led to many fragile constructions which are especially vulnerable to earthquakes. In these sorts of buildings across the world, poor performance usually follows any substantial geographical movement. Ignoring seismic activities will also lead to fewer columns and beams being used. This is beneficial in the design because it provides for flexible, column-free internal space and reduced building costs. The small number of columns results in a larger column spacing and the utilization of long-span beams, typically far higher than the columns' bending strengths. This leads to a significant weak column design, with extensive ground movement, and the creation of a soft-storey mechanism [10].

Seismically designed buildings should withstand service loads and low-intensity earthquakes without damage; moderate ones without damage structurally, but perhaps with some damage in non-structural elements; and heavy earthquakes with structural and non-structural damage, but without breakdown [4].

Reinforced Concrete has a long history of being a popular construction material. Under earthquake conditions, it gives durability and rigidity but not ductility. Because of the lack of seismic design standards in the past, many researchers are focusing on improving the seismic performance of the existing RC structures in active seismic zones rather than rebuilding to the codes to preserve more lives and property [1].

Fig. 2. 1, clarifies the combination of collapse prevention and different levels of damage results in a curve that separates the strength-ductility plane into sufficient and inadequate

zones. Suppose the building withstands a demanding earthquake while causing minimum damage to the structure or its contents. In that case, the primary issue will be drift control, and the needed strength will not be ductility dependant. Because of the system's enhanced inelastic behaviour and energy absorption properties, the strength decreases as ductility increases. To prevent non-structural elements from damage, a maximum drift limit might be set [6].

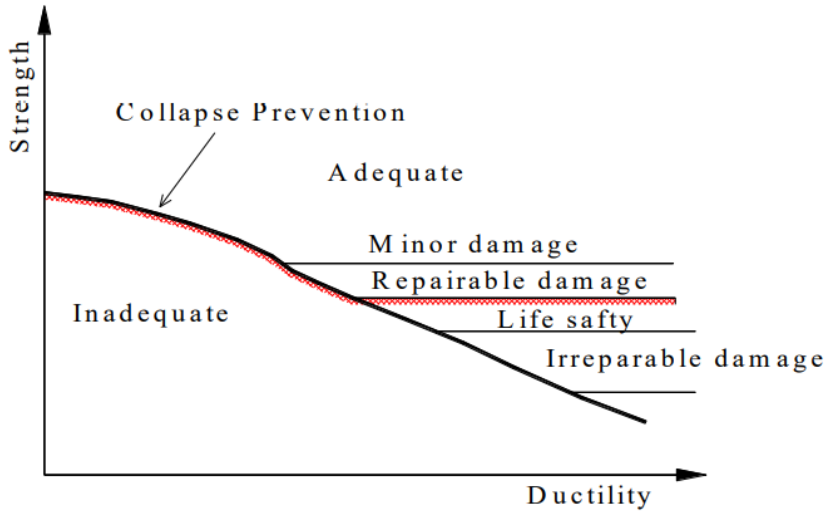

Fig. 2. 1, Ductility – Strength Relationship.

For decades, the researchers evaluated several strategies, Fig. 2. 2 [11], controlled by the technique's seismic performance to redesign the existing RC structures seismically [1]. Seismic retrofitting strategy can meet these purposes: To regain the original structural performance; to improve structural performance in the original structure; and to minimize seismic response [12].

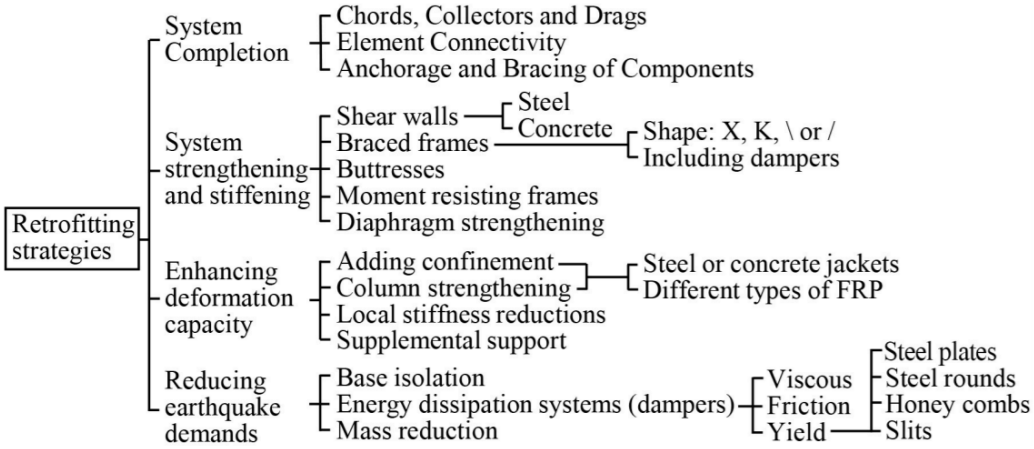

Fig. 2. 2, Retrofitting strategies and potential techniques.

Retrofitting techniques varies at the structure level (global) or the component level (local), Fig. 2. 3.

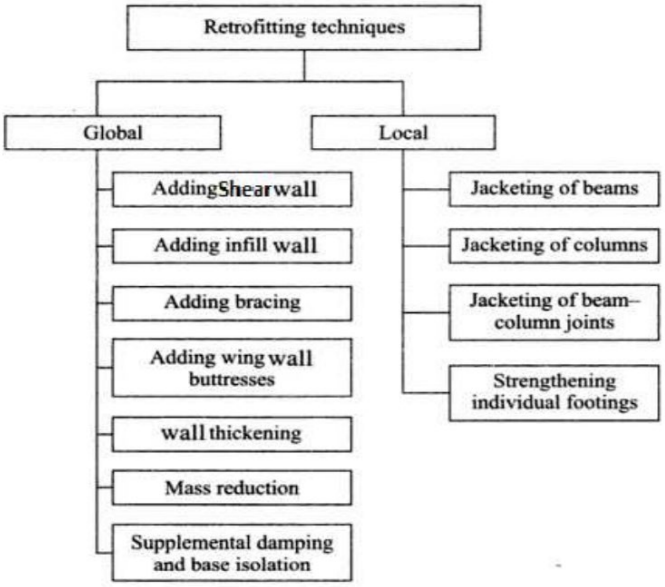

Fig. 2. 3, Global and Local Retrofitting techniques.

- Global Retrofit at the Structure Level: For structure level retrofitting, two methodologies are used:

  - Conventional techniques rely on improving the seismic resistance of existing structures as shear wall, infill walls or Steel braces, or even mixing more than one regarding the effectivity.
  - Unconventional techniques for reducing seismic demands. Here, seismic base isolated and addition supplemented device techniques are the most popular. Fig. 2. 4 [12].
  - Local Retrofitting at the structural element level: The seismically insufficient element's strength is improved at the element level or at the local level. When compared to structure level retrofit, this technique is more cost effective. It includes the utilization of Concrete, Steel, or fiber reinforced polymer (FRP), jackets for confining reinforced Concrete columns, beams, joints, and foundations [1].

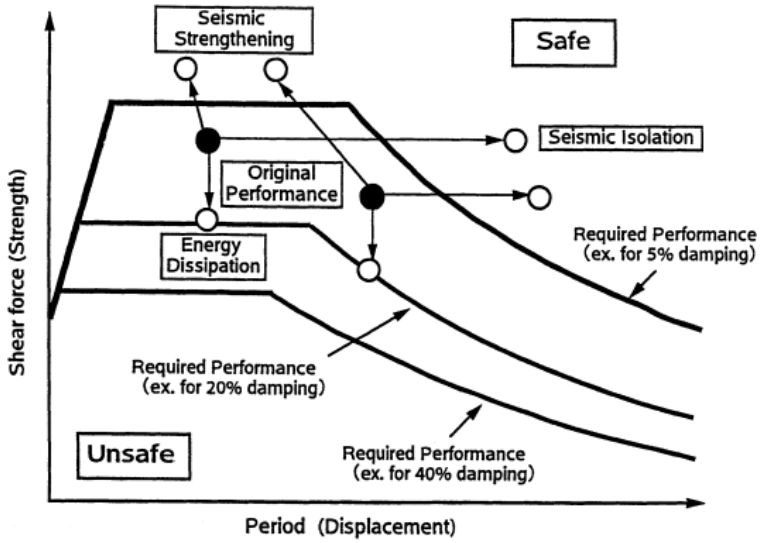

Fig. 2. 4, Seismic retrofitting, seismic isolation, and energy dissipation.

Connector features of any existing Concrete element shown in Fig. 2. 5. For infill walls and sidewalls (a), dowel connections are utilized. The expansion and adhesive anchors for dowel connections (c). Steel components can be easily connected to the existing Concrete using mortar fill or bolted directly to the frames (d) [12].

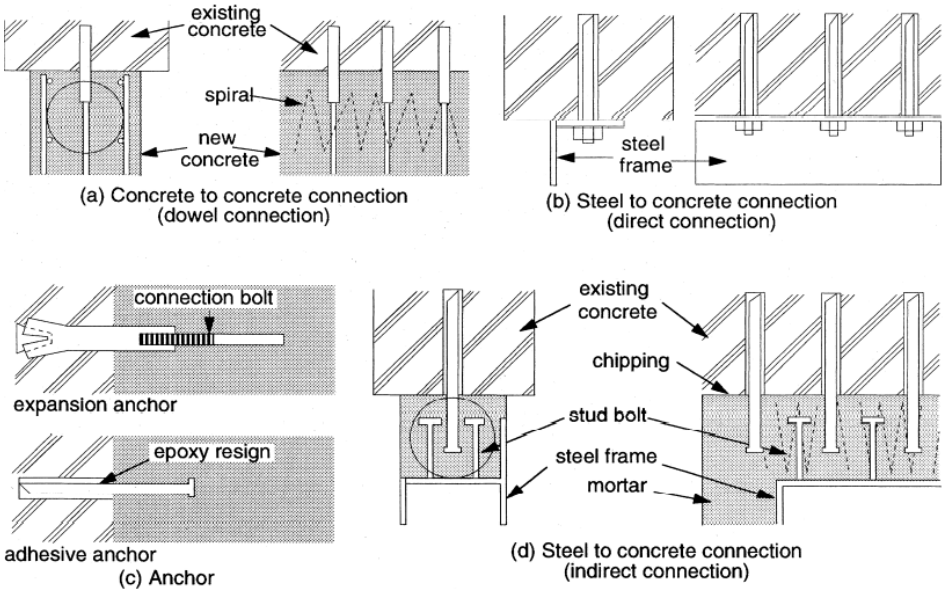

Fig. 2. 5, Connection in retrofitting techniques.

2.1.1. Retrofitting by jacketing

Jacketing is a local retrofitting system, used to enhance the axial, flexural, Fig. 2. 6, and shear strength of existing structure components, Fig. 2. 7, as well as the ductility and stiffness. By enclosing the old section with fresh cast - in - place Concrete or shotcrete and adding longitudinal and transverse reinforcement or a welded wire mesh. To improve the monolithic behaviour of the structure elements, the original section's surface must be roughened using sandblasting or mechanical methods [6].

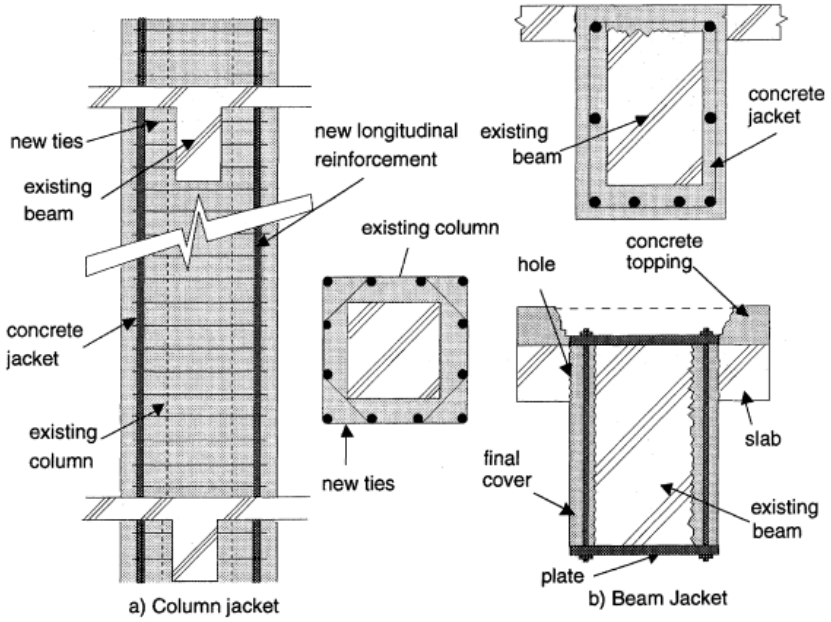

Fig. 2. 6, Jacketing for increasing flexural capacity.

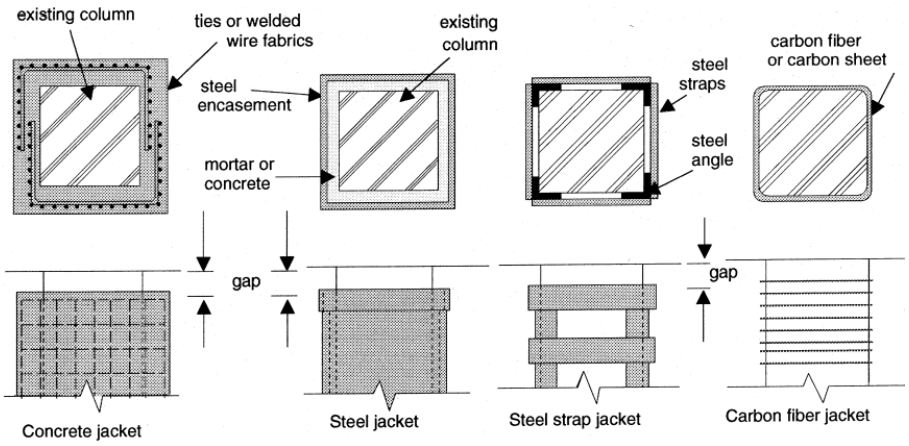

Fig. 2. 7, Jacketing for increasing column shear capacity.

Fig. 2. 8 shows jacketing with moment resisting end connections and jacketing without end connections [13].

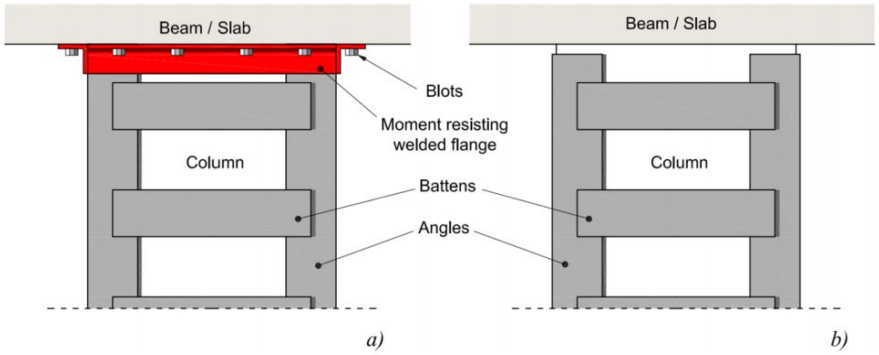

Fig. 2. 8, (a) Jacketing with moment resisting end connections; (b) Jacketing without end connections.

Jacketing system, Fig. 2. 9 illustrates the retrofitting of Column-Beam connection, leads to increase in the lateral strength of the building because of the stiffening of the joint of frames, and improves individual axial and flexural column strength [4].

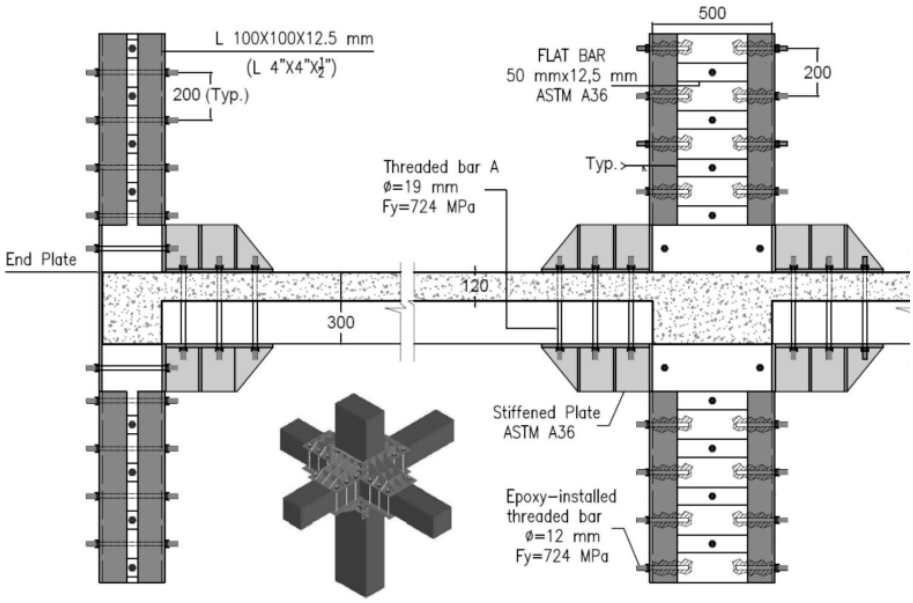

Fig. 2. 9, Retrofitting scheme for RC columns and beam-column joints.

In case of column, a thin gap must be created at the end of the enclosures in Steel or Concrete to avoid an unwanted increase of the shear strength resulting from the increase in the bending capacity. Fig. 2. 10 (b) [12].

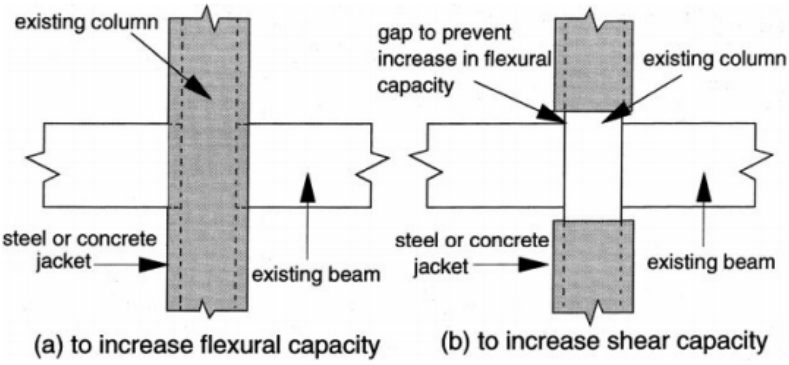

Fig. 2. 10, Jacketing of column.

2.1.2. Retrofitting by shear walls

Adding Concrete walls is a common global retrofitting technique, by infilling specific frame bays with reinforced Concrete, but codes only cover it only if provided the connection of the old and new Concrete assures monolithic behaviour. When walls are properly anchored into the surrounding frame with various types of connections (e.g., shear keys, dowels, chemical anchors), they not only significantly increase the lateral stiffness of the building but also improve the existing non-ductile frames from being subjected to large lateral force demands. The distribution of lateral earthquake stresses on the walls and frame is a significant issue in predicting the seismic performance of a structure enhanced with shear walls [6].

Retrofitting by RC shear wall has been more successful in reducing global drifts and structural damage in frame structures. The additional elements may be cast in location or precast. When adding additional elements, the best position should be examined, which may correspond to the entire height of the structure to reduce torsion [1].

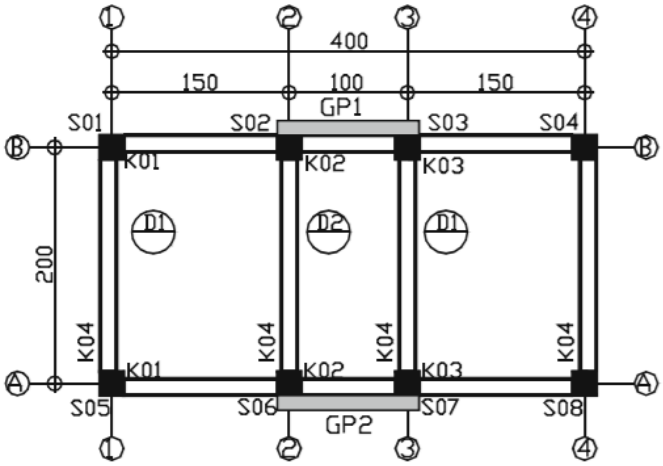

Fig. 2. 11, strengthened structure by RC shear wall

Nowadays, many techniques of applying, shaping, merging shear walls with another retrofitting system, are used to improve shear wall seismic performance. Moreover, shear wall is enhanced by time, and tested with varied materials such as RC, Fig. 2. 11 [14], Timber, Fig. 2. 12 [15], and Steel, Fig. 2. 13 [16].

Precast Concrete (PC) shear walls are increasingly used as lateral load-resistance components because of the acceptable seismic properties and implementation ease in low and medium-sized structures [15].

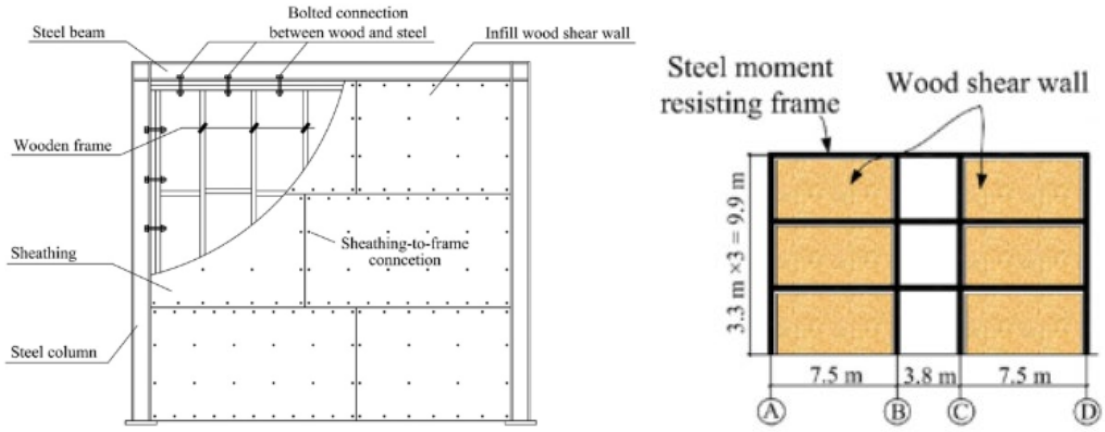

Fig. 2. 12, A Steel-Timber hybrid structural system.

A reduction of bending moments in the columns and beams can be provided by using a Steel plate as a shear wall, while the increase in thickness has a significant influence on column bending moment and has a minor impact on the beam bending moment [17]. With an infill wall with poorly constructed dowels, t can enhance strength significantly by providing a bracing effect.. With dowel failure, external shear walls cannot enhance capacity. The effective utilization of outer shear walls to vulnerable existing structures increases seismic performance if the dowels are correctly designed [14].

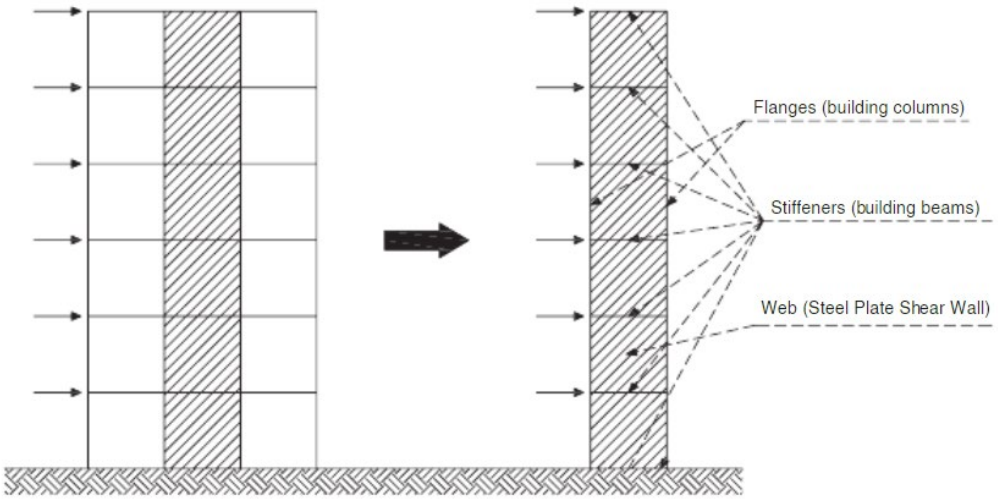

Fig. 2. 13, Steel plate system.

Any new shear wall installation is beneficial for limiting global lateral drifts and decreasing damage in frame structures, minimizing lateral displacement, bending moment, and shear pressures. The effective position of shear walls in the frame system is essential for reducing lateral force [1].

2.1.3. Retrofitting by Steel bracing

Steel bracing is a global retrofitting technique, thought to be an efficient option to upgrade seismic performance of RC building and has been practiced for decades.

Steel bracing may be attached to an existing RC frame in different formats as:

- Bracing could be attached to an exterior face of the frame.
- Bracing could be placed inside an individual unit frame and be attached to the frame through an intermediary Steel frame.
- The Brace could be placed inside the frame and be directly connected to the RC frame.

As the number of storeys increases, the reliability of the X-bracing system in minimizing maximum lateral displacements decreases, and the increase rate in base shear is reduced. In addition, this system reduces the inter-storey drift, which is clearly performed best in the 8-storey frame according to a study in 2020 considering X-bracing system on 4-, 8-, and 12-storey existing RC. frames [18].

One of research on how effects the X, inverted V, ZX, and Zipper bracing systems on the seismic performance of an existing RC building using different types of Steel profiles was published in 2011, Fig. 2. 14.

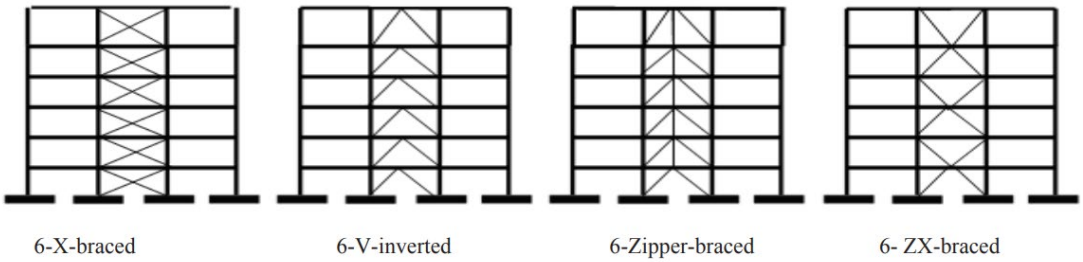

Fig. 2. 14, Bracing system.

The load capacity of the six-storey structure decreases, and the ZX bracing system displays a loss in strength when compared to the other bracing systems. Steel bracing decreases lateral drift on the second and third floor of the six-storey structure. The impact of tiny sections on ductility is minimal for the X and ZX bracing systems for the 6-storey building. However, for increasing section dimensions, the ductility of the structure decreases for the ZX bracing system and remains consistent for the X bracing system. This is explained because when the section is small, the structure has higher ductility because the deformation is maximum, resulting in a high capacity for energy dissipation, whereas for larger sections, the ductility is low because the modulus of rigidity of the structure is large, implying a limited capacity for energy dissipation. The capacity of bracing systems is increased when the section dimensions are increased, and the tube section performed more efficiently than other sections. As a result, Steel bracing can decrease the amount of damage in RC constructions.
As a result, using the ZX and Zipper bracing systems has been determined to be the most efficient in terms of the building's strength capability. The deformation and ductility capabilities are influenced by the section profile [19].

Steel bracing, in case of the high buildings up to 20 storeys, shows various enhancements offered with the addition of uniform or combined concentrated braces. A drop in the torsional performance of braced frames suggests a major improvement compared to unbraced. The structural stiffness of the braced frames can be enhanced. The most effective system is the X braced system with the highest overall performance to reduce

the lateral drifts in the stories. But when comparing bracing techniques, certain advantages can be achieved when combined. However, these improvements are limited in terms of global performance of the frames [18].

Advantage (+) and Disadvantage (-)	*Steel Jacketing*	*Bracing System*	*Shear Walls*
Strength	+	+	+
Stiffness		+	+
Ductility	+		
irregularity		+	+
Force demand		-	-
Deformation Demand		+	+
Familiar materials	+	+	+
Expensive	-		-
Labour intensive	-	-	+
Time-consuming implementation	-		-
Need for corrosion protection	-	-	+
Member stiffness Modifying	-	-	
Weight	-	-	-
Solo	-		+

(+) = Advantege, (-)= Disadvantage, ( )= No effect.

Table 2. 1, Advantages and Disadvantages of retrofitting technique.

The choice of the right rehabilitation solution for a building without a one-all answer is a multi-parametric challenge. RC Shear Walls limit Interstorey drifts effectively, reduce irregularities, and prevent soft storage failure mechanisms. Moreover, Shear Walls are expensive and very disturbing. Bracing retrofitting work takes place on the external frames of the structure, and there is minor damage and disturbance in the living area. There are several forms of bracing that may be used in RC constructions, and the disturbance level and the expense are reasonable. Whereas with jacketing, The added weight and long and accurate implementation time can be classified as disadvantages, but this can be neglected regarding the RC jacketing seismic improvement performance. Effect of local and global retrofit measures on building properties, Table 2. 1, summarizes some advantages and disadvantages of Jacketing, Bracing, and Shear Wall retrofitting techniques [20], [21].

2.2. CLT Panels

Cross-laminated Timber (CLT) panels have been developed in Austria in the late 1990s. Because of the high stiffness, strength, and in-plane stability, it has been popular due to the possibilities offering in construction design. In general, Timber is a remarkably harmless substance to deal with, not toxic, does not decompose into environmental pollutants. CLT is a popular description of applied material in low-rise and medium-rise residential and commercial buildings as multilayer Timber boards [22]. Structures of CLT are increasingly utilized globally and mainly in Europe. However, while the development of numerous multi-storey structures around Europe has been diffused, Eurocodes for CLT designers, notably regarding seismic design, are almost utterly absent [23].

Previous research on CLT panels as building walls has carried out several quasistatic experiences. In 2009, on two CLT structures in Japan, the Trees and Timber Institute of Italy conducted large and minor seismic shake table tests. This shows sufficient seismic performance in the CLT wall panels. Because of the nonlinear behaviour, the CLT panels perform vertical load-bearing members in the bracket and hold-down connection zones, even after failing the connections. CLT wall panels can also have a system-sharing effect and redundancy because they offer gravity and lateral resistance. Therefore, the CLT wall panels can become an efficient lateral load-resistant system to improve the CLT building's seismic performance. The other approach for studying seismic behaviour on the CLT floors used in buildings is the use of the CLT panels as horizontal slabs [24].

2.2.1. Definition and Dimensions

CLT is a two-dimensional solid Timber product for load-bearing applications. It comprises at least three board layers, Fig. 2. 15, glued together over their entire surface area at right angles to one another and resulting in a symmetrical cross-section. It may arrange over three adjacent layers with their fibers running parallel if their joint thickness does not exceed 90mm.

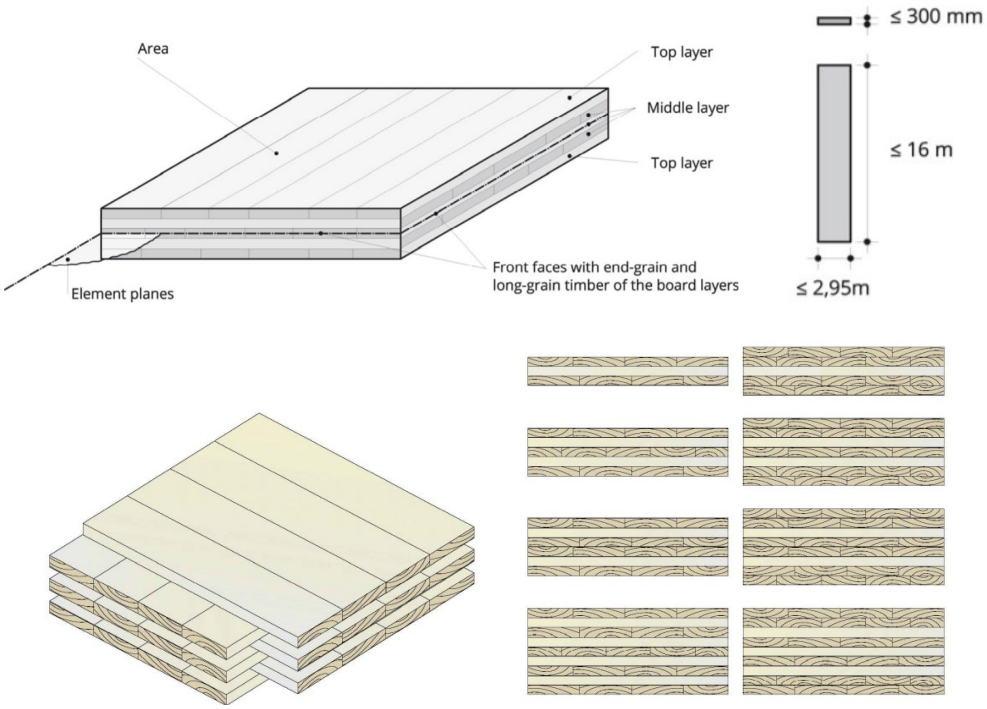

Fig. 2. 15, CLT panel configuration & cross section.

CLT is manufactured in (up to 16m length, up to 2,95 or 3m width, 0,3m or up to 0,5m thickness) [25] [26].

2.2.2. Characteristics

Since 1995, CLT has been produced. Still, it has not been included in standards so far; used through national or European Technical Approvals (ETA). Many standards experts are working on including CLT into Eurocode 5 (EN 1995-1-1).

As a structural element, CLT is used based on technical approvals as roof, wall, and floor elements. Utilization corresponds to an ambient climate of (20 °C, humidity 85% humidity and exceeded for only a few weeks each year).

CLT enhances shear capacity as a vertical element because of the interlocked layers, giving a high shear stiffness.

Table 2. 2, Table 2. 3 below illustrate the characteristic building material values [25].

		Suggested design values	Value range according to approvals
Density (for load assumptions)	γ	5,50 kN/m³	(4,20[1] ÷ 5,50) ÷ 6,00[2] kN/m³
Characteristic minimum value of bulk density	ρ_k	400 kg/m³	350[3] ÷ 400[4] kg/m³
Mean bulk density	ρ_{mean}	450 kg/m³	450 kg/m³

Table 2. 2, General Characteristics building material values.

		Suggested design values	Value range according to approvals
Modulus of elasticity (normal stresses)	$E_{0,mean}$	11.000 N/mm²	11.000 ÷ 12.000 N/mm²
	$E_{0,05}$	9.160 N/mm²	7.330 ÷ 9.160 ÷ 9.650 N/mm²
Modulus of elasticity (transverse to fibre)	$E_{90,mean}$	370 N/mm²	370 N/mm²
Shear modulus	$G_{0,mean}$	690 N/mm²	600 ÷ 690 ÷ 720 N/mm²
	$G_{0,05}$	570 N/mm²	
Rolling shear modulus	$G_{R,mean}$	50 N/mm²	50 ÷ 60 N/mm²

Table 2. 3, Coefficients of stiffness for CLT as a panel.

2.2.3. CLT as Retrofitting Structural Element

Many scholars work on helpful studies in terms of including CLT in the existing buildings' retrofitting process.

CLT panels, as roof diaphragm to retrofit a masonry church, have considered an effective reasonable solution to achieve a significant improvement in terms of lateral wall rocking control [27]. And improve the seismic performance of RC frame and made it stiffer, stronger, and more ductile than the plain frame [28].

CLT panel as an infill allowed RC frame to minimize drift value and reach a higher peak load regarding common masonry infill. CLT has thus high potentialities for retrofitting of RC frames. Fig. 2. 16 illustrates a CLT panels used as an infill shear wall to retrofit RC building seismically, (a), RC building layout with CLT infill shear walls. (b), An example of CLT infill panel for the integrated seismic and energy retrofit [29].

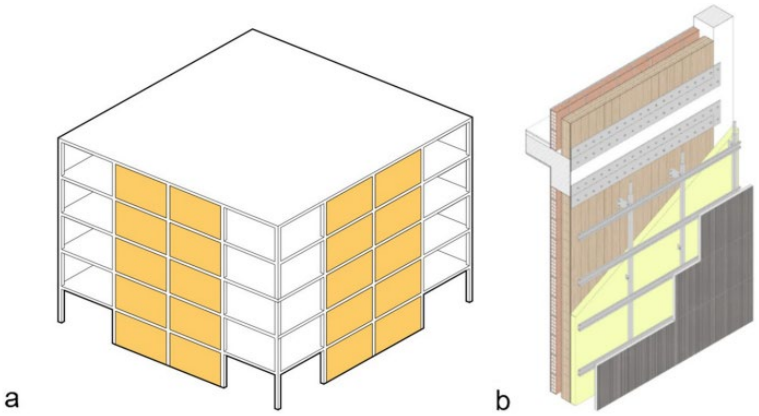

Fig. 2. 16, CLT panels used as infill shear walls for RC buildings retrofit.

2.2.4. Advantages and Disadvantages of CLT

As a structural material, CLT has a negative carbon footprint in terms of an environmental impact compared to the other materials. Its strength-to-weight ratio makes it more popular in the construction market. A lighter CLT structure has fewer gravity loads, thus a minor foundation system. CLT products are ready to install, provide a shortened time of construction, requiring less qualified staff. The CLT panel is not ductile, but the panel-to-panel connection provides this ductility. CLT contributes little to seismic forces as a structural material but showed high shear resistance because of its high stiffness.

	Structural Properties	Hygrothermal Properties	Construction Site
R.c. frame	• High stiffness • Good connection to existing walls	• High thermal conductivity • Risk of thermal bridges	• Difficult casting stage due to presence of existing structure • Irreversible
Steel frame	• High strength and stiffness • Prestress required to ensure structural collaboration with existing portion	• High thermal conductivity • Risk of thermal bridges	• Not always simple handling of prefabricated elements • Fast installation • Reversible due to dry connections
Wooden frame	• Great lightweight • Low stiffness and great deformability • Suitable only for thin masonry panels	• Good thermal properties but not covering building envelope • Reduced durability when exposed to prolonged moisture	• Easy handling due to lightweight • Fast installation • Reversible and recyclable (sustainable)
CLT panel	• Significant lightweight • High stiffness	• Good thermal properties • Reduced durability when exposed to prolonged moisture	• Facilitate handling due to lightweight, possible difficult in-site assembly movements due to presence of existing structure • Fast installation • Reversible and recyclable (sustainable)

Table 2. 4, Comparison between various materials for new inner structure

However, One of CLT disadvantages is the large volume of wood required for manufacturing. It uses three times more wood than a wood-frame system, that can be a problem in countries with deforestation. The shortcomings in the installation and the lack of proper linings are an additional controversial issue. In addition, many people may believe that wood can not withstand time, so it requires higher maintenance costs [26].
A conventional wood installation staff can lift, set, and screw down CLT wood panels, and with a manufacturer-provided installation plan, it goes even faster. Like other industry panels (i.e., precast Concrete), CLT panels provide easy handling during construction and a high level of prefabrication facilitation and rapid project completion [30].

A comparison among different building materials included in a study of an advance strategy for seismic and energy improvement of the existing masonry buildings with CLT panels, Table 2. 4, CLT panels show a good feasibility in terms of stiffness, weight, installation, and positive environmental behaviour [31].

CHAPTER 3

This chapter has three sections:

1- First section: A summarized content about the seismic analysis.

2- Second section is considering the Response Spectrum analysis method, and displays the selected case study with the characteristics of the used materials. Three submitted models as:

- Building A_0: The existing RC building designed for PGA = 0.15g, modelled as 2D RC frame, plays the base model of seismic performance that will be assessed for PGA = 0.35 after retrofitting by CLT panels. The structural, geometrical characteristics, and FEM are illustrated.

- Building A_{ret}: Investigating the seismic performance of the 2D RC Frame A_0 retrofitted by CLT panels for PGA = 0.35g. Four 2D RC models are considered. The first three models are retrofitted by three layered, five layered, and three and five layered CLT panels connected to the beams. Fourth one is retrofitted by three layered CLT connected to the columns. The details of the structural and geometrical characteristics, CLT panels, connectors, and FEM are illustrated.

- Building B: The reference Building designed for PGA = 0.35g, modelled as 2D RC frame designed for PGA = 0.35g, to be seismically a reference to evaluate the seismic performance of the retrofitted models. The structural, geometric, and FEM features are described.

3- Third section is about the Pushover analysis, presenting the case study with the modelling presumptions, FEM, and Capacity Spectrum Method.

3.1. Seismic Design

Earthquake engineering has grown in the last several decades as an engineering area to estimate earthquakes' consequences and avoid them. It has become a subject for seismologists, structural and geotechnical engineers, architects, urban planners, IT, and social scientists. The issue is both fascinating and challenging, making its practitioners aware of a broad range of booming fields [32].

In history, Earthquake engineering is a new field, and it is a development of the 20th century. While certain old buildings have been extraordinarily resistant to earthquake forces for ages, their seismic resistance has been accomplished without seismic analysis by good, conceptual design. Early requirements concerning resistance in earthquakes for structures, such as in Lima, Peru, and Lisbon, Portugal, were constrained by the buildings' standards and upper limits after the catastrophic earthquakes.of 1699 and 1755. Seismic analysis was initially recommended for engineering in Italy in 1909. The static equivalent process prevailed until 1978, Table 3. 1. The same static approach percolated worldwide to seismic countries. First, innovative engineers employed it, and then building codes were created. The standard design method was used until the 1940s by the construction regulations and is still frequently employed in regular structures with the seismic factors updated values. The time test was an appropriate approach to measure the seismic resistance of most buildings. Better techniques would develop, but the discovery of a proper method of seismic force analysis is historically the first fundamental change or jump in the state-of-the-art. Dynamics were initially introduced from the three essential characteristics of seismic structure response. Later, seismic load gradation for various structural systems approximately considered inelastic behaviour, while unpredictability was implicitly considered using multiple safety factors, The expanded deployment and operation of dense networks, combined with high-quality earthquake records and the observation of damage recorded and vital progress in numerical modelling and calculation provide trained researchers and engineers with a better understanding of the physical process of earthquakes, which allows them to develop more precise and efficient tooling [33].

1909 Italy	The first seismic regulations for buildings worldwide, with provisions for equivalent static analysis. In the first storey, the horizontal force was equal to 1/12th of the weight above, and in the second and third storeys, 1/8th of the weight above.
1924 Japan	The first seismic code in Japan. The seismic coefficient was equal to 10%.
1927 USA	First edition of the uniform building code (UBC) with optional seismic provisions. The seismic coefficient varied between 7.5% and 10% of the total dead load plus the live load of the building, depending on soil conditions.
1933 USA	First mandatory seismic codes in the United States (the Field and Riley acts in California). The seismic coefficient varied from 2% to 10%.
1943 USA	Los Angeles enacted the first code, which related the seismic coefficient to the flexibility of the building.
1956 USA	San Francisco enacted a code with explicit dependence of the seismic loads on the building period.
1957 USSR	Implementation of the modal response spectrum method, which later became the main analysis procedure in Europe.
1959 USA	The SEAOC model code took into account the impact of the energy dissipation capacity of structures in the inelastic range.
1977 Italy/ Slovenia	A very simple pushover procedure for masonry buildings was implemented in a regional code in Friuli, Italy.
1978 USA	The start of modern codes with ATC 3-06 guidelines (probabilistic seismic maps, force reduction R-factors).
1981 Yugoslavia	Adoption of linear and nonlinear response history analysis for very important buildings and prototypes of prefabricated buildings in the seismic code.
1986 USA	The pushover-based Capacity Spectrum Method was implemented in the "Tri-services" guidelines.
2010 USA	Explicit probabilistic analysis permitted in ASCE 7-10.

Table 3. 1, Develop the analytical criteria for seismic codes.

The main aim of all forms of building structural systems is the efficient transmission of gravity loads. Dead, live, and snow load are the common loads coming from gravity. In addition to these vertical loads, structures are also susceptible to lateral wind, explosion, or seismic loads. Lateral loads can create significant tension, lead to swaying or vibration. The structure thus requires enough strength against vertical loads and enough rigidity in order to withstand lateral stresses [34].

Seismic analysis is a method to estimate structural responses in designing and/or upgrading existing hazardous buildings. The issue is problematic because of the dynamic, nonlinear, and unpredictable structural reaction to severe earthquakes. In structural

engineering, these three characteristics are uncommon, where most difficulties are static, linear, and predictable. Seismic analysis methods are offered in seismic codes, designed for real applications. After computers became widely available, i.e., in the late 1960s and the 1970s, the rapid development of methods for seismic analysis and supporting software was documented. Nowadays, there are almost no limits related to computation because of enormous growth in computing power, numerical methods, and software [33].

In Europe, the design, assessment, and retrofitting of structures for earthquake resistance was published in 1998, with detailed criteria of Basic principles of conceptual design, Methods of analysis, Safety verifications, and Damage limitation. Analysis methods, according to EC8, divides into these methods, the lateral force, pushover, modal response spectrum, and the time method [35].

3.2. Case Study (RSA)

The Response Spectrum Method is used to design the existing suggested building for PGA=0.15g and 0.35g, By SAP2000.

(RSA), The Response Spectrum Method is a linear dynamic analysis, expresses the graphic or the steady reaction (displacement, velocity, or accelerations) of a sequence of natural frequency oscillators pushed by the same base vibration or shock to move. The maximum building reaction is directly assessed by the elastic or inelastic design spectrum that characterizes the site's earthquake and considers the building performance criteria. RS analysis creates mechanisms that absorb energy from an earthquake actively or passively [36].

EC8 includes Interstorey Drift in Damage Limitation, verifying according to equations in APPENDIX B reported in EC8. The drift between the storeys is the most significant relative shift between two storeys, normalized up to the height [37]. The interstorey horizontal relative displacement ratio to the interstorey height defines the interstorey Drift Ratio (IDR) [38]. Standards for the study case are set to $d_r \cdot \nu \leq 0.0075$ for buildings having ductile nonstructural elements, where d_r is the design Interstorey Drift. The reduction factor that takes into account the lower return period of the seismic action associated with the Damage Limitation requirement $\nu = 0.5$. This recommendation is for II importance classes for buildings. The behaviour factor q is 2 for structural ductility class (DCL(LOW)), the displacement behaviour factor q_d is equal to q.

Whereas, a seismic activity estimate of the most significant expected lateral force at the structure's bottom presents Base Shear. Base shear is included in the Safety Verifications to compute the base shear using the seismic zone, soil material, and building EC8 lateral force equations, included in APPENDIX B [39]. Furthermore, the design of the column needs the calculation of the cross-section failure surface, stated as regards the strong axial load and the bending moment components of the main axes. This is commonly known as the P-M interaction curve [40].

Every building is of importance classes II (ordinary building), DCL, presented by 2D RC frame of which is 8 Storeys with 3,3m height for each, 3 Spans with 5m for each, Fig. 3. 1, RC of 25/30 Concrete quality. Steel of B450C Rebar, Table 3. 2, [41] and Table 3. 3, [42], respectively. CLT as a retrofitting material in Table 3. 4, [9]. Every storey is loaded by 27.75 kN/m Dead, 8 kN/m Live Loades, except the roof with 23 kN/m Dead load. Load details in APPENDIX A.

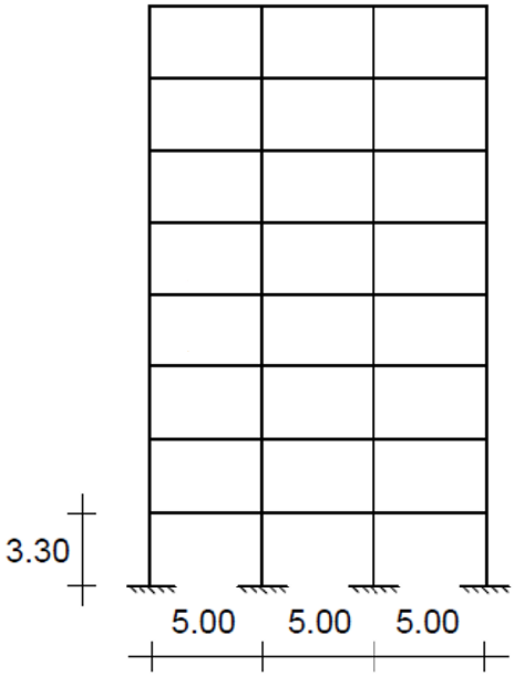

Fig. 3. 1, Study Case, 2D RC Frame.

Symbol	*Description*	*B450C*
D (mm)	Diameter	6 ÷ 50
f_y *(MPa)*	Minimum Yield Stress	450
f_u *(MPa)*	Minimum Tensile Stress	540
E_{cm} *(MPa)*	Elastic modulus	210
v	Poisson's ratio	0,3
a	Coefficient of thermal expansion	$1{,}17.10^{-5}$

Table 3. 2, Study Case, Material characteristics, Steel.

Symbol	*Description*	*C25/30*
f_{ck} *(MPa)*	Characteristic cylinder compressive strength	25
E_{cm} *(MPa)*	Elastic modulus	31476
ρ *(kg/m^3)*	Density	2500
γ *(kN/m^3)*	Unit weight	25
v	Poisson's ratio	0,2
a	Coefficient of thermal expansion	10×10^{-6}
G (MPa)	Shear modulus	13115

Table 3. 3, Study Case, Material characteristics, Concrete.

Symbol	*Description*	*CLT*
E_1, E_3 *(N/mm^2)*	Modulus of elasticity (outer layers)	173.33
E_2 *(N/mm^2)*	Modulus of elasticity (inner layer)	5200
G_{12}, G_{23} *(N/mm^2)*	Rolling shear modulus	100
G_{13} *(N/mm^2)*	Longitudinal shear modulus	400
ρ *(kg/m^3)*	Density	439
v	Poisson's ratio	0.35
a	Coefficient of thermal expansion	0

Table 3. 4, Study Case, Material characteristics, CLT.

3.2.1. Building A_0

Building A_0 is the suggested existing RC building designed for PGA = 0.15g. 2D RC frame, the structural and geometrical characteristics in Fig. 3. 2 are shown in Table 3. 5. Building A_0 will be tested for several CLT panels based on retrofitting solutions, CHAPTER 4 presents and the results and comparison.

Storey	*Column*	*Beam*	*Height*	*Span*
1	C1	B1	3.3m	3*5m
2	C2	B1	3.3m	3*5m
3	C3	B1	3.3m	3*5m
4	C4	B1	3.3m	3*5m
5	C5	B1	3.3m	3*5m
6	C6	B1	3.3m	3*5m
7	C7	B1	3.3m	3*5m
8	C8	B1	3.3m	3*5m

Table 3. 5, Building A_0, structural and geometrical characteristics.

3.2.1.1. FEM, A_0

Using SAP2000 to model a 2D frame of Building A_0 as a low ductile structure DCL, designed according to Eurocode 8 for PGA=0.15g by RSA method, Considering B as a ground type in Norway, Table 3. 6. The structural elements in details are in APPENDIX A.

RSA	*S*	*Tb*	*Tc*	*Td*	*β*	*q*	*Damping*
PGA=0.15g	1.3	0.1	0.25	1.5	0.2	2	0.05

Table 3. 6, Model A_0, PGA=0,15g.

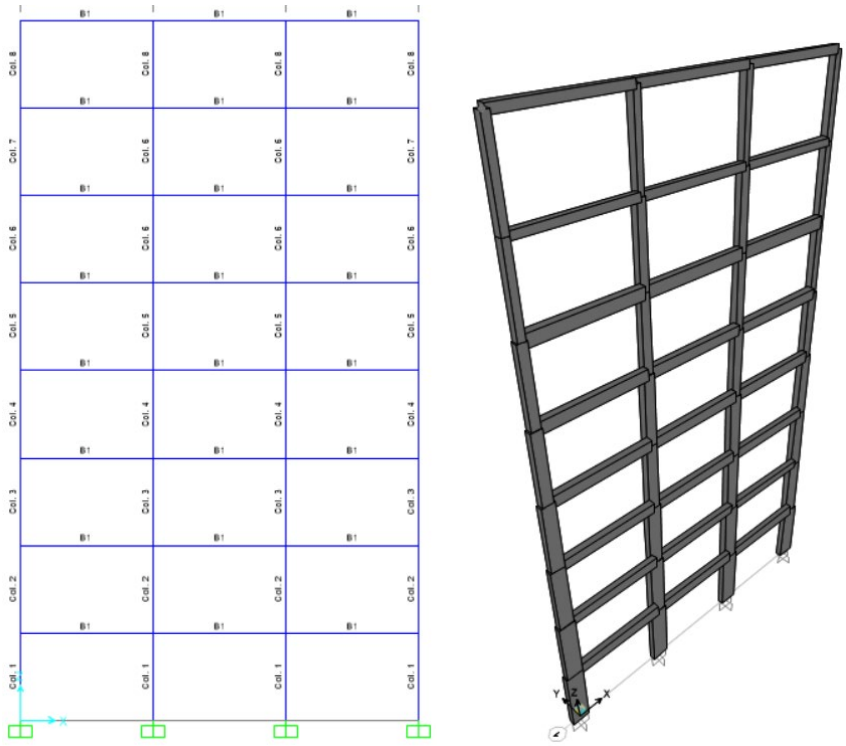

Fig. 3. 2, Model A_0, 2D RC Frame.

Designing process, Fig. 3. 3 shows high BEAM-COLUMN Capacity Ratio values. Columns and capacity values in Table 3. 7.

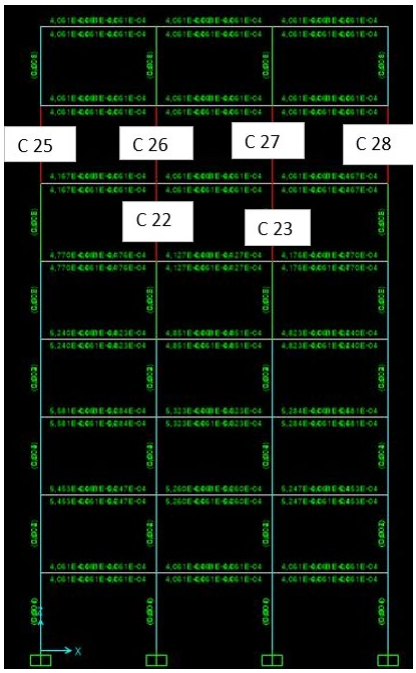

Fig. 3. 3, Model A_0, Design, Columns Failure.

Beam-Column Capacity Ratios

Column	Capacity
22 = C6	1.227
23 = C6	1.227
25 = C7	1.091
26 = C7	1.779
27 = C7	1.779
28 = C7	1.091

Table 3. 7, Model A_0, Design, Capacity Ratio.

Beams B1 replaced by B2 in 7th and 8th storeys, the two-middle column C7 in the 7th storey are also replaced by C6, Table 3. 8 shows the changes in structural characteristics.

Storey	*Column*	*Beam*	*Height*	*Span*
1	C1	B1	3.3m	3*5m
2	C2	B1	3.3m	3*5m
3	C3	B1	3.3m	3*5m
4	C4	B1	3.3m	3*5m
5	C5	B1	3.3m	3*5m
6	C6	B1	3.3m	3*5m
7	C7-C6-C6-C7	B2	3.3m	3*5m
8	C8	B2	3.3m	3*5m

Table 3. 8, Model A_0, Design, Structural and Geometrical characteristics.

3.2.2. Building A_{ret}

Building A_{ret} is the suggested existing RC building A_0 retrofitted by CLT panels, Fig. 3. 4, as supporting elements., investigated seismically for PGA = 0.35g, Table 3. 9.

RSA	*S*	*Tb*	*Tc*	*Td*	*β*	*q*	*Damping*
PGA=0.35g	1.3	0.1	0.25	1.5	0.2	2	0.05

Table 3. 9, Model $A_{ret,}$ PGA=0.35g.

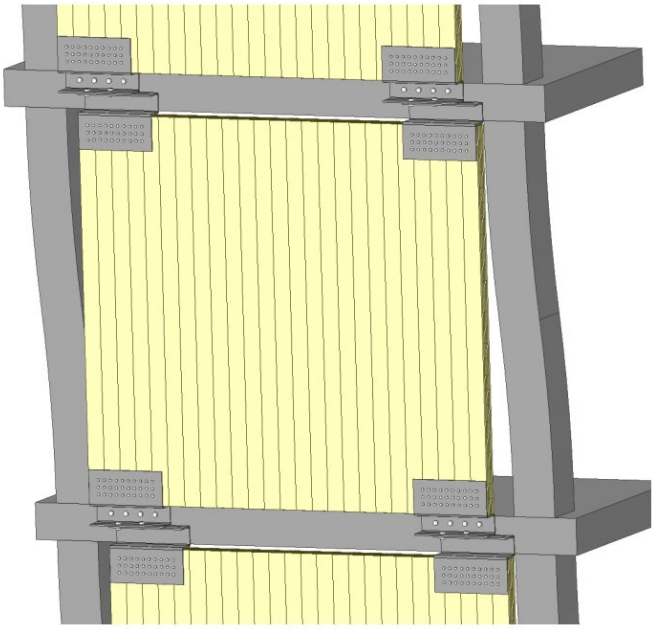

Fig. 3. 4, CLT panels as a retrofitting technique.

3.2.2.1. FEM, A_{ret}

In SAP2000, a 2D RC Frame is modelled with CLT panels, CLT material is added as a new orthotropic material, Table 3. 4. Sections are simulated as a layered shell section, Fig. 3. 5 (a), 3cm thickness for each, two CLT sections are modelled, 3 layered and 5 layered shells, Table 3. 10 and Table 3. 11, respectively.

Body constrains are used to connect the CLT panels to the beams to free its movement on X-axis, Fig. 3. 5 (b). In Fig. 3. 5 (c), the body constrains are connecting the CLT panels to the Columns to free its movement on X-axis. When a body constraint is added, means that all of its restricted joints move together as a three-dimensional rigid body with a body constraint. By default, each joint linked participates in all degrees of freedom. A subset of freedom degrees can be chosen to be restricted. At least two joints to have any effect on the model must be included in any body constrain, APPENDIX A.

All layered shells are divided by 10*6 to locate the bodies between the panels and the 2D RC frame, as illustrated in Fig. 3. 5 (b), (c).

CLT Elements are suggested into three layout models A_{ret_1}, A_{ret_2}, A_{ret_2}, and A_{ret_4}. In these suggestions, the CLT panels, at the base level, are connected to three unloaded B1 Beams added.

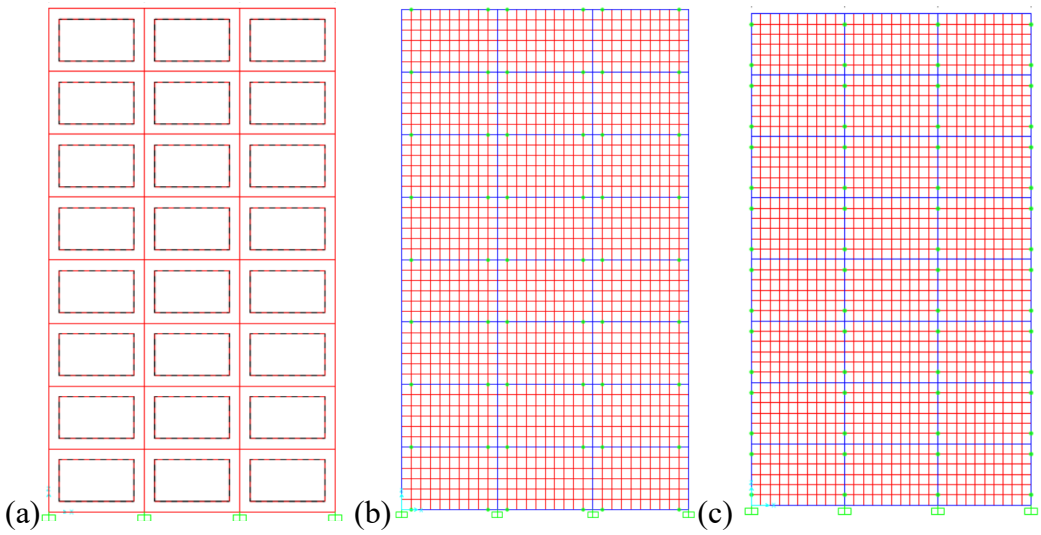

Fig. 3. 5, CLT panels Modelling.

Layer	*Distance*	*Thickness*	*Section*	*Material*
1	0.00	0.03	Shell	CLT
2	0.03	0.03	Shell	CLT
3	0.06	0.03	Shell	CLT

Table 3. 10, 3 Layered CLT panel shell section.

Layer	*Distance*	*Thickness*	*Section*	*Material*
1	0.00	0.03	Shell	CLT
2	0.03	0.03	Shell	CLT
3	0.06	0.03	Shell	CLT
4	0.09	0.03	Shell	CLT
5	0.012	0.03	Shell	CLT

Table 3. 11, 5 Layered CLT panel shell section.

- Model A_{ret_1}: CLT panels, as three layered shell sections, are used to retrofit the 2D RC frame assessed for PGA=0.35g, Table 3. 12. CLT panels are covering the whole Model, the connectors here are CLT-Beam set, Fig. 3. 5 (b).

Storey	*Column*	*Beam*	*Height*	*Span*	*layer*	*Connector*
1	C1	B1	3.3m	3*5m	3	*CLT-Beam*
2	C2	B1	3.3m	3*5m	3	*CLT-Beam*
3	C3	B1	3.3m	3*5m	3	*CLT-Beam*
4	C4	B1	3.3m	3*5m	3	*CLT-Beam*
5	C5	B1	3.3m	3*5m	3	*CLT-Beam*
6	C6	B1	3.3m	3*5m	3	*CLT-Beam*
7	C7-C6-C6-C7	B2	3.3m	3*5m	3	*CLT-Beam*
8	C8	B2	3.3m	3*5m	3	*CLT-Beam*

Table 3. 12, Model A_{ret_1}, CLT, Structural, Geometrical characteristics.

- Model A_{ret_2}: CLT panels, as five layered shell sections, are used to retrofit the 2D RC frame assessed for PGA=0.35g, Table 3. 13. CLT panels are covering the whole Model, the connectors here are CLT-Beam set, Fig. 3. 5 (b).

Storey	*Column*	*Beam*	*Height*	*Span*	*layer*	*Connector*
1	C1	B1	3.3m	3*5m	5	*CLT-Beam*
2	C2	B1	3.3m	3*5m	5	*CLT-Beam*
3	C3	B1	3.3m	3*5m	5	*CLT-Beam*
4	C4	B1	3.3m	3*5m	5	*CLT-Beam*
5	C5	B1	3.3m	3*5m	5	*CLT-Beam*
6	C6	B1	3.3m	3*5m	5	*CLT-Beam*
7	C7-C6-C6-C7	B2	3.3m	3*5m	5	*CLT-Beam*
8	C8	B2	3.3m	3*5m	5	*CLT-Beam*

Table 3. 13, Model A_{ret_2}, CLT, Structural, Geometrical characteristics.

- Model A_{ret_3}: CLT panels, as three layered shell sections covering the 1st, 2nd, 3rd, and 4th storey, and five layered shell sections covering the 5th, 6th, 7th, and 8th storey, are used to retrofit the 2D RC frame assessed for PGA=0.35g, the connectors here are CLT-Beam set, Table 3. 14, Fig. 3. 5 (b).

Storey	*Column*	*Beam*	*Height*	*Span*	*layer*	*Connector*
1	C1	B1	3.3m	3*5m	3	*CLT-Beam*
2	C2	B1	3.3m	3*5m	3	*CLT-Beam*
3	C3	B1	3.3m	3*5m	3	*CLT-Beam*
4	C4	B1	3.3m	3*5m	3	*CLT-Beam*
5	C5	B1	3.3m	3*5m	5	*CLT-Beam*
6	C6	B1	3.3m	3*5m	5	*CLT-Beam*
7	C7-C6-C6-C7	B2	3.3m	3*5m	5	*CLT-Beam*
8	C8	B2	3.3m	3*5m	5	*CLT-Beam*

Table 3. 14, Model A_{ret_3}, CLT, Structural, Geometrical characteristics.

- Model A_{ret_4}: CLT panels, as three layered shell sections, are used to retrofit the 2D RC frame assessed for PGA=0.35g, the connectors here are CLT-Column set, Table 3. 15, Fig. 3. 5 (c).

Storey	*Column*	*Beam*	*Height*	*Span*	*layer*	*Connector*
1	C1	B1	3.3m	3*5m	3	*CLT-Column*
2	C2	B1	3.3m	3*5m	3	*CLT- Column*
3	C3	B1	3.3m	3*5m	3	*CLT- Column*
4	C4	B1	3.3m	3*5m	3	*CLT- Column*
5	C5	B1	3.3m	3*5m	3	*CLT- Column*
6	C6	B1	3.3m	3*5m	3	*CLT- Column*
7	C7-C6-C6-C7	B2	3.3m	3*5m	3	*CLT- Column*
8	C8	B2	3.3m	3*5m	3	*CLT- Column*

Table 3. 15, Model A_{ret_4}, CLT, Structural, Geometrical characteristics.

3.2.3. Building B

Building B is the suggested existing RC building designed for PGA = 0.35g. the structural and geometrical characteristics are shown in Fig. 3. 6, Table 3.4. 3.

The structural elements in details are in APPENDIX A.

Building B is a reference building to compare results of the various retrofitting solutions to assess whether the retrofitting technique satisfies the seismic safety requirements compared to the results of a newly designed Building B.

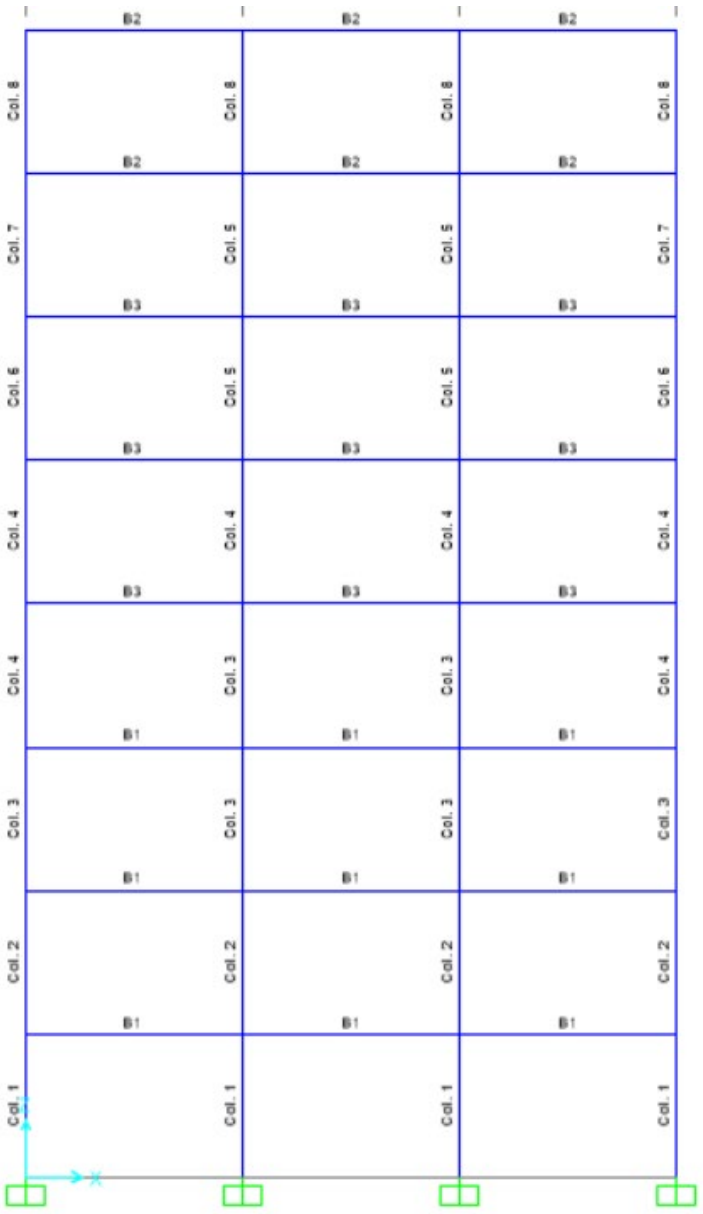

Fig. 3. 6, Model B.

3.2.3.1. FEM, B

Using SAP2000 to model a 2D frame of Building B as a low ductile structure DCL, designed according to Eurocode 8 for PGA=0.35g by RSA method, Table 3. 16. Considering B as a ground type in Norway.

RSA	*S*	*Tb*	*Tc*	*Td*	*β*	*q*	*Damping*
PGA=0.35g	1.3	0.1	0.25	1.5	0.2	2	0.05

Table 3. 16, Model B, PGA=0.35g.

Fig. 3. 7, the design procedures show high-capacity ratio values of Beam-Column. In addition, axial force and biaxial moment check displays risk levels. Columns and capacity values are in Table 3. 17.

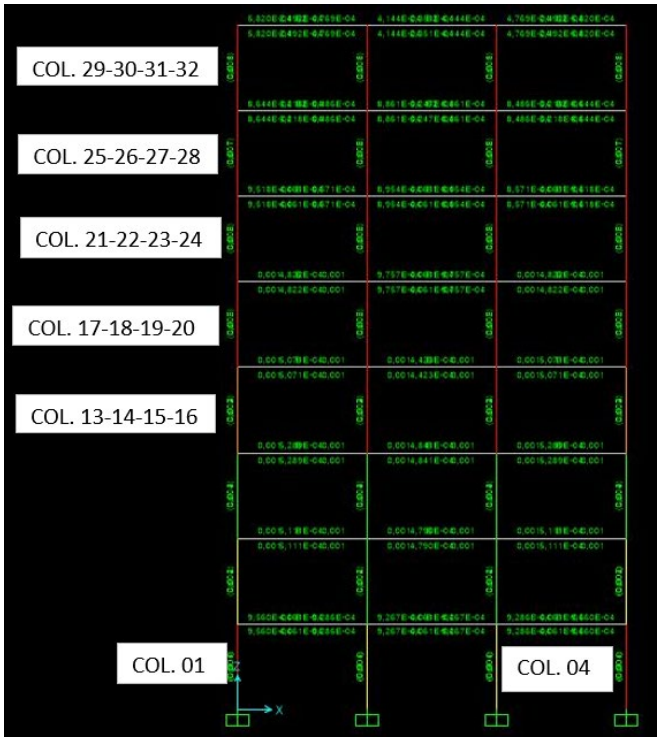

Fig. 3. 7, Model B, Design, Columns Failure.

Capacity Ratios

Column	Beam-Column	Axial force and biaxial moment
1	---	1.076
4	---	1.076
13	0.885	0.961
14	1.273	1.123
15	1.273	1.123
16	0.885	0.961
17	1.024	---
18	1.472	1.236
19	1.472	1.236
20	1.024	---
21	1.326	1.232
22	1.683	1.501
23	1.683	1.501
24	1.326	1.232
25	0.876	1.264
26	1.189	1.665
27	1.189	1.665
28	0.876	1.264
29	---	1.046
30	---	1.579
31	---	1.579
32	---	1.046

Table 3. 17, Model B, Design, Capacity Ratio.

The designing process required many Steel and columns cross-section design steps, and a B2 beam cross-section is in use in addition. The design process in details shown in APPENDIX A.

Table 3. 1 illustrates the ultimate design of a 2D RC frame for PGA = 0.35g. the resulting seismic performance of this Model will be a reference to compare the seismic performance of the Model A_{ret}.

Storey	*Column*	*Beam*	*Height*	*Span*
1	C1	B1	3.3m	3*5m
2	C2	B1	3.3m	3*5m
3	C3	B1	3.3m	3*5m
4	C4-C3-C3-C4	B3	3.3m	3*5m
5	C4	B3	3.3m	3*5m
6	C6-C5-C5C6	B3	3.3m	3*5m
7	C7-C5-C5-C7	B2	3.3m	3*5m
8	C8	B2	3.3m	3*5m

Table 3. 18, Model B, Design, Structural and Geometrical characteristics.

3.3. Case Study (POA)

This Case Study evaluates the seismic performance of the down-mentioned Models and determines the acceptable damage level considering the Model inelastic Behaviour, by Pushover Method.

(POA), The pushover method is a static nonlinear technique. A computer model of a structure undergoes a pre-defined lateral load application, representing approximately the relative inertia forces created at locations of substantial mass. The load intensity is increased, i.e., the structure is pushed, and the fracture sequence, the plastic hinge development, and a load of failure of the different structural components are recorded because of the increased lateral load. This procedure continues until a specified limit of displacement. It is primarily built on the presumption that the structure's response is governed by the initial mode of vibration and the first few modes of vibration and that it remains constant throughout the structure's elastic and inelastic response. This offers a basis for turning a dynamic problem into a theoretically flawed static problem [43].

This section presents the modeling process of two Models by SAP2000 using the POA:

- Model A_{ret}: four suggested solutions for Building A_{ret}, modelled by SAP2000, will be assessed by POA for PGA=0.35g.

- Model B: the Reference Model will be assessed by the POA for PGA = 0.35g.

3.3.1. Modelling Presumptions

The modelling of POA based on:

1- All structural inputs are previously mentioned inputs for the testing Models.

2- The testing Models is the constitutive model designed for PGA=0.35 by RSA. This is not an alternative to the design based on linear-elastic analysis (RSA), but to assess the structural performance of the retrofitted modal.

3- The testing Models maintain the configuration of the Response Spectrum already specified.

4- POA requires the force-deformation curve development for beams and columns critical section (Force–deformation relationship of a typical plastic hinge.), Fig. 3. 8 [44]:

- Point A matches to the unloaded condition.
- Load deformation relation is defined by the linear response from A to an effective yield B.
- Then the stiffness decreases from point B to C.
- At point C, the resistance is equal to the nominal strength, then there is a dramatic fall in lateral load resistance to point D, the response at reduced resistance to E, and finally, no resistance.
- The BC line's slope is usually set to between 0 and 10% of the initial slope.
- The CD line refers to an initial failure of the element.
- The DE Line represents the element's residual strength. [45]

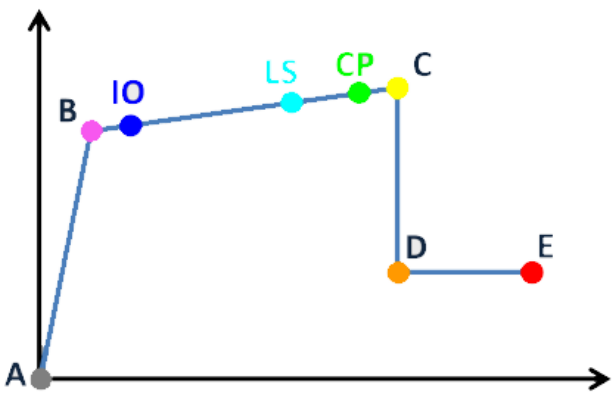

Fig. 3. 8, Elements' Performance criteria.

FEMA specifies these points to determine the hinge rotation behavior of RC elements. The points between B and C show the hinge's acceptance criteria, which are Immediate Occupancy (IO), Life Safety (LS), and Compliance (CP) (Collapse Prevention), Table 3. 19, [46].

Damage Control and Building Performance Levels

Level	Discribtion
Immediate Occupancy (IO)	There is some minimal damage and no long-term drift. The structure's initial strength and stiffness are kept. Facades, partitions, and ceilings, as well as structural elements, have minor cracks. The fire protection system is operational.
Life Safety (LS)	Damage is moderate. Some drift is unavoidable. In all storeys, there is some residual strength and stiffness. Partitions have been damaged. It's possible that the structure is beyond economical repair.
Collapse Prevention (CP)	Damage that is severe. Drifts that are large and permanent. However, load-bearing columns and walls work despite the lack of residual stiffness and strength. The structure is on its way to collapse.

Table 3. 19, Damage Control and Building Performance Levels.

3.3.2. FEM Model

Using SAP2000 to analyse the uo-mentioned Models by POA under these procedures:

1- Gravity Load is arranged with nonlinear state.

2- Pushover Load is added with nonlinear static state continues from the nonlinear Gravity End, Load Pattern (ACC, UX; -1), the Load Application on displacement Control using UX at Joint 32. Using monitored displacement 4% of the total height with 1.056m, [47].

3- The testing Models consider nonlinear behavior of elements. Hinges are added with recomendatios of PM3 hinge for columns, and M3 for Beams. The default hinge properties (from tabels in ASCE 41-13 [47], provided by SAP2000), are used with no considerations due to simplicity, Fig. 3. 9.

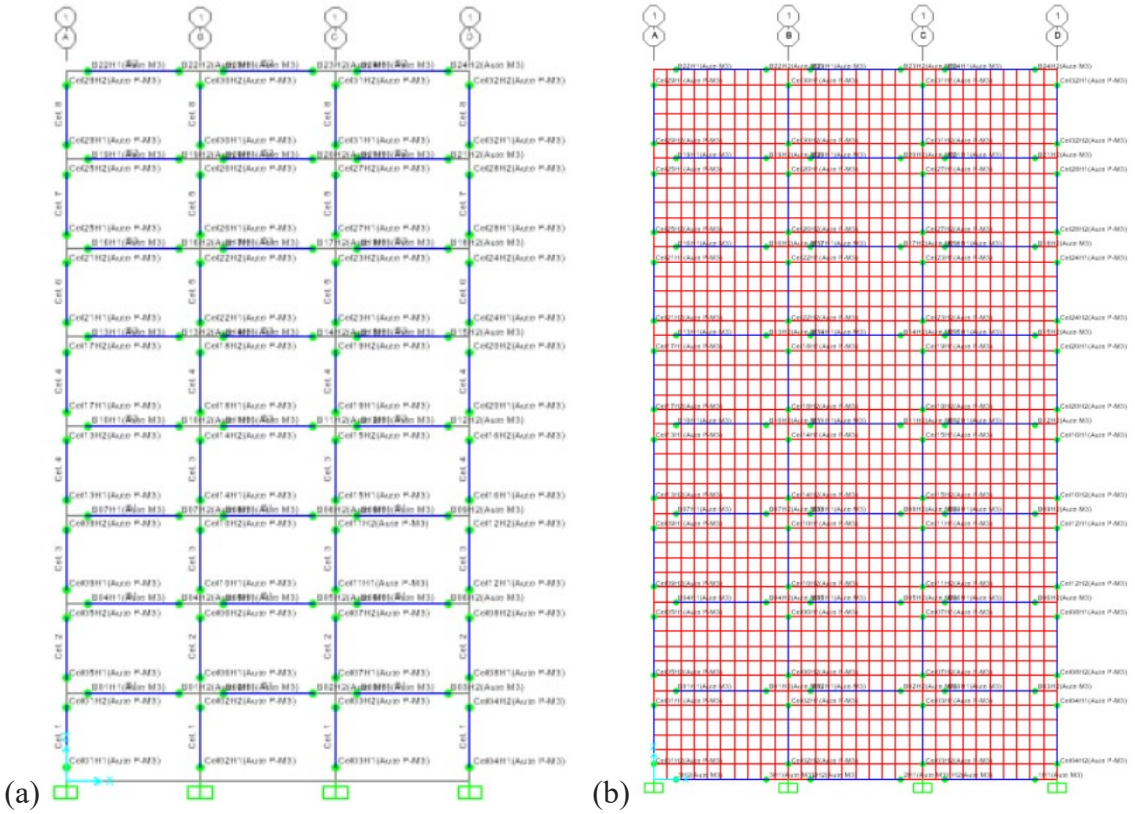

Fig. 3. 9, Hinges in POA Case Study.

4- Regarding the CLT Panels, the Material Behaviour set to nonlinear behaviour.

3.3.2.1. Capacity Spectrum (CSM)

Capacity Spectrum Method (CSM), according to the Applied Technology Council (ATC-40), is a nonlinear static analysis implementation affords a graphical expected seismic performance of the existing or retrofitted structure by the intersection of the structure's capacity spectrum representation with a representation of demand spectrum (the earthquake's displacement demand) on the model. The performance point is at the intersection, and the estimated displacement demand on the structure for the specified level of seismic hazard is at the displacement coordinate of the performance point [48]. Fig. 3. 10 [43].

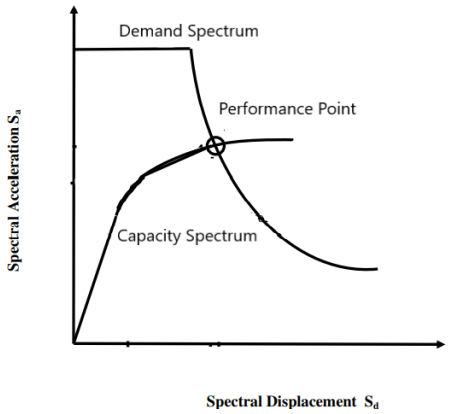

Fig. 3. 10, CSM.

- Capacity Spectrum: The capacity curve converted from shear force vs. roof displacement coordinates into spectral acceleration vs. spectral displacement coordinates [48]. Conversion to a single-degree-of-freedom equivalent system and derivation of the capacity curve in Fig. 3. 11 [49].
-

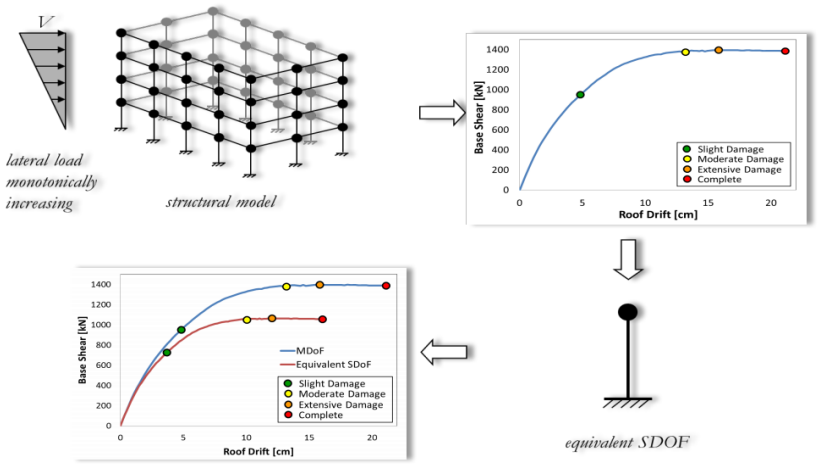

Fig. 3. 11, Capacity Spectrum.

- Demand Spectrum: The 5% damped reduced response spectrum used to represent the earthquake ground motion in CSM [48]. Fig. 3. 12 shows the elastic spectrum to Demand spectrum conversion [43].

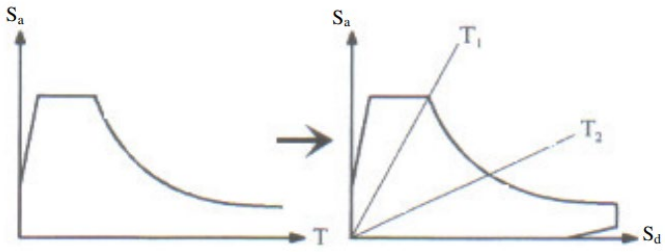

Fig. 3. 12, Demand Spectrum.

- Performance point: At the intersection of the Capacity Spectrum with the Demand Spectrum in CSM, the performance point determines the peak displacement [48].

CSM implementation is commonly used in structural engineering. SAP2000 has already implemented these default nonlinear properties [50], and CSM is used to evaluate the POA results.

CHAPTER 4

This chapter displays the result of :

- RSA: Results of each model of the case study, and comparison discuss the effectivity of CLT panels on the seismic performance of the model A_{ret}, examining the records of displacement, Interstorey drift, base reaction, and the periods and frequencies, compared to the reference B.

- POA: Results of each model of the case study, with a comparison that discusses the effectivity of CLT panels on the seismic performance of the model A_{ret}, by examining the records of Capacity Curve, Capacity Spectrum, and the Performance Point compared to the reference B.

4.1. RSA Results

In this section, the RSA is carried out using the SAP2000. A two-dimensional model is being designed for PGA= 0.15g regarding the suggusted existing Building A_0, and PGA= 0.35g regarding the Reference Building B, and the suggested retrofitted Building A_{ret}. The results of lateral Displacement, Interstorey Drift, Base Shear, Period and Frequency, and the (P-M) Interaction Curve of the six Models are displayed.

4.1.1. Model A_0

4.1.1.1. Lateral Displacement

The resulting displacements of the Model A_0 from RSA can be seen in Table 4. 1, max axial X displacement at the roof of the Model is 2.62 cm. Deformed shape in Fig. 4. 1.

Model A_0, Δx

Point	H	Δx
9	3.3	0.0269
8	3.3	0.0223
7	3.3	0.0181
6	3.3	0.0144
5	3.3	0.011
4	3.3	0.0076
3	3.3	0.0042
2	3.3	0.0014
1	3.3	0

Values(m).

Table 4. 1, Model A_0, Δx.

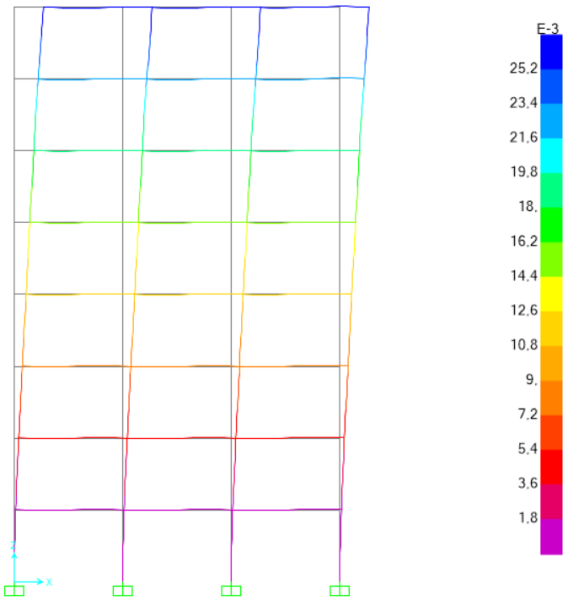

Fig. 4. 1, Model A_0, Deformation.

4.1.1.2. Interstorey Drift

Checking the Interstorey Drift Limit results from RSA in Table 4. 3, shows less drift than the limitation of 24.75mm in the Model A_0 assessed for PGA = 0.15g. While the IDR graph, Fig. 4. 2, computed according to the previous resulting displacements in Table 4. 2, shows that the IDR has a peak at the top storey with about 0.14%, and a stable value of about 0.1% along with the 3rd, 4th, and the 5th storeys. IDR graph displays continuous flow without abrupt changes.

Model A_0, Interstorey Drift Ratio

Storey	Level	I. D. R. %
8	26.4	0.1394
7	23.1	0.1273
6	19.8	0.1121
5	16.5	0.1030
4	13.2	0.1030
3	9.9	0.1030
2	6.6	0.0848
1	3.3	0.0424

Table 4. 2, Model A_0, IDR.

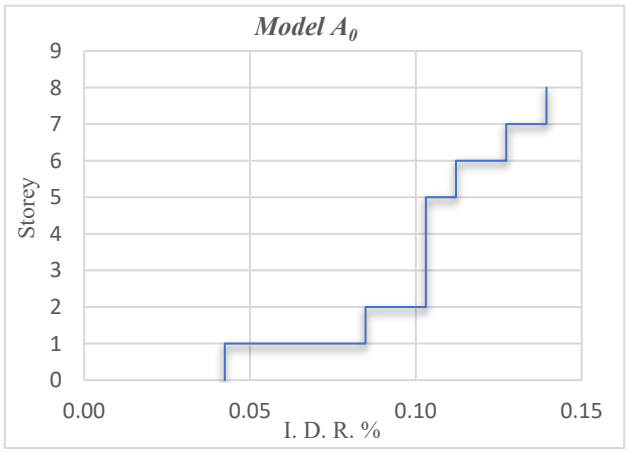

Fig. 4. 2, Model A_0, IDR.

Model A_0: Interstorey Drift limit Check

storey	Δx	q_d	ν	d_{si}	d_r	d_r*ν	Limit: 24.75
8	26.9	2	0.5	53.8	9.2	4.6	TRUE
7	22.3	2	0.5	44.6	8.4	4.2	TRUE
6	18.1	2	0.5	36.2	7.4	3.7	TRUE
5	14.4	2	0.5	28.8	6.8	3.4	TRUE
4	11	2	0.5	22.0	6.8	3.4	TRUE
3	7.6	2	0.5	15.2	6.8	3.4	TRUE
2	4.2	2	0.5	8.4	5.6	2.8	TRUE
1	1.4	2	0.5	2.8	2.8	1.4	TRUE

The values of Δx, d_{si}, d_r, and Limit are in mm.

Table 4. 3, Model A_0, Interstorey Drift Limit Check.

4.1.1.3. Base Reaction

The resulting Base Shear value from RSA in the Model A_0 assessed for PGA = 0.15g is about 236 kN, Table 4. 4.

Model A_0: Base Reaction

F_X	F_Z	M_Y
236.18	0.00	3638.40

Values in kN-m.

Table 4. 4, Model A_0, Base Reactions.

4.1.1.4. Period and Frequency

The max resulting period from RSA in the Model A_0 assessed for PGA = 0.15g is about 1.13 sec reported in Mode 1, while the Mode 12 gives the max resulting frequency value, about 21 Cyc/sec, Table 4. 5.

Model A_0: Modal Periods and Frequencies

Mode	Period	Frequency
1	1.13	0.88
2	0.48	2.10
3	0.28	3.62
4	0.18	5.44
5	0.14	7.14
6	0.11	9.36
7	0.10	9.70
8	0.10	10.04
9	0.08	12.70
10	0.08	12.74
11	0.07	13.96
12	0.05	20.92

Values in sec-Cyc.

Table 4. 5, Model A_0, Modal Periods and Frequencies.

4.1.1.5. (P-M) Interaction Curve

For the seismic performance of a column, the impact of axial force on capacity is essential in terms of strength and ductility. The P-M Interaction Curve of the Model A_0 assessed for PGA= 0.15g represents the possible failure combination for the columns bent around the axis x. The capacity of a P-M combination must be checked by generating a failure surface results from a compressive Concrete failure analysis for columns and the PM Demands combination (resulting from the RSA) on the same line emitting from the center of a coordinate system.

Because of the nonexistence of Demands interaction points outside the Capacity Curve, Fig. 4. 3, Fig. 4. 4, Fig. 4. 5, Fig. 4. 6, Fig. 4. 7, Fig. 4. 8, and Fig. 4. 9. Therefore, no exceeding the nominal column's strength, and no failure in any column, exactly a complete ductile performance for the PGA 0.15g.

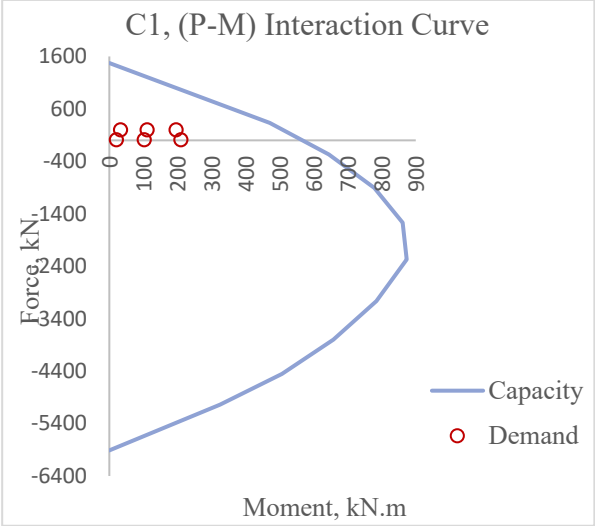

Fig. 4. 3, Model A_0, (P-M) Interaction Curve, C1.

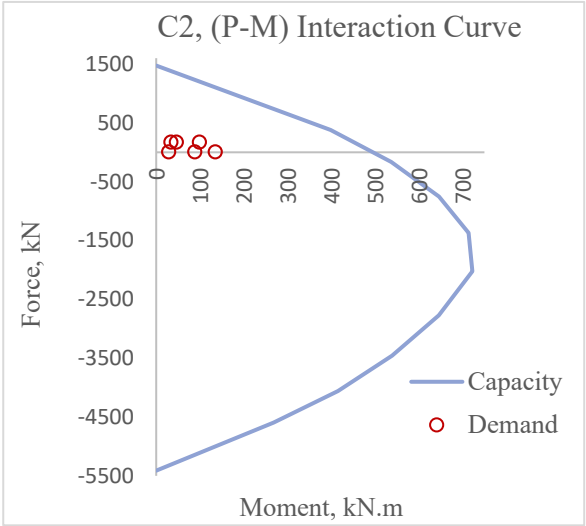

Fig. 4. 4, Model A_0, (P-M) Interaction Curve, C2.

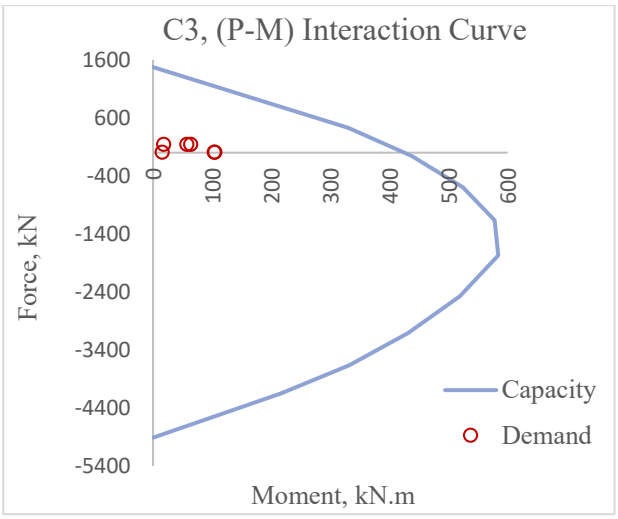

Fig. 4. 5, Model A_0, (P-M) Interaction Curve, C3.

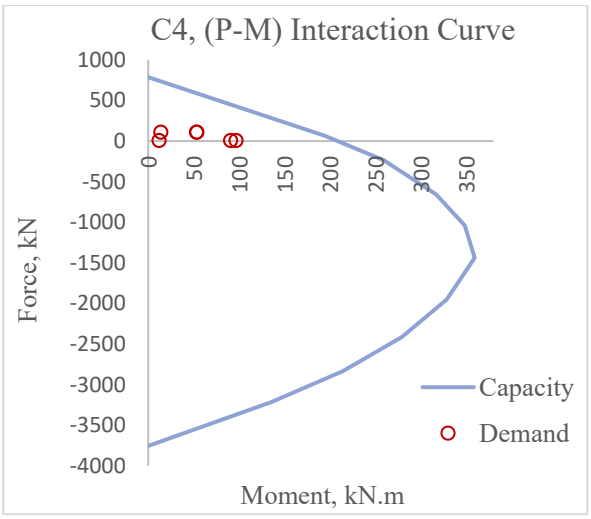

Fig. 4. 6, Model A_0, (P-M) Interaction Curve, C4.

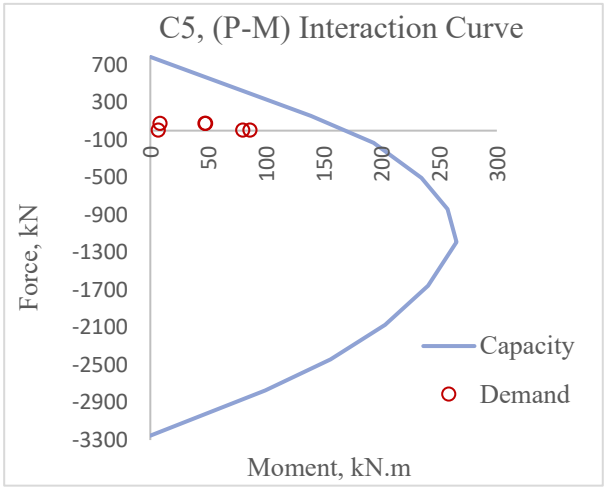

Fig. 4. 7, Model A_0, (P-M) Interaction Curve, C5.

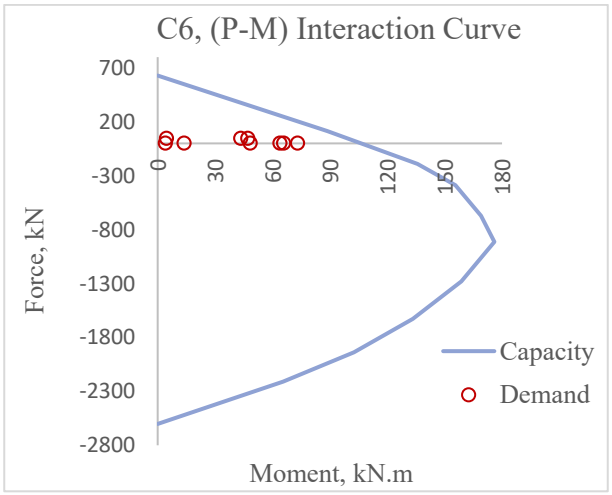

Fig. 4. 8, Model A_0, (P-M) Interaction Curve, C6.

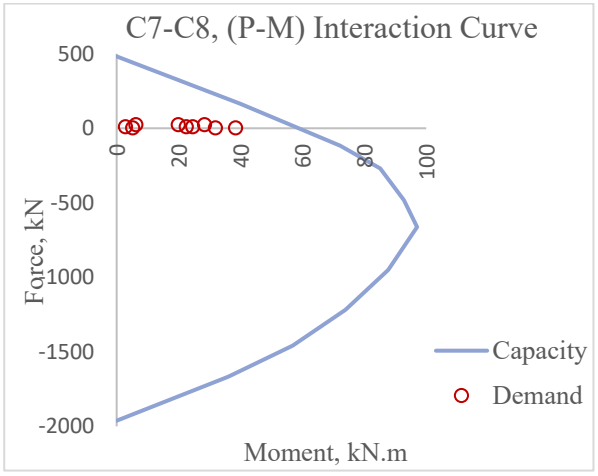

Fig. 4. 9, Model A_0(P-M) Interaction Curve, C7. C8.

4.1.2. Model A_{ret}

4.1.2.1. Model A_{ret_1}

4.1.2.1.1. Lateral Displacement

The resulting displacements of Model A_{ret_1} from RSA can be seen in Table 4. 6, max axial X displacement at the . of the Model is 3.59 cm under PGA = 0.35g. Deformed shape in Fig. 4. 10.

Model A_{ret_1}, Δx

Point	H	Δx
9	3.3	0.0359
8	3.3	0.0331
7	3.3	0.0288
6	3.3	0.0236
5	3.3	0.0185
4	3.3	0.0132
3	3.3	0.0079
2	3.3	0.0029
1	3.3	0

Values(m).

Table 4. 6, Model A_{ret_1}, Δx.

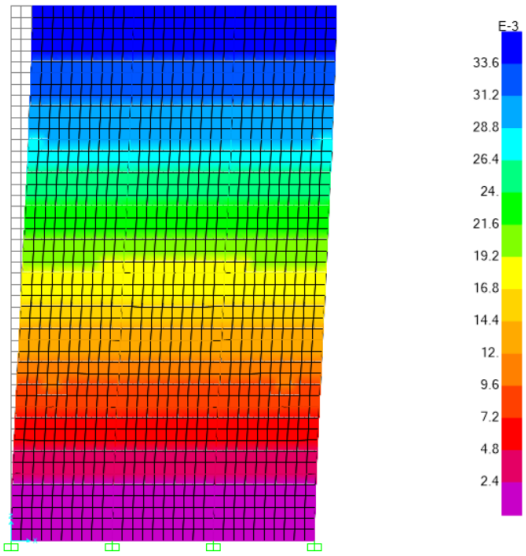

Fig. 4. 10, Model A_{ret_1}, Deformation.

4.1.2.1.2. Interstorey Drift

In the Model A_{ret_1} assessed for PGA = 0.35g, checking the Interstorey Drift Limit results from RSA, In Table 4. 8, Data shows less drift than the limitation of 24.75mm. Whereas, IDR graph, Fig. 4. 11, computed according to the previous resulting displacements in Table 4. 7, shows that the IDR is about 0.08% at the top storey and a stable peak value of about 0.15 to 0.16% between the 3rd and 6th storey. IDR graph doesn't display a

continuous flow, but a staggered one, starting to retract after the 4th storey and shows a severe regression after the 6th storey to the end.

Model A_{ret_1}, Interstorey Drift Ratio

Storey	Level	I. D. R. %
8	26.4	0.0848
7	23.1	0.1303
6	19.8	0.1576
5	16.5	0.1545
4	13.2	0.1606
3	9.9	0.1606
2	6.6	0.1515
1	3.3	0.0879

Values(m).

Table 4. 7, Model A_{ret_1}, IDR.

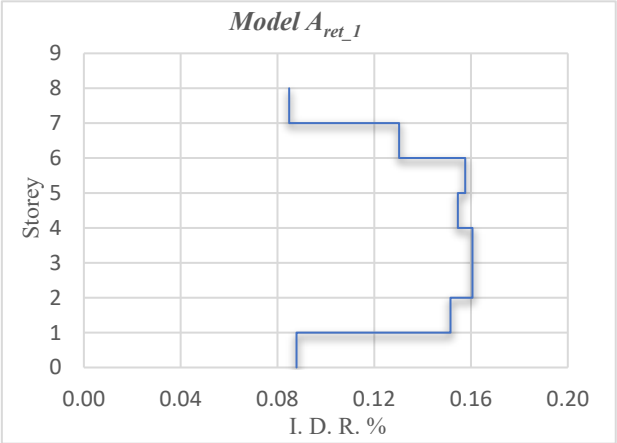

Fig. 4. 11, Model A_{ret_1}, IDR.

Model A_{ret_1}: Interstorey Drift limit Check

storey	d_m	q_d	ν	d_{si}	d_r	d_r*ν	Limit: 24.75
8	35.9	2	0.5	71.8	5.6	2.8	TRUE
7	33.1	2	0.5	66.2	8.6	4.3	TRUE
6	28.8	2	0.5	57.6	10.4	5.2	TRUE
5	23.6	2	0.5	47.2	10.2	5.1	TRUE
4	18.5	2	0.5	37.0	10.6	5.3	TRUE
3	13.2	2	0.5	26.4	10.6	5.3	TRUE
2	7.9	2	0.5	15.8	10.0	5	TRUE
1	2.9	2	0.5	5.8	5.8	2.9	TRUE

The values of Δx, d_{si}, d_r, and Limit are in mm.

Table 4. 8, Model A_{ret_1}, Interstorey Drift Check.

4.1.2.1.3. Base Reaction

The resulting Base Shear value from RSA in the Model A_{ret_1} assessed for PGA = 0.35g is 925.5 kN,Table 4. 9.

Model A_{ret_1}: Base Reaction

F_X	F_Z	M_Y
925.50	0.00	14930.20

Values in kN-m.

Table 4. 9, Model A_{ret_1}, Base Reactions.

4.1.2.1.4. Period and Frequency

The max resulting period from RSA in the Model A_{ret_1} assessed for PGA = 0.35g is about 0.7 sec reported in Mode 1, while the Mode 12 gives the max resulting frequency value, about 29 Cyc/sec,Table 4. 10.

Model A_{ret_1}: Modal Periods and Frequencies

Mode	Period	Frequency
1	0.71	1.41
2	0.27	3.69
3	0.16	6.09
4	0.12	8.44
5	0.09	10.56
6	0.08	12.56
7	0.06	16.43
8	0.05	22.14
9	0.04	22.88
10	0.04	22.92
11	0.04	24.38
12	0.03	29.17

Values in sec-Cyc.

Table 4. 10, Model A_{ret_1}, Modal Periods and Frequencies.

4.1.2.2. Model A_{ret_2}

4.1.2.2.1. Lateral Displacement

The resulting displacements of Model A_{ret_2} from RSA can be seen in Table 4. 11, max axial X displacement at the roof of the Model is 3.24 cm under PGA= 0.35g. Deformed shape in Fig. 4. 12.

Model A_{ret_2}, Δx

Point	H	Δx
9	3.3	0.0324
8	3.3	0.0303
7	3.3	0.0268
6	3.3	0.0224
5	3.3	0.0178
4	3.3	0.0128
3	3.3	0.0078
2	3.3	0.0029
1	3.3	0

Values(m).

Table 4. 11, Model A_{ret_2}, Δx.

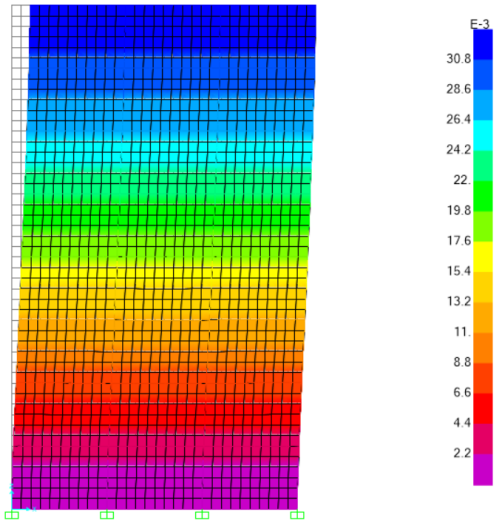

Fig. 4. 12, Model A_{ret_2}, Deformation.

4.1.2.2.2. Interstorey Drift

In the 2D RC Frame, A_{ret_2} assessed for PGA = 0.35g, checking the Interstorey Drift Limit results from RSA, Table 4. 13 illustrates less drift values than the limitation of 24.75mm. While the IDR graph, Fig. 4. 13, plotted according to the previous resulting displacements in Table 4. 12, shows that the IDR is about 0.06% at the top storey and has a stable peak value of about 0.15% between 3rd and 4th storeys. IDR graph displays a continuous flow to the 4th storey, but retracts at the 5th storey, and shows a severe regression after the 6th storey to the end.

Model A_{ret_2}, Interstorey Drift Ratio

Storey	Level	I. D. R. %
8	26.4	0.0636
7	23.1	0.1061
6	19.8	0.1333
5	16.5	0.1394
4	13.2	0.1515
3	9.9	0.1515
2	6.6	0.1485
1	3.3	0.0879

Table 4. 12, Model A_{ret_2}, IDR.

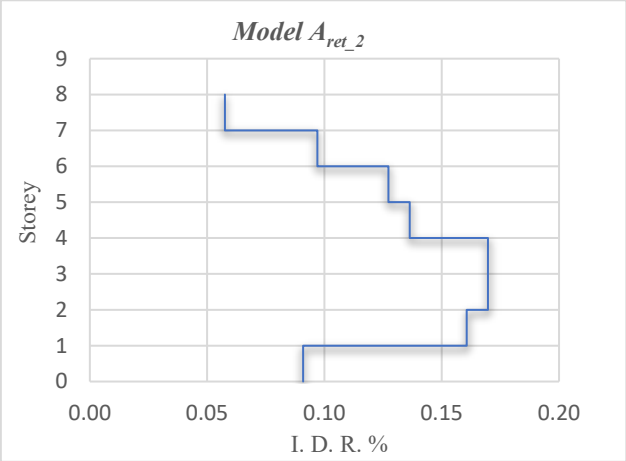

Fig. 4. 13, Model A_{ret_2}, IDR.

Model A_{ret_2}: Interstorey Drift limit Check

storey	Δx	q_d	ν	d_{si}	d_r	d_r*ν	Limit: 24.75
8	32.4	2	0.5	64.8	4.2	2.1	TRUE
7	30.3	2	0.5	60.6	7.0	3.5	TRUE
6	26.8	2	0.5	53.6	8.8	4.4	TRUE
5	22.4	2	0.5	44.8	9.2	4.6	TRUE
4	17.8	2	0.5	35.6	10.0	5	TRUE
3	12.8	2	0.5	25.6	10.0	5	TRUE
2	7.8	2	0.5	15.6	9.8	4.9	TRUE
1	2.9	2	0.5	5.8	5.8	2.9	TRUE

The values of Δx, d_{si}, d_r, and Limit are in mm.

Table 4. 13, Model A_{ret_2}, Interstorey Drift Check.

4.1.2.2.3. Base Reaction

The resulting Base Shear value from RSA in the Model A_{ret_2} assessed for PGA = 0.35g is 1032 kN, Table 4. 14.

Model A_{ret_2}: Base Reaction

F_X	F_Z	M_Y
1032.28	0.00	16837.39

Values in kN-m.

Table 4. 14, Model A_{ret_2}, Base Reactions.

4.1.2.2.4. Period and Frequency

The max resulting period from RSA in the Model A_{ret_2} assessed for PGA = 0.35g is about 0.65 sec reported in Mode 1, while the Mode 12 gives the max resulting frequency value, about 31 Cyc/sec, Table 4. 15.

Model A_{ret_2}: Modal Periods and Frequencies

Mode	Period	Frequency
1	0.65	1.53
2	0.24	4.11
3	0.15	6.80
4	0.11	9.41
5	0.08	11.86
6	0.07	13.72
7	0.06	17.25
8	0.04	22.93
9	0.04	23.48
10	0.04	24.01
11	0.04	26.40
12	0.03	30.74

Values in sec-Cyc.

Table 4. 15, Model A_{ret_2}, Modal Periods and Frequencies.

4.1.2.3. Model A_{ret_3}

4.1.2.3.1. Lateral Displacement

The resulting displacements of Model A_{ret_3} from RSA can be seen in Table 4. 16, max axial X displacement at the roof of the Model is 3,33 cm under PGA =0.35g. Deformed shape in Fig. 4. 14.

Model A_{ret_3}, Δx

Point	H	Δx
9	3.3	0.0333
8	3.3	0.0314
7	3.3	0.0282
6	3.3	0.024
5	3.3	0.0195
4	3.3	0.0139
3	3.3	0.0083
2	3.3	0.003
1	3.3	0

Values(m).

Table 4. 16, Model A_{ret_3}, Δx.

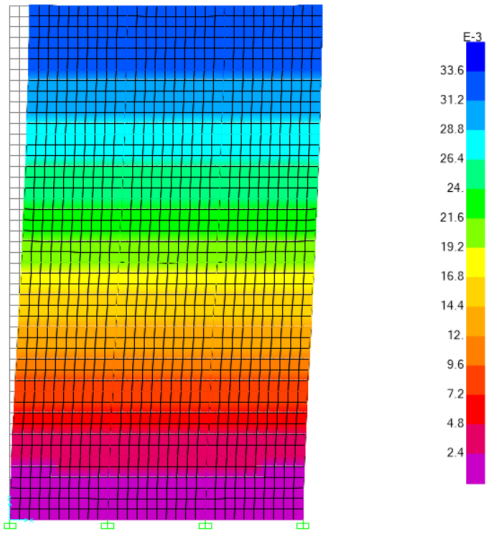

Fig. 4. 14, Model A_{ret_3}, Deformation.

4.1.2.3.2. Interstorey Drift

Checking the Interstorey Drift Limit results, Table 4. 18, from RSA of Model A_{ret_3} assessed for PGA = 0.35g, show less drift values than the limitation of 24.75mm.

However, the IDR graph, outlined in Fig. 4. 15 according to the previous resulting displacements in Table 4. 17, shows that the IDR is about 0.06% at the top storey and a stable peak value of about 0.15 to 16% between 2nd and 4th storey. IDR graph displays a continuous flow to the 4th storey, but retracts harshly after that showing a severe regression from the 6th storey to the top.

Model A_{ret_3}, Interstorey Drift Ratio

Storey	Level	I. D. R. %
8	26.4	0.0576
7	23.1	0.0970
6	19.8	0.1273
5	16.5	0.1364
4	13.2	0.1697
3	9.9	0.1697
2	6.6	0.1515
1	3.3	0.1000

Table 4. 17, Model A_{ret_3}, IDR.

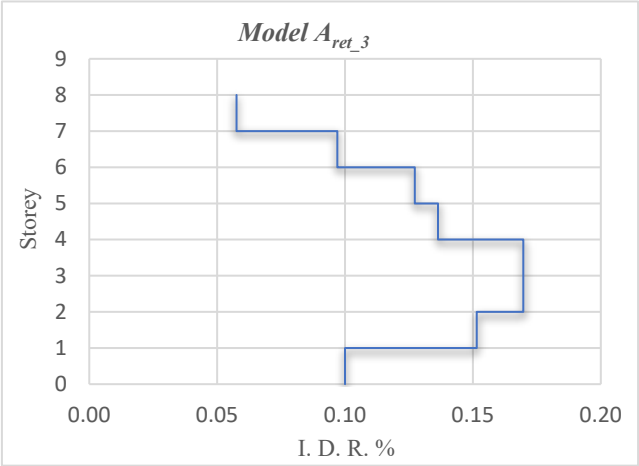

Fig. 4. 15, Model A_{ret_3}, IDR.

Model A_{ret_3}: Interstorey Drift limit Check

storey	Δx	q_d	ν	d_{si}	d_r	d_r*ν	Limit: 24.75
8	33.3	2	0.5	66.6	3.8	1.9	TRUE
7	31.4	2	0.5	62.8	6.4	3.2	TRUE
6	28.2	2	0.5	56.4	8.4	4.2	TRUE
5	24	2	0.5	48.0	9.0	4.5	TRUE
4	19.5	2	0.5	39.0	11.2	5.6	TRUE
3	13.9	2	0.5	27.8	11.2	5.6	TRUE
2	8.3	2	0.5	16.6	10.0	5	TRUE
1	3.3	2	0.5	6.6	6.6	3.3	TRUE

The values of Δx, d_{si}, d_r, and Limit are in mm.

Table 4. 18, Model A_{ret_3}, Interstorey Drift Check.

4.1.2.3.3. Base Reaction

The resulting Base Shear value from RSA in the Model A_{ret_3} assessed for PGA = 0.35g is about 972 kN, Table 4. 19.

Model A_{ret_3}: Base Reaction

F_X	Fz	My
972.52	0.00	15952.98

Values in kN-m.

Table 4. 19, Model A_{ret_3}, Base Reactions.

4.1.2.3.4. Period and Frequency

The max resulting period from RSA in the Model A_{ret_3} assessed for PGA = 0.35g is about 0.7 sec reported in Mode 1, while the Mode 12 gives the max resulting frequency value, about 31 Cyc/sec, Table 4. 20.

Model A_{ret_3}: Modal Periods and Frequencies

Mode	Period	Frequency
1	0.689	1.451
2	0.247	4.053
3	0.150	6.678
4	0.108	9.222
5	0.085	11.770
6	0.074	13.602
7	0.060	16.738
8	0.044	22.921
9	0.044	22.933
10	0.042	23.989
11	0.038	26.383
12	0.033	30.642

Values in sec-Cyc.

Table 4. 20, Model A_{ret_3}, Modal Periods and Frequencies.

4.1.2.4. Model A_{ret_4}

4.1.2.4.1. Lateral Displacement

The resulting displacements of Model A_{ret_4} from RSA can be seen in Table 4. 21, max axial X displacement at the roof of the Model is 2.04 cm under PGA =0.35g. Deformed shape in Fig. 4. 16.

Model A_{ret_4}, Δx

Point	H	Δx
9	3.3	0.0204
8	3.3	0.0179
7	3.3	0.0142
6	3.3	0.0101
5	3.3	0.007
4	3.3	0.0046
3	3.3	0.0027
2	3.3	0.0012
1	3.3	0

Values(m).

Table 4. 21, Model A_{ret_4}, Δx.

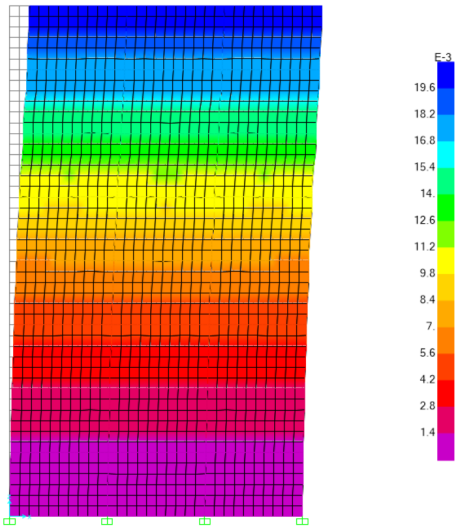

Fig. 4. 16, Model A_{ret_4}, Deformation.

4.1.2.4.2. Interstorey Drift

Checking the Interstorey Drift Limit results from RSA in Table 4. 23, shows less drift than the limitation of 24.75mm in the Model A_{ret_4} assessed for PGA = 0.35g. While the IDR graph, Fig. 4. 17, plotted according to the previous resulting displacements in Table 4. 22, shows that the IDR has a peak at the 6th with about 0.12% and displays continuous flow without abrupt changes until it retracts from the 7th storey to the top to reach a value of 0.07% at the top.

Model A_{ret_4}, Interstorey Drift Ratio

Storey	Level	I. D. R. %
8	26.4	0.0758
7	23.1	0.1121
6	19.8	0.1242
5	16.5	0.0939
4	13.2	0.0727
3	9.9	0.0576
2	6.6	0.0455
1	3.3	0.0364

Table 4. 22, Model A_{ret_4}, IDR.

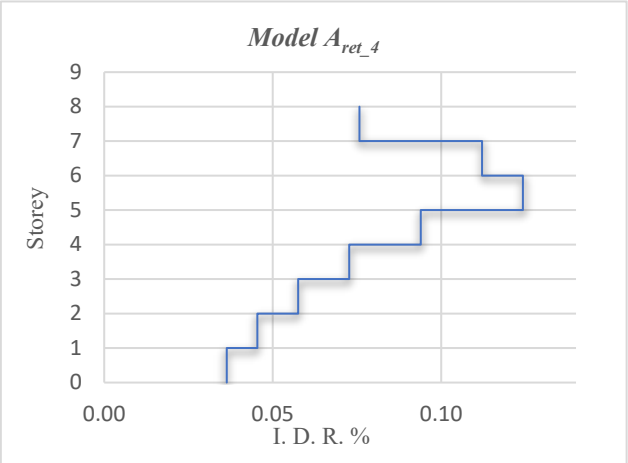

Fig. 4. 17 , Model A_{ret_4}, IDR.

Model A_{ret_4}: Interstorey Drift limit Check

storey	Δx	q_d	ν	d_{si}	d_r	d_r*ν	Limit: 24.75
8	20.4	2	0.5	40.8	5.0	2.5	TRUE
7	17.9	2	0.5	35.8	7.4	3.7	TRUE
6	14.2	2	0.5	28.4	8.2	4.1	TRUE
5	10.1	2	0.5	20.2	6.2	3.1	TRUE
4	7	2	0.5	14.0	4.8	2.4	TRUE
3	4.6	2	0.5	9.2	3.8	1.9	TRUE
2	2.7	2	0.5	5.4	3.0	1.5	TRUE
1	1.2	2	0.5	2.4	2.4	1.2	TRUE

The values of Δx, dsi, dr, and Limit are in mm.

Table 4. 23, Model A_{ret_4}, Interstorey Drift Check.

4.1.2.4.3. Base Reaction

The resulting Base Shear value from RSA in the Model A_{ret_4} assessed for PGA = 0.35g is about 1700 kN, Table 4. 24.

Model A_{ret_4}: Base Reaction

F_X	Fz	My
1700.68	0.00	30519.55

Values in kN-m.

Table 4. 24, Model A_{ret_4}, Base Reactions.

4.1.2.4.4. Period and Frequency

The max resulting period from RSA in the Model A_{ret_4} assessed for PGA = 0.35g is about 0.35 sec reported in Mode 1, while the Mode 12 gives the max resulting frequency value, about 24 Cyc/sec, Table 4. 25.

Model A_{ret_4}: Modal Periods and Frequencies

Mode	Period	Frequency
1	0.349	2.863
2	0.148	6.771
3	0.095	10.479
4	0.072	13.922
5	0.064	15.664
6	0.061	16.276
7	0.060	16.682
8	0.058	17.302
9	0.048	20.946
10	0.044	22.695
11	0.043	23.142
12	0.042	23.691

Values in sec-Cyc.

Table 4. 25, Model A_{ret_3}, Modal Periods and Frequencies.

4.1.2.4. Model A_{ret}, (P-M) Interaction Curve

For the seismic performance of a column, the impact of axial force on capacity is essential in terms of strength and ductility. The P-M Interaction Curve of the Model A_{ret} assessed for PGA= 0.35g represents the possible failure combination for the columns bent around the axis x. The capacity of a PM combination must be checked by generating a failure surface results from a compressive Concrete failure analysis for columns and the PM Demands combination (resulting from the RSA) on the same line emitting from the center of a coordinate system. Table 4. 26 shows the effectivity of A_{ret} Models in keeping the seismic Demands within the columns' according to every Storey.

Comparisn , Model A_{ret} effectivity in P-M interaction Curve.

Storey	A_{ret_1}	A_{ret_2}	A_{ret_3}	A_{ret_4}
1	+	+	+	+
2	++	++	++	++
3	++	++	++	++
4	++	+	+	+
5	+	++	++	+
6	+	++	++	-
7	++	++	++	-
8	++	++	++	-

(++)= Non Exceedance, (+)= Exceedance, (-)= Failure

Table 4. 26, Model A_{ret} Effectivity in P-M interaction Curve.

The columns in the 1st Storey are showing a ductile performance and some of the P-M Demand points are exceeding the Capacity Curve in the all A_{ret} Models . Fig. 4. 18.

Fig. 4. 19 and Fig. 4. 20 are presenting the columns in the 2nd and 3rd Storey, respectively. The columns performe ductile against the PGA 0.35g. and there is a non-exceedance of the nominal column's strength. That can be seen in the A_{ret} Models.

The 4th Storey's columns are showing a high ductile performance relevant to the Frame A_{ret_1}, and no exceeding the Capacity Curve. But, the columns in Models A_{ret_2}, A_{ret_3}, and A_{ret_4} are exceeding with some P-M Demands points the Capacity Curve, which presenting a certin ductile level. Fig. 4. 21.

In the 5th and 6th Storey, the columns in Models A_{ret_2} and A_{ret_3} orm ductile against the PGA 0.35g. and there is a non-exceedance of the nominal column's strength. The Model A_{ret_1} columns are exceeding the nominal column's strength with some P-M Demands points to the Capacity Curve, which presents a certain ductile level. Meantime, the columns of Models A_{ret_1}, A_{ret_2}, A_{ret_3} in the 7th and 8th Storey show a flexible performance, and some of the P-M Demand points exceed the Capacity Curve same as the 2nd and 3rd Storey. Fig. 4. 22 and Fig. 4. 23.

On the other hand, a failure in the 6th, 7th, and 8th Storey columns relative to the Model A_{ret_4}, Fig. 4. 23 and Fig. 4. 24, respectively.

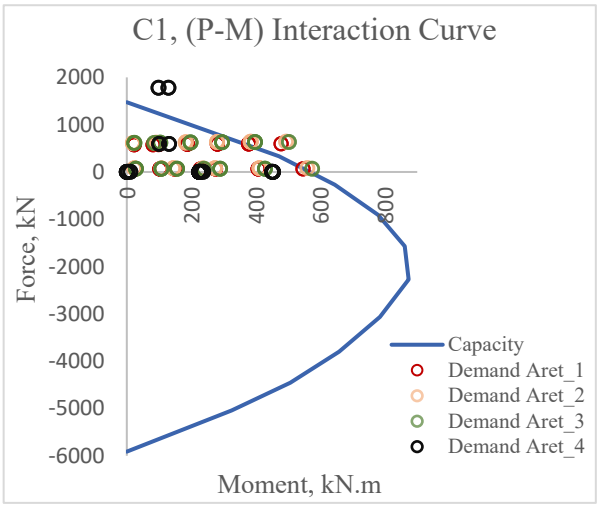

Fig. 4. 18, Model A_{ret}, (P-M) Interaction Curve, C1.

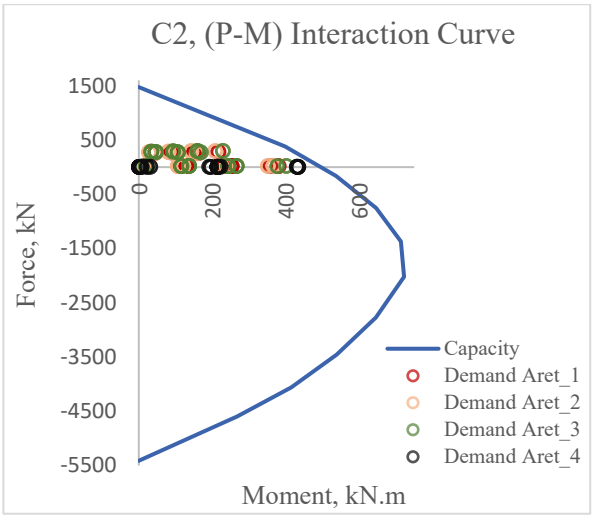

Fig. 4. 19, Model A_{ret}, (P-M) Interaction Curve, C2.

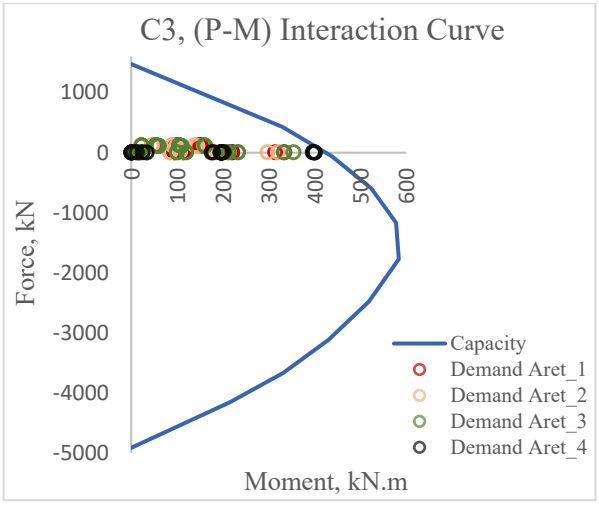

Fig. 4. 20, Model A_{ret}, (P-M) Interaction Curve, C3.

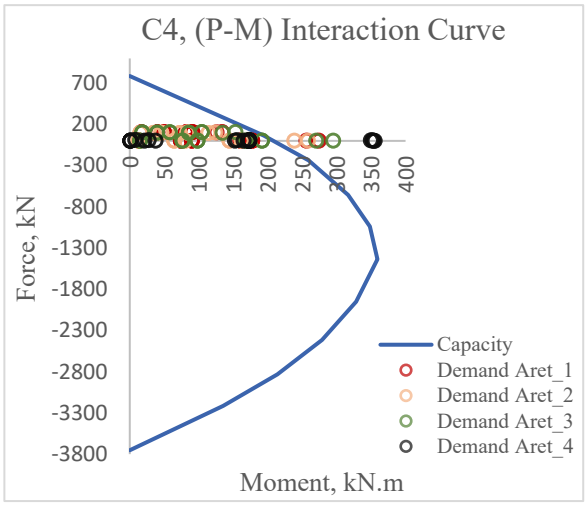

Fig. 4. 21, Model A_{ret}, (P-M) Interaction Curve, C4.

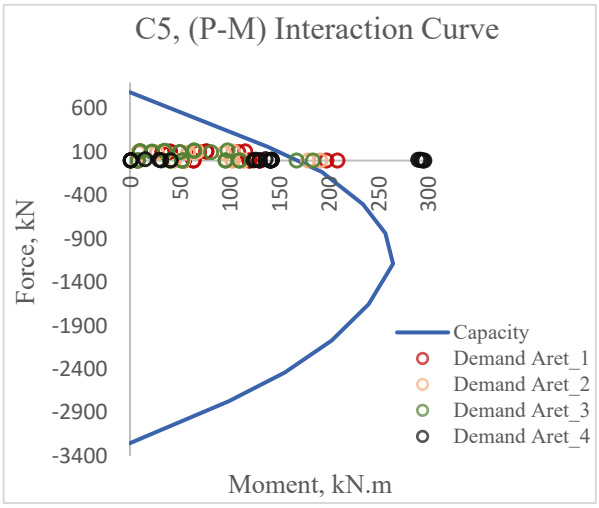

Fig. 4. 22, Model A_{ret}, (P-M) Interaction Curve, C5.

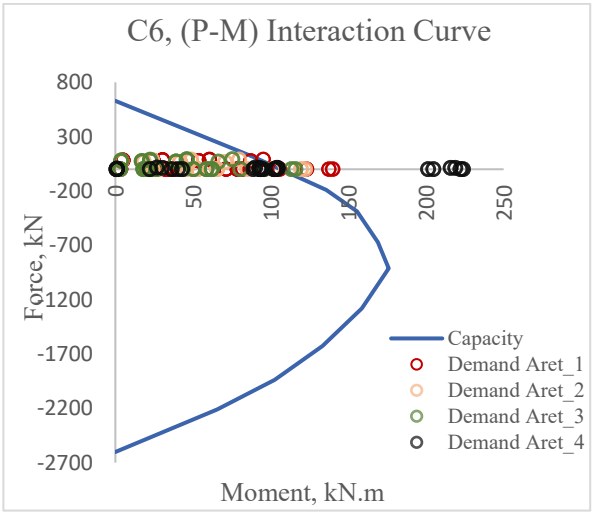

Fig. 4. 23, Model A_{ret}, (P-M) Interaction Curve, C6.

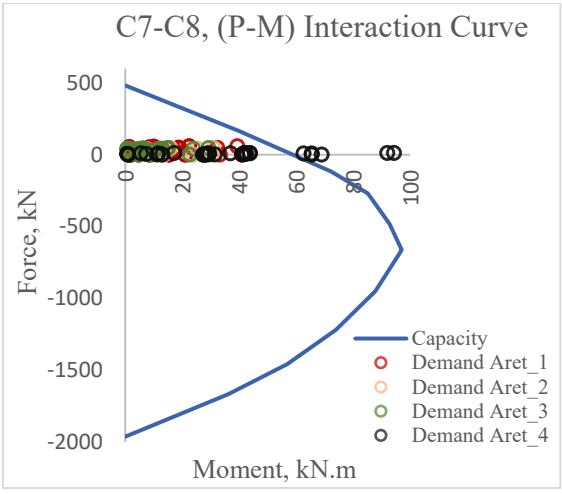

Fig. 4. 24, Model A_{ret}, (P-M) Interaction Curve, C7. C8.

4.1.3. Model B

4.1.3.1. Lateral Displacement

The resulting displacements of Model B from RSA can be seen in Table 4. 27, max axial X displacement at the roof of the Model is 6,55 cm under PGA = 0.35g. Deformed shape in Fig. 4. 25.

Model B, Δx

Point	H	Δx
9	3.3	0.0655
8	3.3	0.0553
7	3.3	0.0454
6	3.3	0.0355
5	3.3	0.0258
4	3.3	0.0172
3	3.3	0.0096
2	3.3	0.0031
1	3.3	0

Values(m).

Table 4. 27, Model B, Δx.

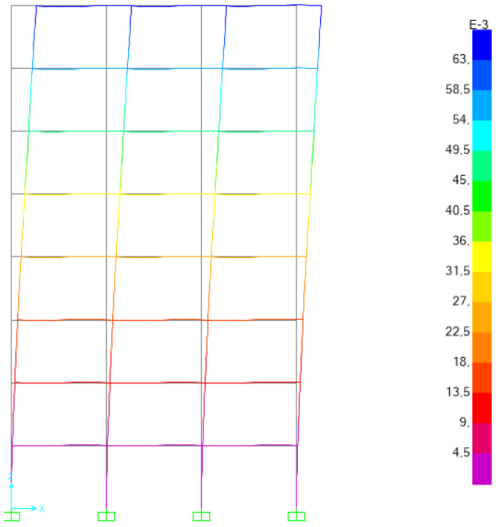

Fig. 4. 25, Model B, Deformation.

4.1.3.2. Interstorey Drift

Checking the Interstorey Drift Limit results from RSA in Table 4. 29, shows less drift than the limitation of 24.75mm in the Model A_0 assessed for PGA = 0.15g. While the IDR graph, Fig. 4. 26, computed according to the previous resulting displacements in Table 4. 28, shows that the IDR has a peak at the top storey with about 0.14%, and a stable value of about 0.1% along with the 3rd, 4th, and the 5th storeys. IDR graph displays continuous flow without abrupt changes.

Model B, Interstorey drift Ratio

Storey	Level	I. D. R. %
8	26.4	0.3091
7	23.1	0.3000
6	19.8	0.3000
5	16.5	0.2939
4	13.2	0.2606
3	9.9	0.2303
2	6.6	0.1969
1	3.3	0.0939

Table 4. 28, Model B, IDR.

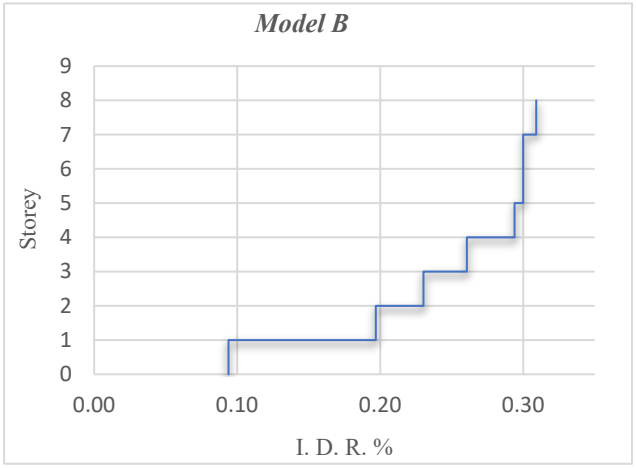

Fig. 4. 26, Model B, IDR..

Model A_0: Interstorey Drift limit Check

storey	Δx	q_d	ν	d_{si}	d_r	d_r*ν	Limit: 24.75
8	65.5	2	0.5	131.0	20.4	10.2	TRUE
7	55.3	2	0.5	110.6	19.8	9.9	TRUE
6	45.4	2	0.5	90.8	19.8	9.9	TRUE
5	35.5	2	0.5	71.0	19.4	9.7	TRUE
4	25.8	2	0.5	51.6	17.2	8.6	TRUE
3	17.2	2	0.5	34.4	15.2	7.6	TRUE
2	9.6	2	0.5	19.2	13.0	6.5	TRUE
1	3.1	2	0.5	6.2	6.2	3.1	TRUE

The values of Δx, d_{si}, d_r, and Limit are in mm.

Table 4. 29, Model B, Interstorey Drift Check.

4.1.3.3. Base Reaction

The resulting Base Shear value from RSA in the Model A_{ret_4} assessed for PGA = 0.35g is about 535.14 kN, Table 4. 30.

Model B: Base Reaction

F_X	F_Z	M_Y
535.14	0.00	7887.73

Values in kN-m.

Table 4. 30, Model B, Base Reactions.

4.1.3.4. Period and Frequency

The max resulting period from RSA in the Model B assessed for PGA = 0.35g is about 1.2 sec reported in Mode 1, while the Mode 12 gives the max resulting frequency value, about 21 Cyc/sec, Table 4. 31.

Model B: Modal Periods and Frequencies

Mode	Period	Frequency
1	1.21	0.83
2	0.47	2.11
3	0.28	3.57
4	0.18	5.48
5	0.13	7.82
6	0.10	9.69
7	0.10	10.17
8	0.09	10.70
9	0.08	12.81
10	0.08	12.83
11	0.07	15.20
12	0.05	21.13

Values in sec-Cyc.

Table 4. 31, Model B, Modal Periods and Frequencies.

4.1.3.5. (P-M) interaction curve

For the seismic performance of a column, the impact of axial force on capacity is essential in terms of strength and ductility. The P-M Interaction Curve of the Model B assessed for PGA= 0.35g represents the possible failure combination for the columns bent around the axis x. The capacity of a PM combination must be checked by generating a failure surface results from a compressive Concrete failure analysis for columns and the PM Demands combination (resulting from the RSA) on the same line emitting from the center of a coordinate system, Fig. 4. 27 to Fig. 4. 33.

Because of the nonexistence of Demands interaction points outside the Capacity Curve, therefore, no exceeding the nominal column's strength, and no failure in any column, exactly a complete ductile performance for the PGA 0.35g.

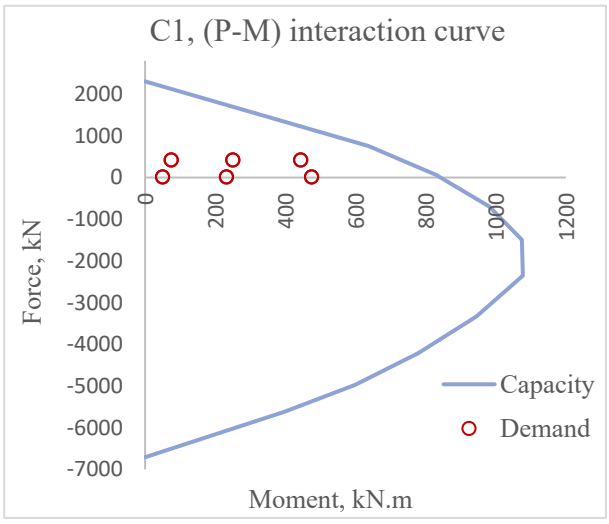

Fig. 4. 27, Model B, (P-M) interaction curve, C1.

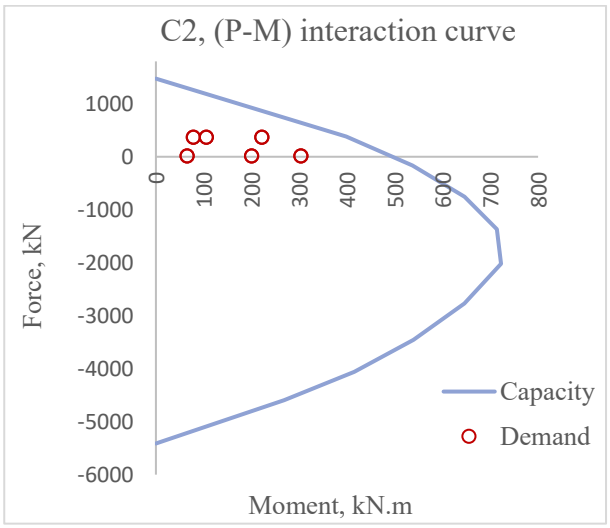

Fig. 4. 28, Model B, (P-M) interaction curve, C2.

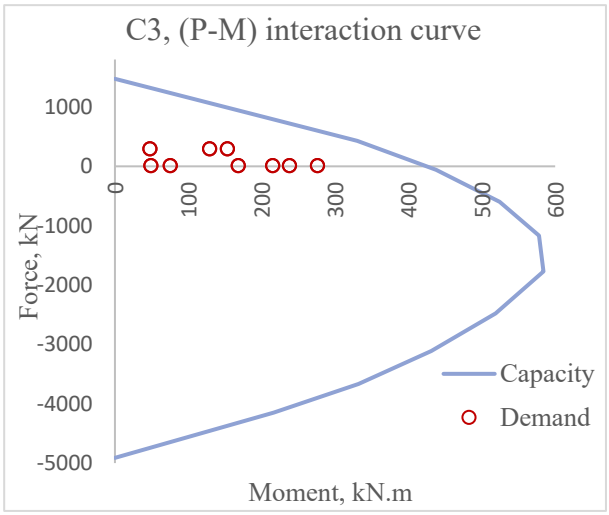

Fig. 4. 29, Model B, (P-M) interaction curve, C3.

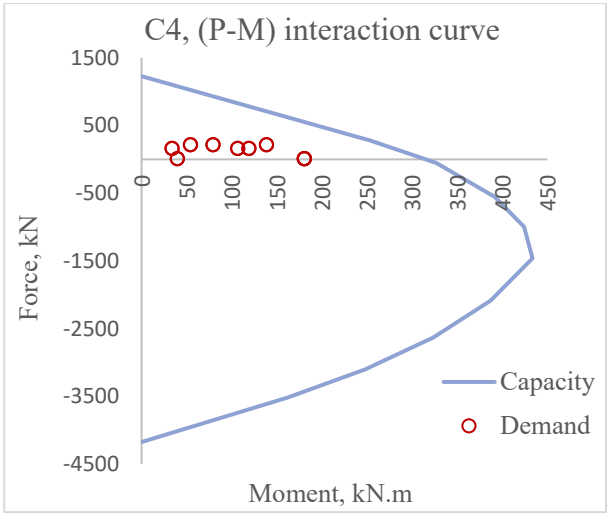

Fig. 4. 30, Model B, (P-M) interaction curve, C4.

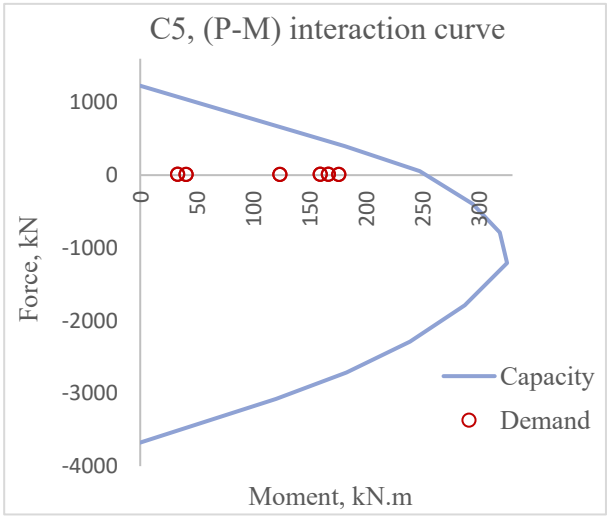

Fig. 4. 31, Model B, (P-M) interaction curve, C5.

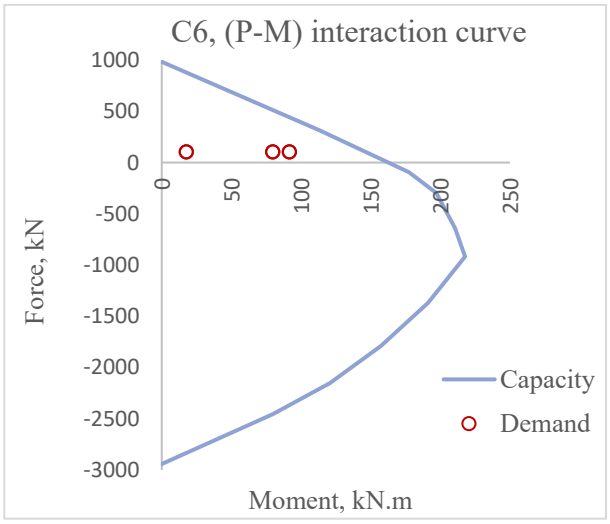

Fig. 4. 32, Model B, (P-M) interaction curve, C6.

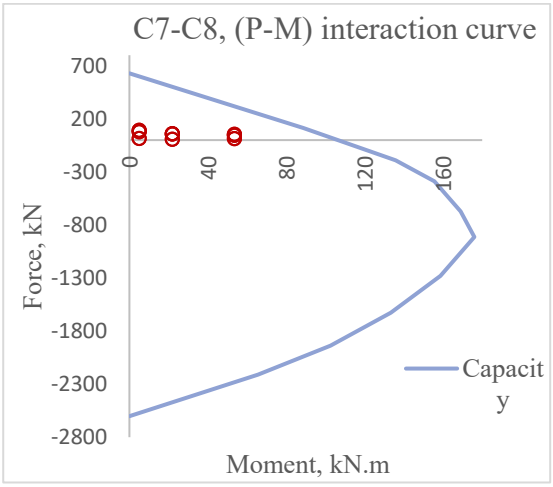

Fig. 4. 33, Model B, (P-M) interaction curve, C7. C8.

4.1.4. RSA Comparison

Assessment of CLT Panels as a retrofitting solution described in CHAPTER 3 in four suggestions: Models A_{ret_1}, A_{ret_2}, A_{ret_3}, and A_{ret_4}. Deformation, IDR, Base Reaction, Modal Period and Frequency, and The P-M interaction curve. The RSA Data of the suggested retrofitting solutions is compared with the RSA results of the reference Model B.

4.1.4.1. Lateral Displacement

RSA results demonstrate that the CLT panels, as a retrofitting solution, provide an effective contribution regarding the Lateral Displacement, reducing the values compared to with Model B displacement values; as Table 4. 33 shows, A_{ret_4} reduces the Δx value by about 69% with 2,04cm on the top. The suggested solutions presented by Models A_{ret_1}, A_{ret_2}, and A_{ret_3} contribute with 45%, 50%, and 49%, respectively, to max Δx value reduction. As displayed in Table 4. 32 and Fig. 4. 34, The Models A_{ret_1}, A_{ret_2}, and A_{ret_3} take part with convergent displacement values on the roof point, 3.6cm, 3.24, and 3.33cm, respectively.

Comparison, Deformation Δx

Storey	A_0	*B*	A_{ret_1}	A_{ret_2}	A_{ret_3}	A_{ret_4}
8	2.69	6.55	3.59	3.24	3.33	2.04
7	2.23	5.53	3.31	3.03	3.14	1.79
6	1.81	4.54	2.88	2.68	2.82	1.42
5	1.44	3.55	2.36	2.24	2.4	1.01
4	1.1	2.58	1.85	1.78	1.95	0.7
3	0.76	1.72	1.32	1.28	1.39	0.46
2	0.42	0.96	0.79	0.78	0.83	0.27
1	0.14	0.31	0.29	0.29	0.3	0.12

Values (cm)

Table 4. 32, Comparison, Lateral Displacement.

Comparison, Lateral Displacement.

Storey	A_{ret_1}	A_{ret_2}	A_{ret_3}	A_{ret_4}
8	- 45.19	- 50.53	- 49.16	- 68.85

Values (%).

Table 4. 33, Comparison, Lateral Displacement, Variations.

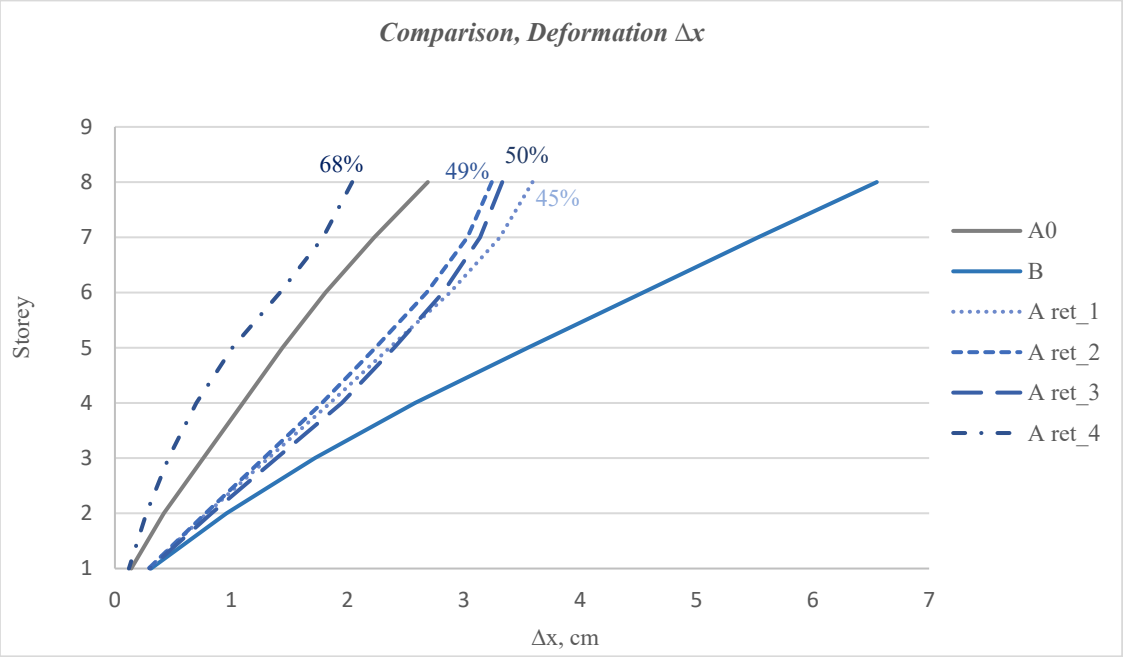

Fig. 4. 34, Comparison, Lateral Displacement vs. Storey.

4.1.4.2. Interstorey Drift

Checking the RSA results of Interstorey Drift Limit under PGA = 0.35g for retrofitting by CLT Panels in the four suggested solutions fulfill the limitation of EC8 with values under 24.75mm.

In terms of IDR values got from RSA, Fig. 4. 35, the solutions presented in Models A_{ret_1}, A_{ret_2}, and A_{ret_3} show a swayed flow, retracting at the 5th Storey and a severe regression after the 6th Storey to the end. IDR varies over the height of the three Models with less ductile performance and a severe regression on the upper Storeys. Highest IDR values are

0.08%, 0.06%, and 0.06% in A_{ret_1}, A_{ret_2}, and A_{ret_3}, respectively, as shown in Table 4. 34.

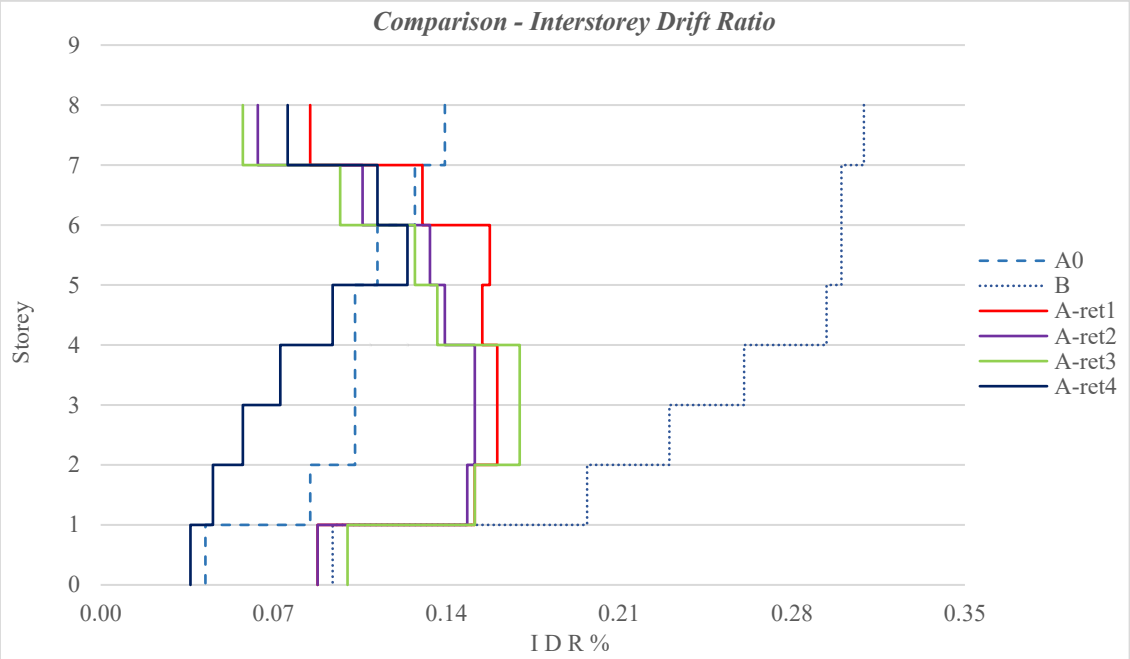

Fig. 4. 35, Comparison, IDR.

The three suggested solutions contribute by an average of 42% to 58%, decreasing the IDR value on top storeys in comparison with Reference B. at the same time, the three Solutions contribute to increasing the peak IDR value by an average of 7% to 14%, contrasted to Reference B, Table 4. 35, referring to less ductile performance.

Comparison, IDR

Solution	*Top Value*	*Peak Value*	*Retraction starting*
A_{ret_1}	0.08	0.16 between 3rd and 6th Storey	at the 5th Storey
A_{ret_2}	0.06	0.15 between 3rd and 4th Storey	at the 5th Storey
A_{ret_3}	0.06	0.16 between 2rd and 4th Storey	at the 5th Storey
A_{ret_4}	0.07	0.12 6th Storey	at the 7th Storey
Reference			
B	0.14	0.14 on top Storey	Non

Values (%).

Table 4. 34, Comparison, IDR.

However, the solution displayed in Model A_{ret_4}, offers a less flexible Frame with IDR of 0.07% on top storey, Table 4. 34. The IDR graph, in Fig. 4. 35, retracts severely after the 6th storey. Meanwhile, it shows a ductile flow from the 1st to 6th Storey. Compared to Reference B, the flexible performance decreases along with the contribution percentage in IDR, reaching the half top storey value, and about 14% of Peak value compared to Reference B, Table 4. 35.

Comparison, IDR

Value	*Aret_1*	*Aret_2*	*Aret_3*	*Aret_4*
On top	-42.86	-57.14	-57.14	-50.00
Peak	+14.29	+7.14	+14.29	-14.29

Values (%).

Table 4. 35, Comparison, IDR Variations.

4.1.4.3. Base Reaction

Regarding Base Reaction, Fig. 4. 36, RSA results show approximately double the value of Model B for the three suggested solutions A_{ret_1}, A_{ret_2}, and A_{ret_3}. However, it is over three times in Model A_{ret_4} relating to both shear and moment. CLT Panels increase the Base Shear by about 42%, 48%, 45%, and 68%, in the four suggested solution respectively.

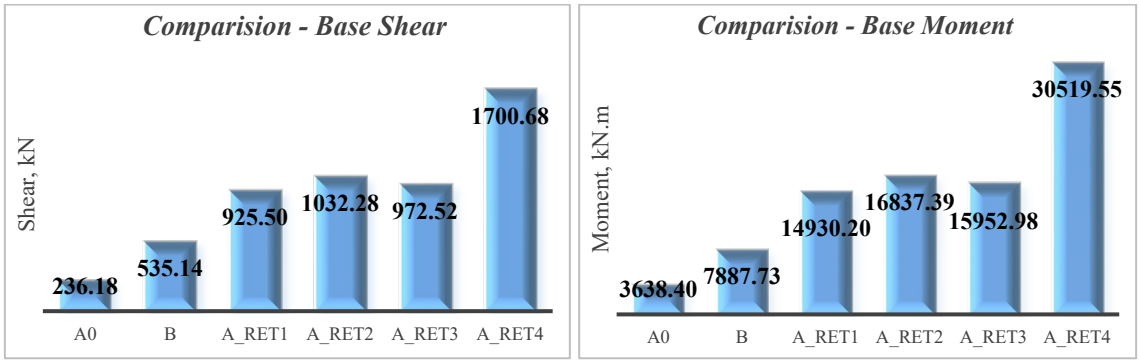

Values (kN-M).

Fig. 4. 36, Comparison, Base Reaction.

Notwithstanding, the base reactions values increase with a reduction of up to less than half the Displacement value compared to Reference B throughout every storey in the suggested Solutions presented in the Models A_{ret_1}, A_{ret_2}, and A_{ret_3}. While the Displacement values achieve minimal levels and correspond to max values in base reactions in the suggested Solution presented in the Model A_{ret_4}, Fig. 4. 37.

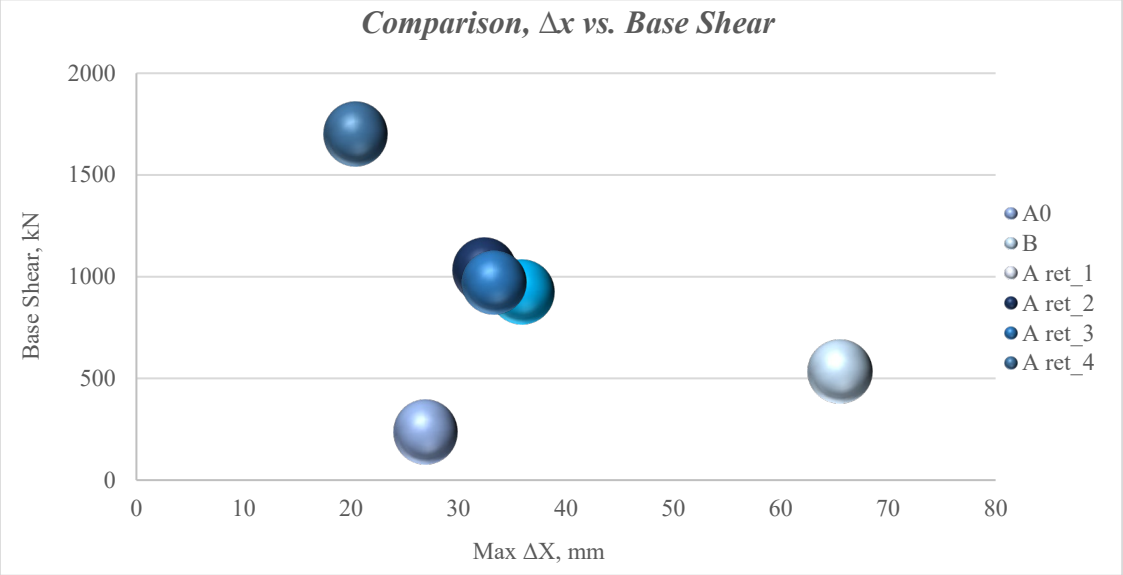

Fig. 4. 37, Comparison, Base Shear vs. Max Roof Lateral Displacement.

CLT Panels increase the Base Shear by about 73%, 93%, 82%, and 218%. While in terms of the Self Weight, the increase is by 26%, 48%, 45%, and 68% in the four suggested Solutions A_{ret_1}, A_{ret_2}, A_{ret_3}, and A_{ret_4}, respectively.

CLT panels affect base Shear value by max about 48% increase when the connection is CLT-Beam and about 68% increase when the connection is CLT-column, Table 4. 36

Comparison, Self Weight, Base Shear

Model	*B*	A_{ret_1}	A_{ret_2}	A_{ret_3}	A_{ret_4}
Self Weight	846.20	1064.87	1167.16	1116.01	1064.87
Change Ratio		+25.84	+37.93	+31.88	+25.84
Base Shear	535.14	925.50	1032.28	972.52	1700.68
Change Ratio		+72.95	+92.90	+81.73	+217.80

Values (kN-%).

Table 4. 36,Comparison, Self Weight & Base Reaction Variations..

4.1.4.4. Period and Frequency

RSA results show that the CLT panels, as a retrofitting solution, in terms of Modal Period contribute to decreasing the first Modal Period over 40% compared to Referance B in the suggested Solutions A_{ret_1}, A_{ret_2}, and A_{ret_3}. Maximum reduction in the first Modal Period was observed the fourth presented solution A_{ret_4} by about 70%, Table 4. 37.

Fig. 4. 38 shows the changes in the Modal Period over 12 Modes. The suggested Solutions A_{ret_1}, A_{ret_2}, and A_{ret_3} show a convergent flow with a decrease of 40% compared to Reference B. On the contrary, the suggested Solution A_{ret_4} provides a short Modal Period from the beginning, flows, to an extent, in harmony with the other after the 5th Mode.

Comparison, Period

Model	*B*	*A_{ret_1}*	*A_{ret_2}*	*A_{ret_3}*	*A_{ret_4}*
Mode 1	1.21	0.71	0.65	0.69	0.35
Change Ratio		-41.32	-46.28	-42.98	-71.07
Mode 12	0.05	0.03	0.03	0.03	0.042
Change Ratio		-40	-40	-40	-16

Values (sec-%).

Table 4. 37, Comparison, Modal Period, Variations..

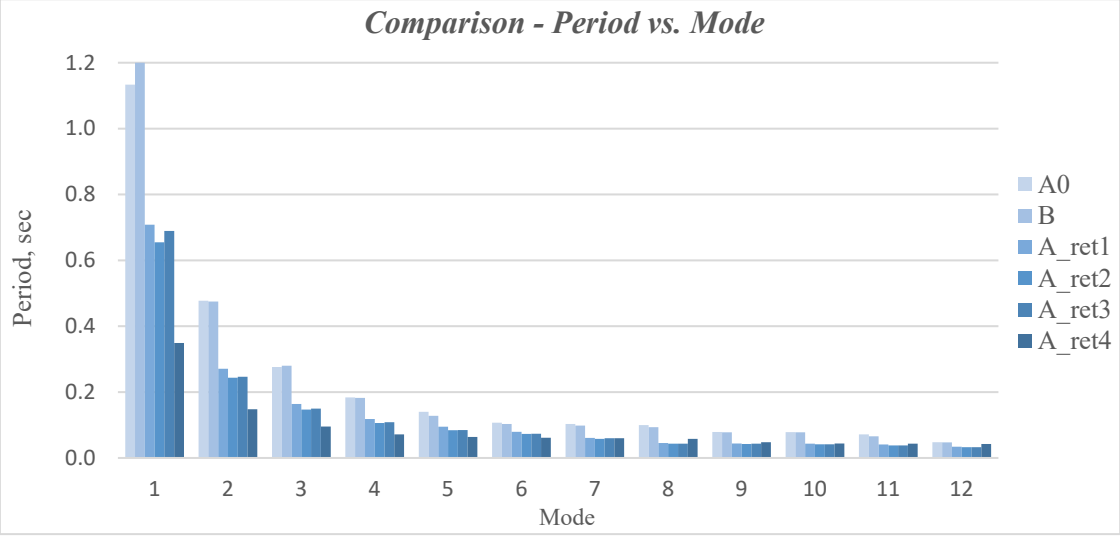

Fig. 4. 38, Comparison, Modal Period.

Regarding Modal Frequency, CLT panels increase the first Modal Frequency up to 84% compared to Reference B in the suggested Solutions A_{ret_1}, A_{ret_2}, and A_{ret_3}. The maximum rise in the first Modal Frequency was observed in the fourth presented Solution A_{ret_4} by about 144%, Table 4. 38.

The variations in the Modal Frequency over 12 modes displayed in Fig. 4. 39, presents a convergent flow with a increase of 45% compared to Reference B in the suggested Solutions A_{ret_1}, A_{ret_2}, and A_{ret_3}. On the contrary, the suggested Solution A_{ret_4} provides a first Modal Frequency with 2.86 Hz to reach nearly the Reference b value in the 12th mode.

Comparison, Frequency

Model	*B*	*A_{ret_1}*	*A_{ret_2}*	*A_{ret_3}*	*A_{ret_4}*
Mode 1	0.83	1.41	1.53	1.45	2.86
Change Ratio		+69.88	+84.34	+74.70	+144.58
Mode 12	21.13	29.17	30.74	30.64	23.69
Change Ratio		+38.05	+45.48	+45.01	+12.12

Values (Cyc/sec-%).

Table 4. 38, Comparison, Modal Frequency, Variations.

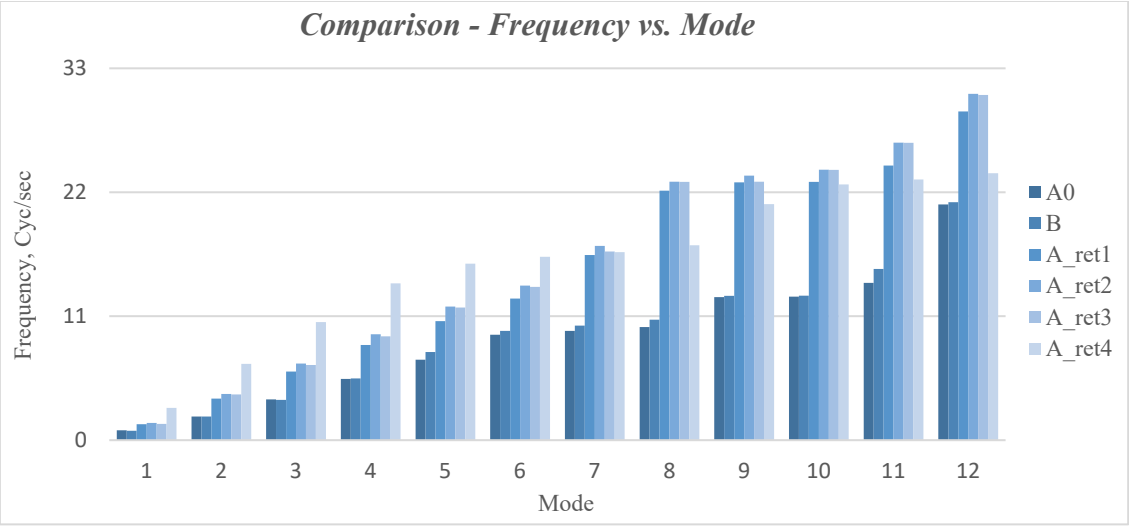

Fig. 4. 39, Comparison, Modal Frequency.

CLT panels technique shortens the period considerably compared to Reference B because the CLT panels system maximizes the overall stiffness of the suggested solutions Model, which results in a rise in the frequency of vibration and minimizing the period, as displayed in Fig. 4. 40.

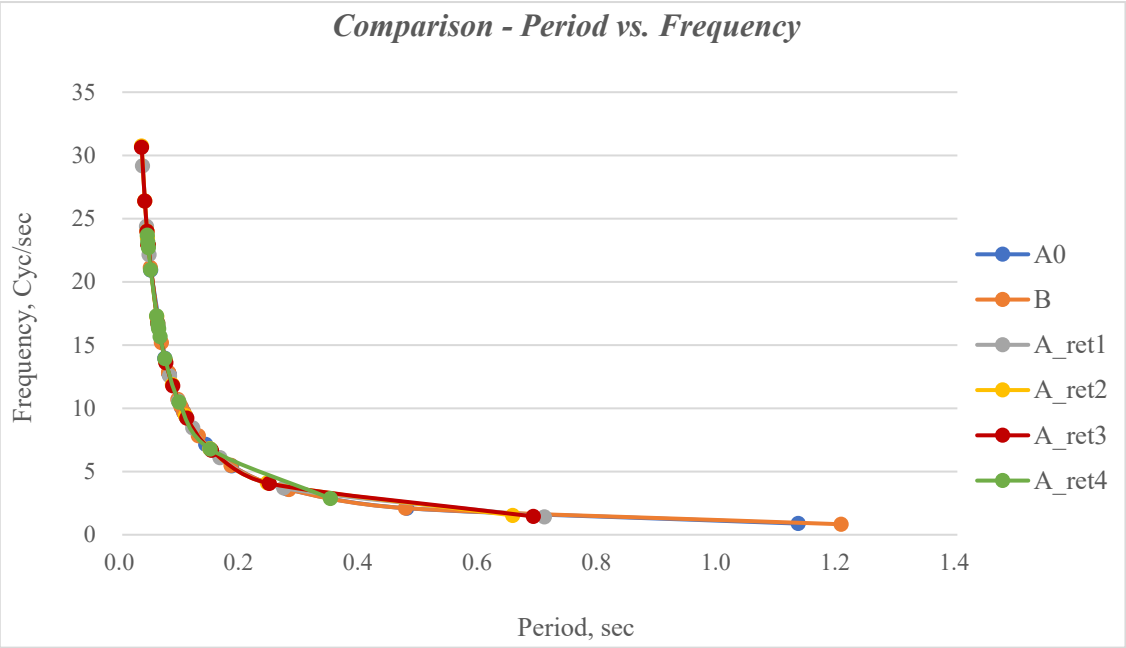

Fig. 4. 40, Comparison, Modal Period and Frequency.

4.1.4.5. (P-M) interaction curve

RSA results show CLT panels, as a retrofitting solution, regarding the suggested Solutions in Models A_{ret_1}, A_{ret_2} and A_{ret_3}, contribute effectively in keeping the seismic Demands within the Columns' capacity, as displayed in Fig. 4. 41to Fig. 4. 47. Compared to Reference B and the up-mentioned Solutions, the seismic Demands of columns (6), (7), and (8) exceed the columns' capacity, which may lead to failure, as shown in Fig. 4. 46 and Fig. 4. 47.

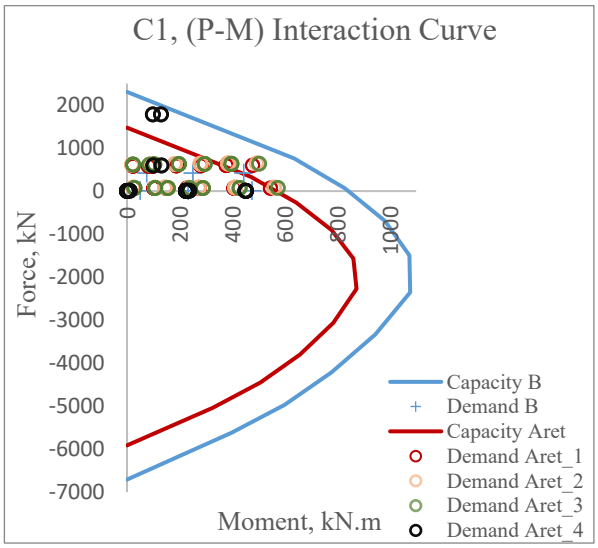

Fig. 4. 41, Comparison, (P-M) Interaction Curve, C1.

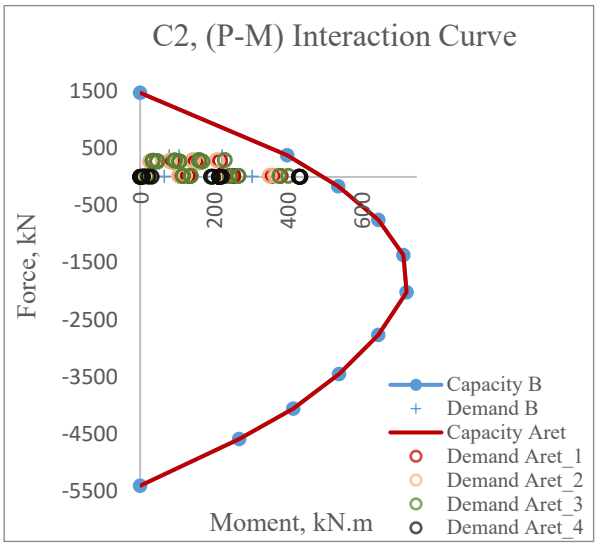

Fig. 4. 42, Comparison, (P-M) Interaction Curve, C2.

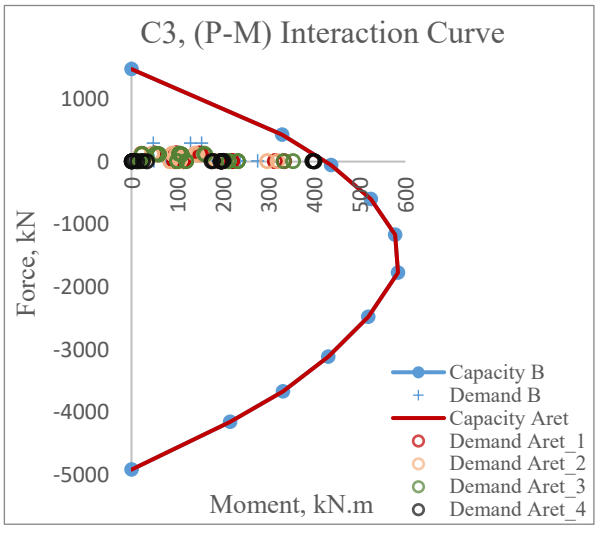

Fig. 4. 43, Comparison, (P-M) Interaction Curve, C3.

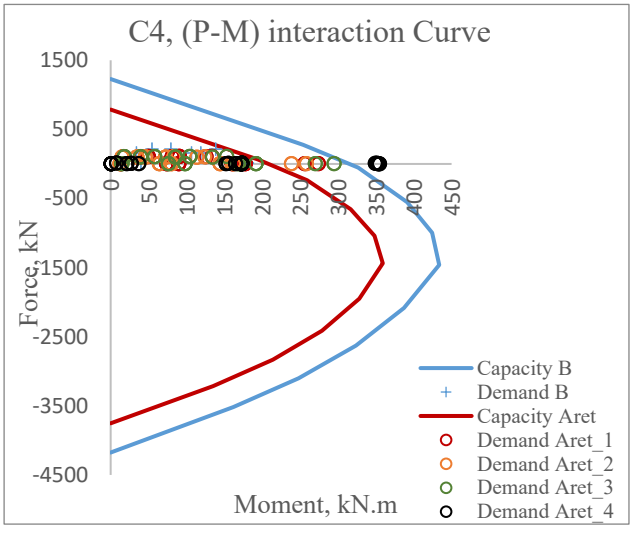

Fig. 4. 44, Comparison, (P-M) Interaction Curve, C4.

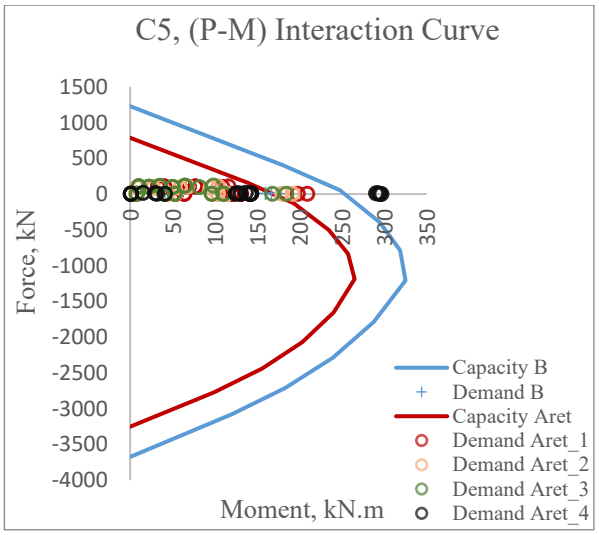

Fig. 4. 45, Comparison, (P-M) Interaction Curve, C5.

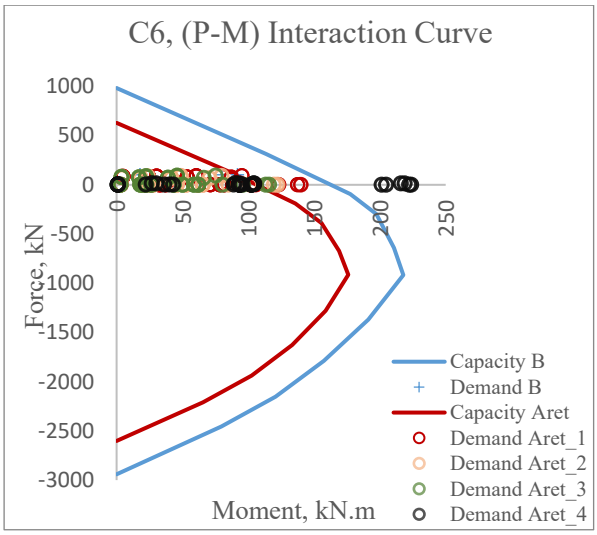

Fig. 4. 46, Comparison, (P-M) Interaction Curve, C6.

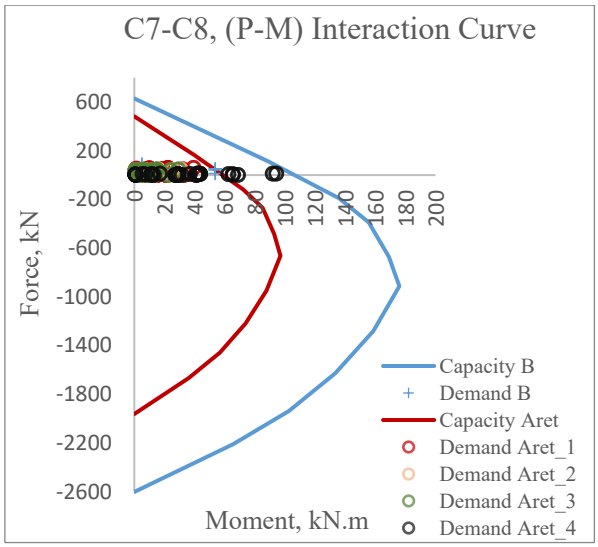

Fig. 4. 47, Comparison, (P-M) Interaction Curve, C7. C8.

The seismic Demands after retrofitting by CLT panels, in Models A_{ret_2} and A_{ret_3}, significantly satisfy the columns' capacity compared to the suggested Solution A_{ret_1} as presented in Table 4. 39. While the suggested solution in Model A_{ret_4} can not prevent the failure in Columns (6), (7), and (8), all in comparison with Reference B.

Comparisn , P-M interaction Curve.

Columns	*B*	A_{ret_1}	A_{ret_2}	A_{ret_3}	A_{ret_4}
1	++	+	+	+	+
2	++	++	++	++	++
3	++	++	++	++	++
4	++	+	+	+	+
5	++	+	++	++	+
6	++	+	++	++	-
7	++	++	++	++	-
8	++	++	++	++	-

(++)= Non Exceedance, (+)= Exceedance, (-)= Failure.

Table 4. 39, Comparison, (P-M) Interaction Curve.

4.2. POA Results

In this section, the POA is carried out using the SAP2000. A two-dimensional Model is being tested for the suggested retrofitted building A_{ret} and the Reference B. Beams and columns are already modeled as nonlinear frame elements at the start and the end of the element. CLT Panels' nonlinear behavior is already considered. The FEMA rule, built-in SAP2000 with the IO, LS, and CP limit states for plastic hinges, has been used for the acceptance criteria. The POA is executed separately for the five Models and is achieved using CSM.

The resulting original graphs in APPENDIX B.

4.2.1. Model A_{ret_1}

4.2.1.1. Capacity Curve

The max Roof Displacement reaches the value of 30.2cm with Base Shear value of 3473 kN as shown in Fig. 4. 48.

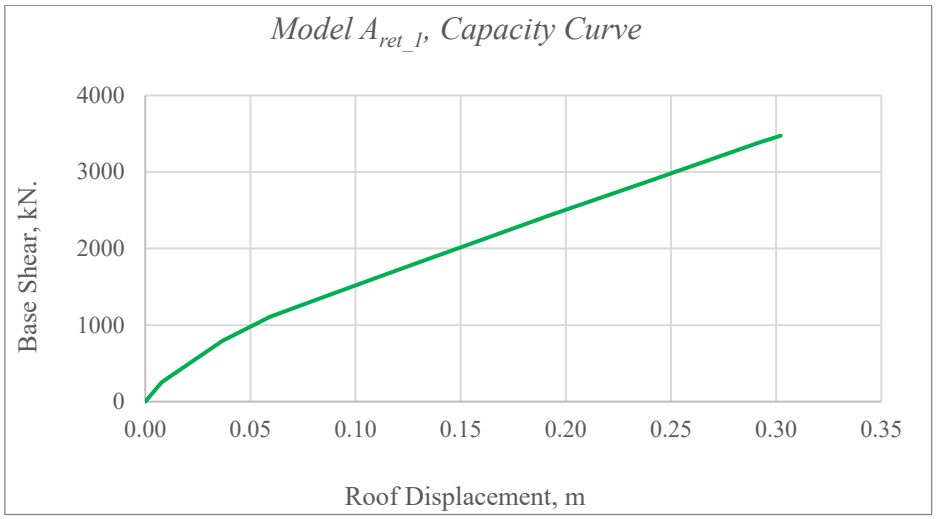

Fig. 4. 48, Model A_{ret_1}, Capacity Curve.

4.2.1.2. CSM

The Performance Point corresponds to an expected Roof Displacement value of 4.6 cm and Base Shear value of 926 kN on time of 0.82 sec, as illustrated in Fig. 4. 49 and Table 4. 40.

Model A_{ret_1}, Performance Point

Parameter	Base Shear	Expected Displacement	T
Value	926	0.046	0.82

Value, kN, m, sec.

Table 4. 40, Model A_{ret_1}, Performance Point.

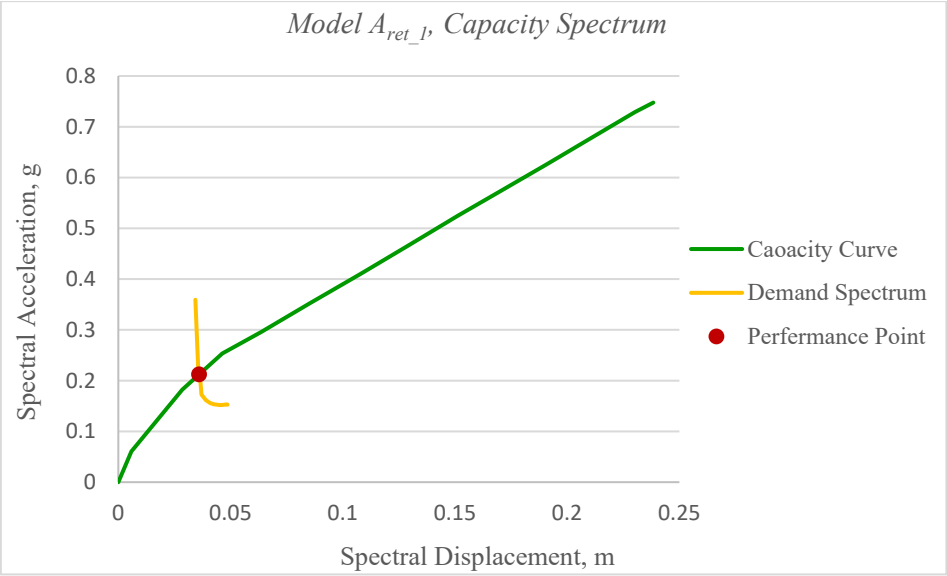

Fig. 4. 49, Model A_{ret_1}, Capacity Spectrum.

At every deformation step of the POA, determine plastic hinge location in the elements and hinges reach the FEMA limit state, IO, LS, and CP using colors for identification as Fig. 4. 50 shows. At the performance point intersection time, plastic hinges form near the elements' ends as considered in the modelling. Thus, the testing Model is adequate because the damage to the structure is still limited considering the structural elements' yielding occurs between B to IO States.

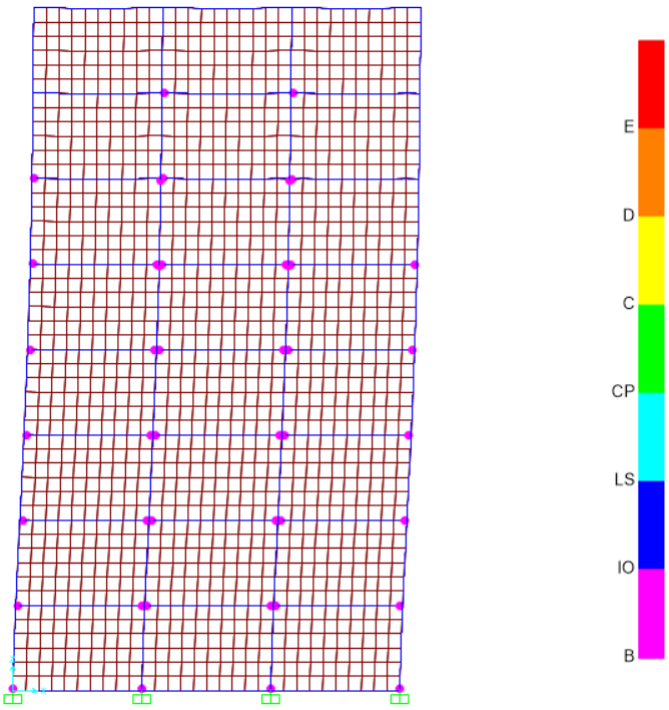

Fig. 4. 50, Model A_{ret_1}, Deformed Shape at the Performance Point step.

4.2.2. Model A_{ret_2}

4.2.2.1. Capacity Curve

The max Roof Displacement reaches the value of 26.35cm with Base Shear value of 4596.3 kN as shown in Fig. 4. 51.

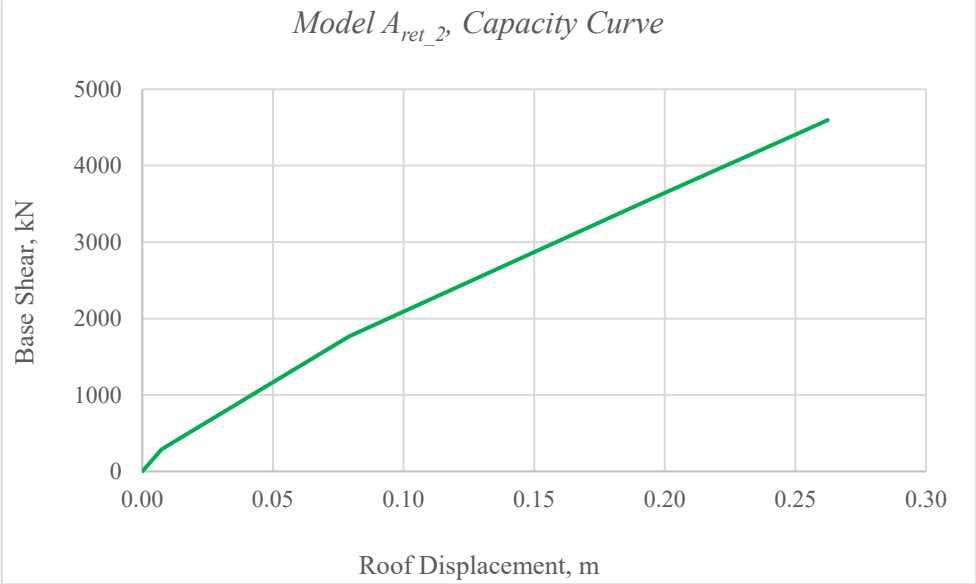

Fig. 4. 51, Model A_{ret_2}, Capacity Curve.

4.2.2.2. CSM

The Performance Point corresponds to to an expected Roof Displacement value of 4.6 cm and Base Shear value of 1079 kN on time of 0.7 sec, as Table 4. 41 and Fig. 4. 52 illustrate.

Model A_{ret_2}, Performance Point

Parameter	Base Shear	Expected Displacement	T
Value	1079	0.046	0.7

Value, kN, m, sec.

Table 4. 41, Model A_{ret_2}, Performance Point.

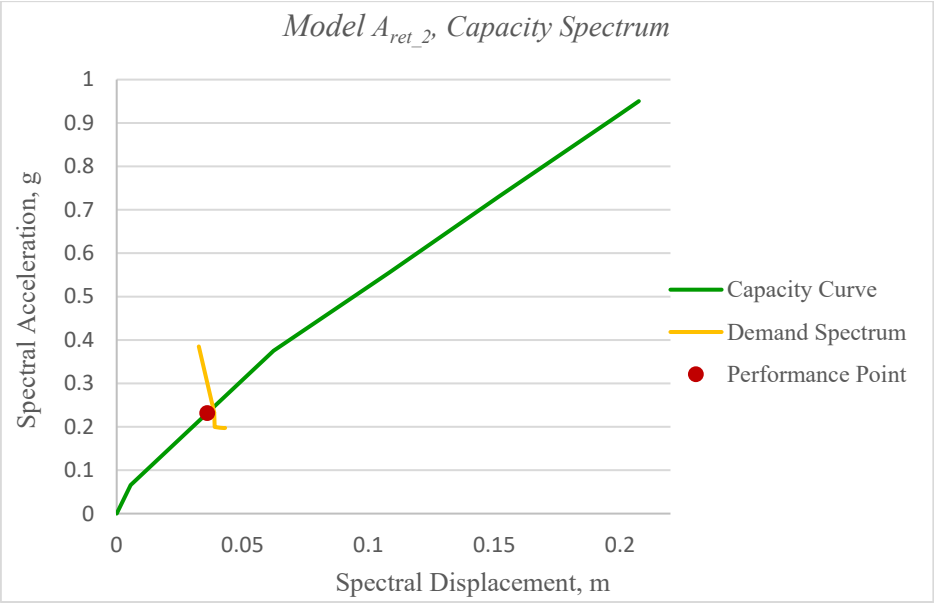

Fig. 4. 52, Model A_{ret_2}, Capacity Spectrum.

At every deformation step of the POA, determine plastic hinge location in the elements and hinges reach the FEMA limit state, IO, LS, and CP using colors for identification as Fig. 4. 53 shows. At the performance point intersection time, plastic hinges form near the elements' ends as considered in the modelling. The damage to the structure is still limited considering the structural elements' yielding occurs between B to IO; Pointing to the most hinges, except the columns' hinges, at the base, that exceed to reach LS State. Thus, the testing Model is satisfactory.

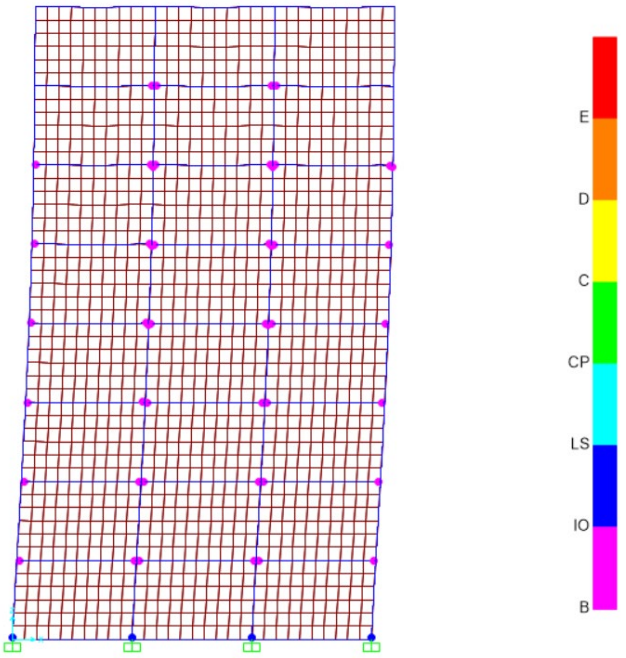

Fig. 4. 53, Model A_{ret_2}, Deformed Shape at the Performance Point step.

4.2.3. Model A_{ret_3}

4.2.3.1. Capacity Curve

The max Roof Displacement reaches the value of 19.15cm with Base Shear value of 2579.77 kN as shown in Fig. 4. 54.

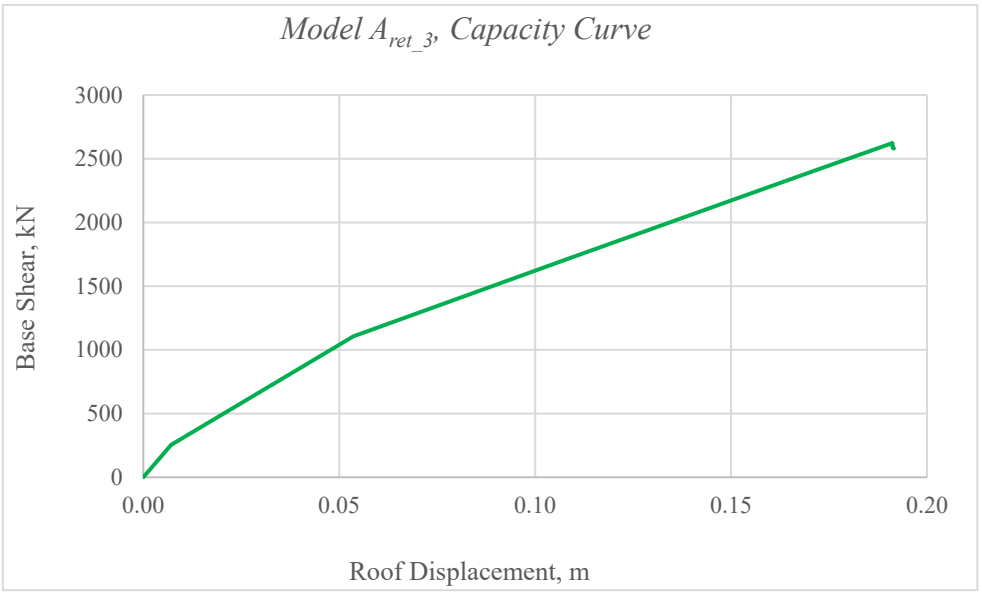

Fig. 4. 54, Model A_{ret_3}, Capacity Curve.

4.2.3.2. CSM

The Performance Point corresponds to to an expected Roof Displacement value of 4.7 cm, and Base Shear value of 985.5 kN on time of 0.8 sec, as shown in Fig. 4. 53 and Table 4. 42.

Model A_{ret_3}, Performance Point

Parameter	Base Shear	Expected Displacement	T
Value	985.5	0.047	0.813

Value, kN, m, sec.

Table 4. 42, Model A_{ret_3}, Performance Point.

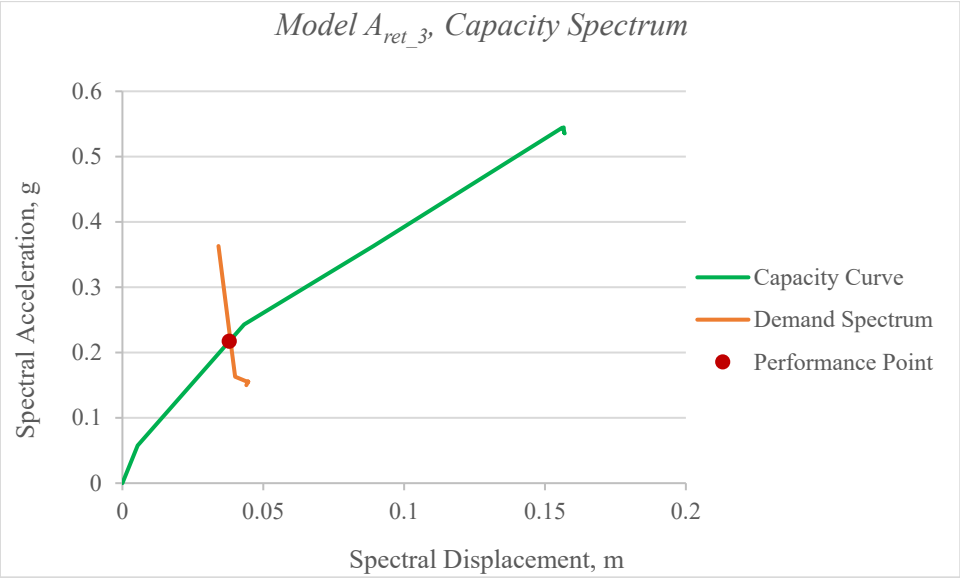

Fig. 4. 55, Model A_{ret_3}, Capacity Spectrum.

At every deformation step of the POA, determine plastic hinge location in the elements and hinges reach the FEMA limit state, IO, LS, and CP using colors for identification as Fig. 4. 56 displays. At the performance point intersection time, plastic hinges form near the elements' ends as considered in the modelling. Thus, the testing Model is adequate because the damage to the structure is still limited considering the structural elements' yielding occurs between B to IO State.

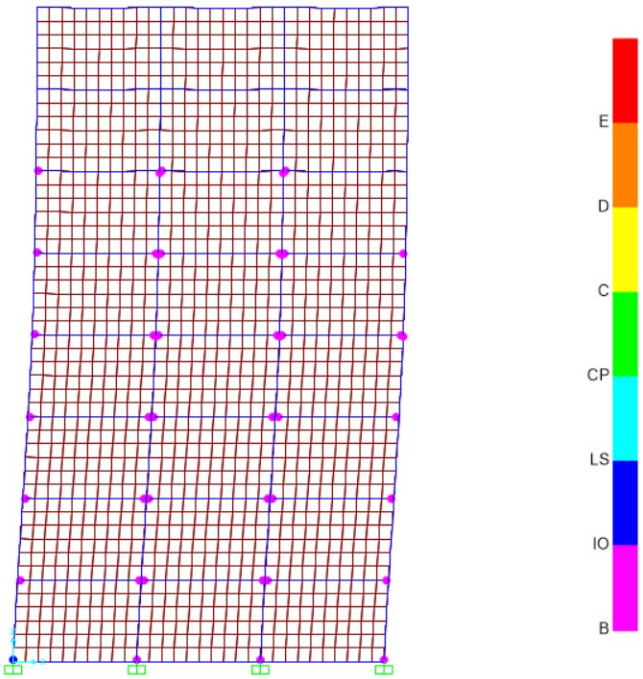

Fig. 4. 56, Model A_{ret_3}, Deformed Shape at the Performance Point step.

4.2.4. Model A_{ret_4}

4.2.4.1. Capacity Curve

The max Roof Displacement reaches the value of 4.5 cm with Base Shear value of 5625.8 kN as shown in Fig. 4. 57.

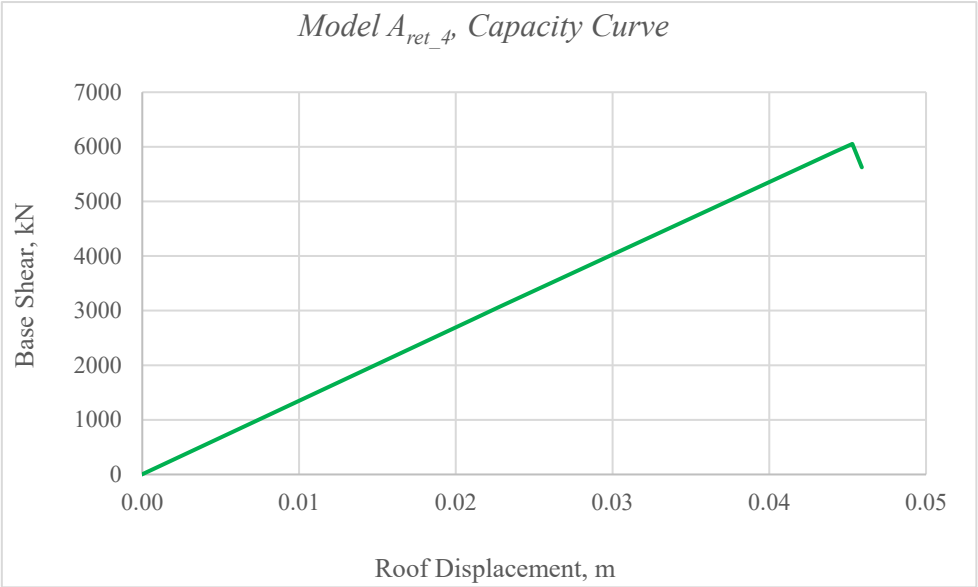

Fig. 4. 57, Model A_{ret_4}, Capacity Curve.

4.2.4.2. CSM

The Performance Point corresponds to to an expected Roof Displacement value of 2.4 cm, and Base Shear value of 3168 kN on time of 0.29 sec, as in Table 4. 43 and Fig. 4. 58.

Model A_{ret_4}, Performance Point

Parameter	Base Shear	Expected Displacement	T
Value	3168	0.024	0.285

Value, kN, m, sec.

Table 4. 43, Model A_{ret_4}, Performance Point.

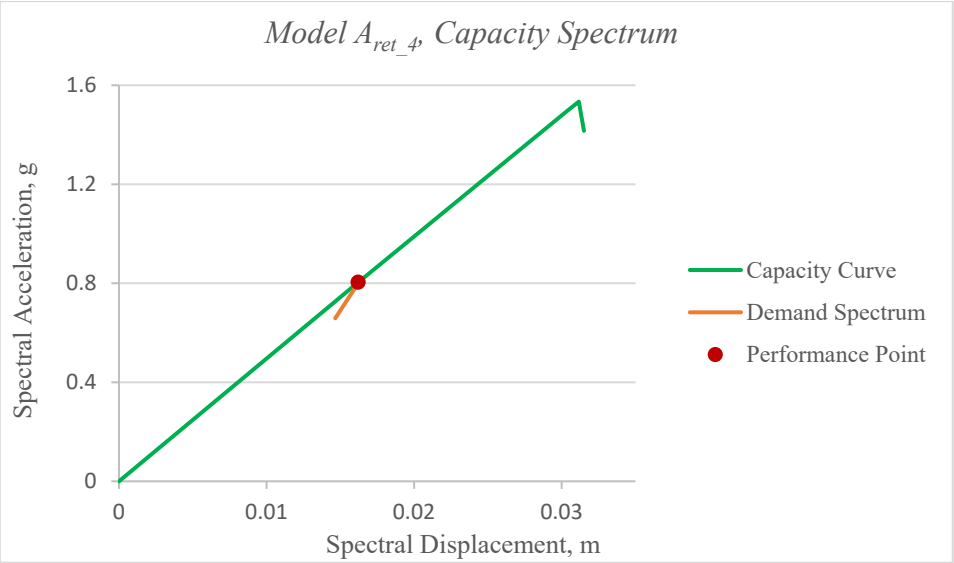

Fig. 4. 58, Model A_{ret_4}, Capacity Spectrum.

At every deformation step of the POA, determine plastic hinge location in the elements and hinges reach the FEMA limit state, IO, LS, and CP using colors for identification as Fig. 4. 59 shows. Regarding the performance point intersection time, a few plastic hinges form near the elements' ends as considered in the modelling and not exceed the IO State. Therefore, the testing Model is adequate.

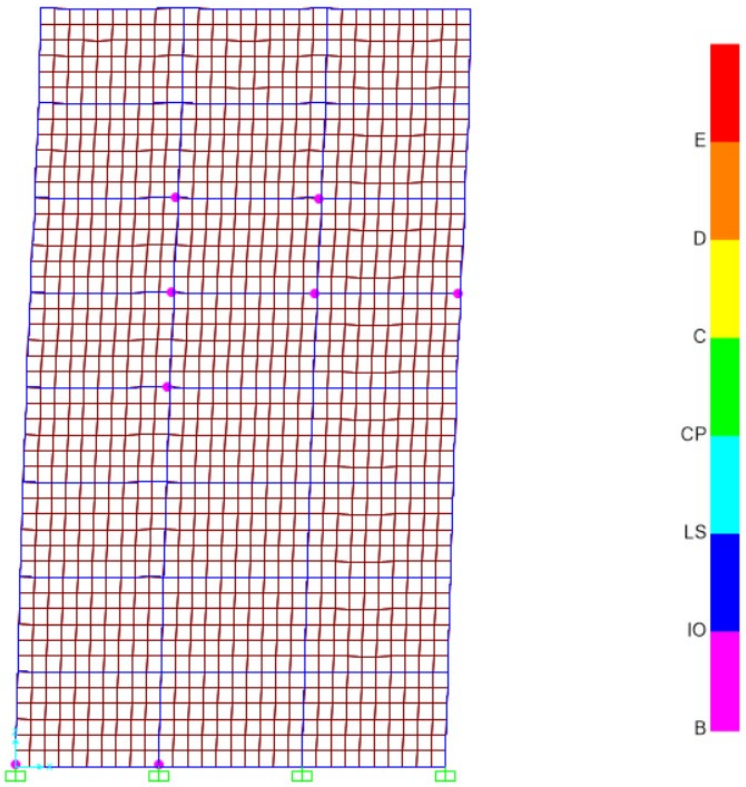

Fig. 4. 59, Model A_{ret_4}, Deformed Shape at the Performance Point step.

4.2.5. Model B

4.2.5.1. Capacity Curve

The max Roof Displacement reaches the value of 42.7 cm with Base Shear value of 350.5 kN as shown in Fig. 4. 60.

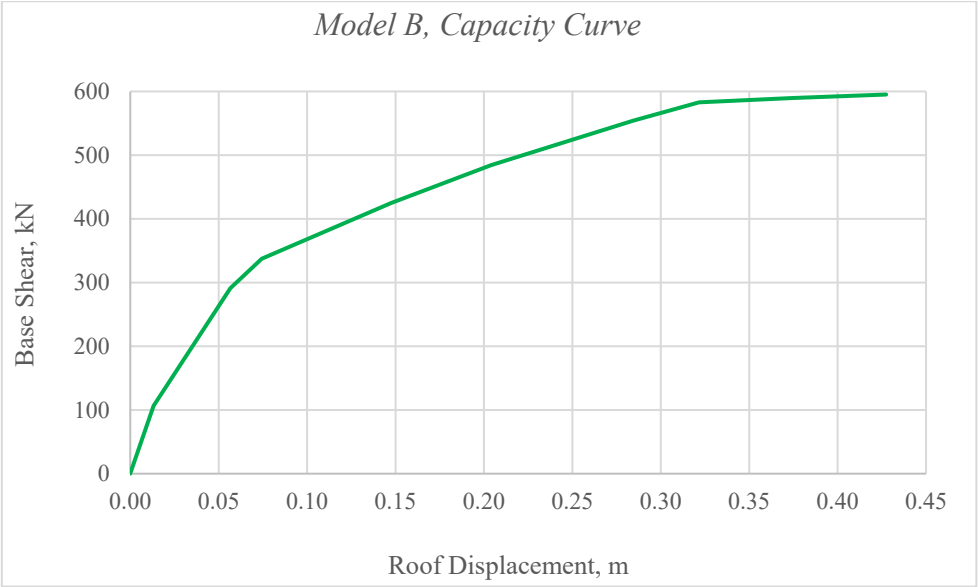

Fig. 4. 60, Model B, Capacity Curve.

4.2.5.2. CSM

The Performance Point corresponds to to an expected Roof Displacement value of 8.5 cm, and Base Shear value of 350.6 kN on time of 1.5 sec as displayed in Fig. 4. 61 and Table 4. 44.

Model B, Performance Point

Parameter	Base Shear	Expected Displacement	T
Value	350.5	0.085	1.525

Value, kN, m, sec.

Table 4. 44, Model B, Performance Point.

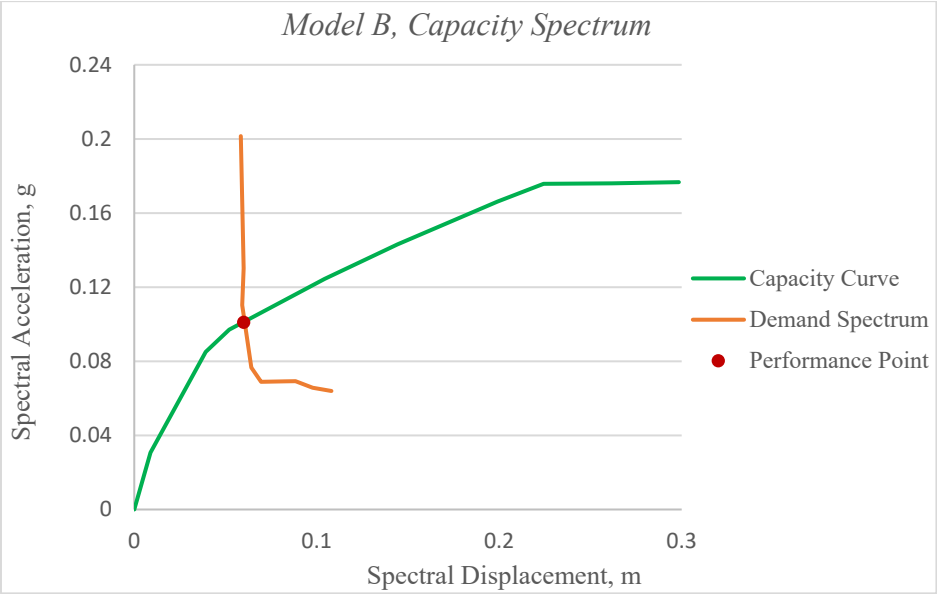

Fig. 4. 61, Model B, Capacity Spectrum.

At every deformation step of the POA, determine plastic hinge location in the elements and hinges reach the FEMA limit state, IO, LS, and CP using colors for identification as Fig. 4. 62 demonstrates. Regarding the performance point intersection time, plastic hinges form near the elements' ends as considered in the modelling and not exceed the IO State. Thus, the testing Model is satisfactory.

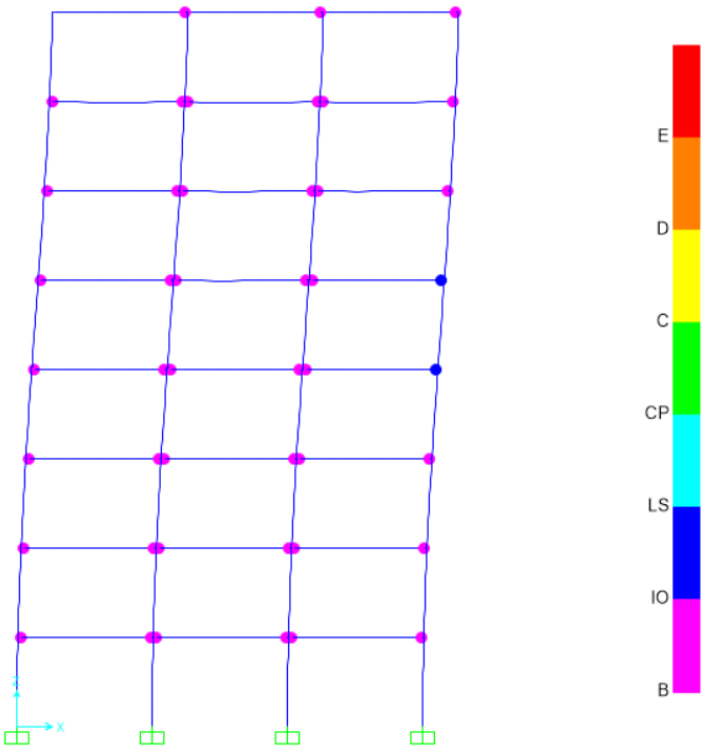

Fig. 4. 62, Model B, Deformed Shape at the Performance Point step..

4.2.6. POA Comparison

4.2.6.1. Capacity Curve

Capacity Curves of the testing Models are presented in Fig. 4. 63. These curves represent the models' behavior with stiffness and ductility. The structural elements may be yielded continuously. At every step, the model experiences loss in stiffness. Therefore, the slope of the Capacity Curve is decreasing.

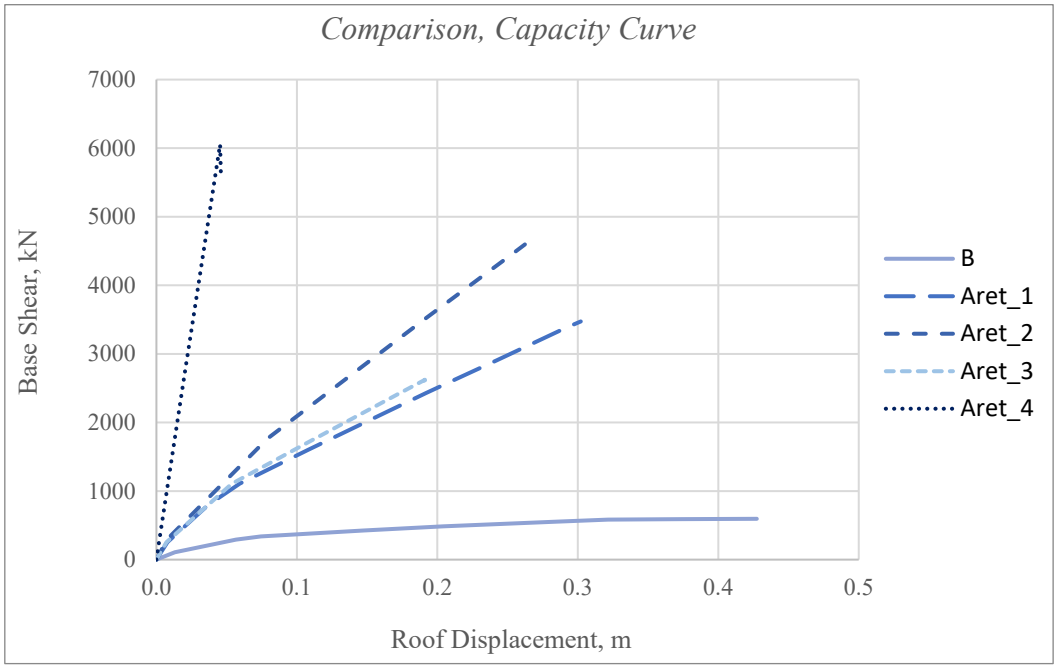

Fig. 4. 63, Comparison, Capacity Curve.

In comparison with the Reference B Model results, the Capacity Curves show that the Model A_{ret_4} has the highest stiffness, the highest max Base Shear value of 5625.8 kN, and the minimum max Roof displacement value of 4.5 cm. While, the resulting values of the Models A_{ret_1}, A_{ret_2}, and A_{ret_3}, provide a decrease in the max roof Displacement value ranging from 29% to 55%, corresponding to an increase in Basse shear value reach to 672%, as shown in Table 4. 45.

Comparison, Capacity Curve

Model	Base Shear	%	Max Roof Displacement	%
A_{ret_1}	3473	+483.6	30.2	-29.3
A_{ret_2}	4596.28	+672.3	26.35	-38.3
A_{ret_3}	2579.77	+333.5	19.15	-55.2
A_{ret_4}	5625.8	+845.3	4.5	-89.5
B	595.13		42.7	

Value, kN, cm, %.

Table 4. 45, Comparision, Capacity Curve.

4.2.6.2. CSM

As Fig. 4. 64 reveals, comparing the Model A_{ret_4} to the Reference B Model, the Model A_{ret_4} provided highest Performance Point. While, the Models A_{ret_1}, A_{ret_2}, and A_{ret_3}, display Performance Points in close proximity to each other.

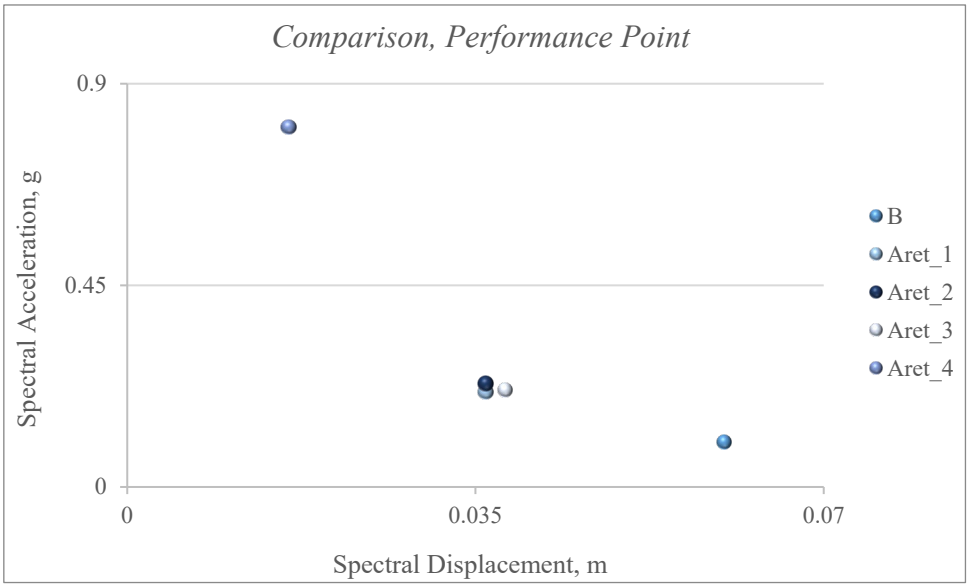

Fig. 4. 64, Comparison, Performance Points.

Compared to the Reference B Model, the Percentage of reducing the effective time and the Max Roof Displacement of the Mode A_{ret_4} Performance Point records the highest values, consequently, the most increased stiffness. Regarding the Models A_{ret_1}, A_{ret_2},

and A_{ret_3}, The reduction proportion is around 45 % and 50 %, respectively, in terms of the expected Roof Displacement and the effective time values as shown in Table 4. 46.

Comparison, Performance Points

Model	Base Shear	%	Expected Displacement	%	T	%
A_{ret_1}	926	+164.2	4.6	-45.9	0.8	-46.7
A_{ret_2}	1079	+207.8	4.6	-45.9	0.7	-53.3
A_{ret_3}	985.5	+181.2	4.7	-44.7	0.8	-46.7
A_{ret_4}	3168	+803.9	2.4	-71.8	0.3	-80.0
B	350.5		8.5		1.5	

Value, kN, cm, sec, %.

Table 4. 46, Comparision, Performance Points.

Comparison of Fig. 4. 50, Fig. 4. 53, Fig. 4. 56, Fig. 4. 59, and Fig. 4. 62, reveals no significant variations in the hinging patterns at the Performance Point state among the suggested Solutions retrofitted by CLT panels, A_{ret_1}, A_{ret_2}, A_{ret_3}, and the Reference B. The hinge locations are consistent. The formation of hinges is not exceeding the IO State, Table 4. 47. In the case of the Model A_{ret_2}, it propagates to LS State in the columns' hinges at the 1st Storey base level. The damage to the structure is still limited; thus, the Models are satisfactory.

Comparison, Damage State

Model	B to IO	IO to LS	Ls to CP
A_{ret_1}			-
A_{ret_2}			-
A_{ret_3}			-
A_{ret_4}			-
B			-

Table 4. 47, Comparison, Damage State.

CHAPTER 5

5.1. Conclusion

This thesis introduced an advanced method of seismic design of concrete structures. Retrofitting solutions of an existing reinforced concrete building by CLT panels have been proposed and analyzed. The four suggested retrofitting solutions vary by CLT panels thickness and the connector locations. CLT panels of 9cm, 15cm, 9-15cm thickness, connected to the beams, were the first three solutions. The fourth one represented retrofitting by CLT panels of 9-15cm connected to the columns. Proper finite element models for four suggested retrofitting solutions, and the reference building, were performed using SAP2000.

A linear dynamic analysis was conducted to design and evaluate the seismic behavior according to Eurocodes criteria using the Response Spectrum analysis. Then, a nonlinear static analysis using Pushover was executed to examine the damage state of the models using the Capacity Spectrum (ATC-40) Method.

The analysis has shown that using CLT panels enhances the seismic performance of the existing building; the determination of CLT panels' thickness and the connectors' location affects the deformation capacity, the ductility, and the stiffness of the structure.

Regarding the linear analysis, implementing CLT panels to the beams reduces the global deformation (the peak roof drift) and the modal period by a decrease of 40%, in contrast with the local deformation (the maximum storey drift) that increases by 7 to 14%. Meanwhile, it adversely affects the base shear values by doubled increase side by side with the stiffness, accompanied by keeping the seismic demands within the columns' capacity. As the CLT panels thickness increases, the roof lateral displacement decreases, and the base shear value and the stiffness increase. On the other hand, connecting CLT panels to the columns contributed in terms of the local and global drift more efficiently. In contrast, it maximized the base shear values and exaggerated the structure's stiffness, while the seismic demands exceeded the columns' capacity in the top storeys.

Concerning the nonlinear analysis, connecting CLT panels to the beams affected the expected roof displacement by a decrease of 45%. While the expected roof displacement was influenced by a 71% decrease with connecting the CLT panels to the columns, the structural damage was limited according to the FEMA in both cases, except that the Capacity Spectrum reflected much more stiffness, considering the final suggested solution.

5.2. Further studies

As a retrofitting technique, the CLT panels can enhance the seismic performance of the existing reinforced concrete buildings, which requires more research to be done.

This study used the SAP2000 to analyze the seismic performance, where adding the cross-laminated timber as new material and connecting the new sections to the original structural elements was challenging.

More studies can be proposed by using different characteristics that the cross-laminated timber can offer, and various types of connectors that the application can offer.

Regarding the nonlinear analysis, this thesis has used the default type of hinges, assuming the same deformation capacity for all columns regardless of their axial load level and weak or strong axis orientation. Advanced studies can be more specific and more accurate concerning the hinges features.

In addition, the ATC-40 was helpful to determine the damage state, which is a traditional old method. Many developed approaches can be more beneficial in further studies.

REFERENCES

1. Alashkar, Y., S. Nazar, and M. Ahmed, *A comparative study of seismic strengthening of RC building by steel bracings and concrete shear walls.* International Journal of Civil and Structural Engineering Research, 2015. **2**(2): p. 24-34.
2. Fragiadakis, M. and M. Papadrakakis, *Performance-based optimum seismic design of reinforced concrete structures.* Earthquake Engineering & Structural Dynamics, 2008. **37**(6): p. 825-844.
3. Fajfar, P. *Analysis in seismic provisions for buildings: past, present and future*. in *European Conference on Earthquake Engineering Thessaloniki, Greece*. 2018. Springer.
4. Villar-Salinas, S., A. Guzmán, and J. Carrillo, *Performance evaluation of structures with reinforced concrete columns retrofitted with steel jacketing.* Journal of Building Engineering, 2021. **33**: p. 101510.
5. Nguyen-Minh, L., et al., *Punching shear resistance of steel fiber reinforced concrete flat slabs.* Procedia Engineering, 2011. **14**: p. 1830-1837.
6. Farghaly, A.A. and A.M. Abdallah, *Evaluation of Seismic Retrofitting Techniques Used in Old Reinforced Concrete Buildings.* Evaluation, 2014. **4**(06).
7. Zhao, X., et al., *Numerical Analysis on Global Serviceability Behaviours of Tall CLT Buildings to the Eurocodes and UK National Annexes.* Buildings, 2021. **11**(3): p. 124.
8. Cho, H.M., et al., *Energy retrofit analysis of cross-laminated timber residential buildings in Seoul, Korea: Insights from a case study of packages.* Energy and Buildings, 2019. **202**: p. 109329.
9. Awad, V., et al., *Experimental Analyses and Numerical Models of CLT Shear Walls under Cyclic Loading.* Wood in Civil Engineering, 2017. **223**.
10. Hashemi, M.J., et al., *Linking seismic resilience into sustainability assessment of limited-ductility RC buildings.* Engineering Structures, 2019. **188**: p. 121-136.
11. Requena-García-Cruz, M.-V., et al., *An index-based method for evaluating seismic retrofitting techniques. Application to a reinforced concrete primary school in Huelva.* Plos one, 2019. **14**(4): p. e0215120.
12. Fukuyama, H. and S. Sugano, *Japanese seismic rehabilitation of concrete buildings after the Hyogoken-Nanbu Earthquake.* Cement and Concrete Composites, 2000. **22**(1): p. 59-79.

13. Di Trapani, F., et al., *Optimal seismic retrofitting of reinforced concrete buildings by steel-jacketing using a genetic algorithm-based framework.* Engineering Structures, 2020. **219**: p. 110864.
14. Kaplan, H., et al., *Seismic strengthening of RC structures with exterior shear walls.* Sadhana, 2011. **36**(1): p. 17-34.
15. Li, Z., et al., *Seismic performance assessment of steel frame infilled with prefabricated wood shear walls.* Journal of constructional steel research, 2018. **140**: p. 62-73.
16. De Matteis, G., A. Formisano, and F. Mazzolani, *An innovative methodology for seismic retrofitting of existing RC buildings by metal shear panels.* Earthquake engineering & structural dynamics, 2009. **38**(1): p. 61-78.
17. MA, I. and H. AE, *Seismic Retrofitting of a RC Building by Adding Steel Plate Shear Walls.* IOSR Journal of Mechanical and Civil Engineering (IOSR-JMCE), 2013. **7**(2): p. 49-62.
18. Rahimi, A. and M.R. Maheri, *The effects of steel X-brace retrofitting of RC frames on the seismic performance of frames and their elements.* Engineering Structures, 2020. **206**: p. 110149.
19. Kadid, A. and D. Yahiaoui, *Seismic assessment of braced RC frames.* Procedia Engineering, 2011. **14**: p. 2899-2905.
20. Gkournelos, P., T. Triantafillou, and D. Bournas, *Seismic upgrading of existing reinforced concrete buildings: A state-of-the-art review.* Engineering Structures, 2021. **240**: p. 112273.
21. Menna, C., et al., *Conceptual design of integrated seismic and energy retrofit interventions.* Journal of Building Engineering, 2021. **38**: p. 102190.
22. Sustersic, I. and B. Dujic. *Seismic strengthening of existing buildings with cross laminated timber panels*. in *Proceedings of the World Conference on Timber Engineering, Auckland, New Zealand*. 2012.
23. Follesa, M., et al., *Seismic design of multi-storey cross laminated timber buildings according to Eurocode 8.* Ingegneria Sismica, 2013. **4**.
24. Yin, X., *The seismic behavior of cross-laminated timber composite slab in high-rise building.* Int J Eng Technol, 2018. **10**(4): p. 325-328.
25. Wallner-Novak, M., J. Koppelhuber, and K. Pock, *Cross-laminated timber structural design—basic design and engineering principles according to Eurocode.* ProHolz: Innsbruck, Austria, 2014.

26. Mallo, M.F.L. and O.A. Espinoza, *Outlook for cross-laminated timber in the United States.* BioResources, 2014. **9**(4): p. 7427-7443.
27. Longarini, N., P. Crespi, and M. Scamardo, *Numerical approaches for cross-laminated timber roof structure optimization in seismic retrofitting of a historical masonry church.* Bulletin of Earthquake Engineering, 2020. **18**(2): p. 487-512.
28. Haba, R., et al., *< Recent research activities> Development of CLT panels bond-in method for seismic retrofitting of RC frame structure.* Sustainable humanosphere: bulletin of Research Institute for Sustainable Humanosphere Kyoto University, 2015. **11**: p. 22-22.
29. Stazi, F., et al., *An experimental and numerical study on CLT panels used as infill shear walls for RC buildings retrofit.* Construction and building materials, 2019. **211**: p. 605-616.
30. Gagnon, S., et al., *CLT Introduction to cross-laminated timber.* In: CLT handbook: cross-laminated timber/edited by Erol Karacabeyli, Brad Douglas.--US ed. 2013; pp. 1-45., 2013: p. 1-57.
31. Valluzzi, M.R., et al., *Nested Buildings: An Innovative Strategy for the Integrated Seismic and Energy Retrofit of Existing Masonry Buildings with CLT Panels.* Sustainability, 2021. **13**(3): p. 1188.
32. Elnashai, A.S. and L. Di Sarno, *Fundamentals of earthquake engineering*. 2008: Wiley New York.
33. Pitilakis, K., *Recent Advances in Earthquake Engineering in Europe: 16th European Conference on Earthquake Engineering-Thessaloniki 2018.* 2018.
34. Kevadkar, M. and P. Kodag, *Lateral load analysis of RCC building.* International Journal of Modern Engineering Research (IJMER), 2013. **3**(3): p. 1428-1434.
35. Sousa, M., et al., *State of harmonised use of the Eurocodes*, in *EUR 29732 EN*. 2019, Publications Office of the European Union Luxembourg.
36. Banginwar, R.S., M. Vyawahare, and P. Modani, *Effect of plans configurations on the seismic behaviour of the structure by response spectrum method.* Int. J. Eng. Res. Appl, 2012. **2**: p. 1439-1443.
37. Ghobarah, A., H. Abou-Elfath, and A. Biddah, *Response-based damage assessment of structures.* Earthquake engineering & structural dynamics, 1999. **28**(1): p. 79-104.
38. Caterino, N., E. Cosenza, and B. Azmoodeh, *Approximate methods to evaluate storey stiffness and interstory drift of RC buildings in seismic area.* Structural engineering and mechanics, 2013. **46**(2): p. 245-267.

39. Khan, M.A., *Earthquake-Resistant Structures: Design, Build, and Retrofit*. 2013: Butterworth-Heinemann.
40. Hashemi, S.S. and M. Vaghefi, *Investigation of bond slip effect on the PM interaction surface of RC columns under biaxial bending.* Scientia Iranica. Transaction A, Civil Engineering, 2015. **22**(2): p. 388.
41. Brooker, O., *How to design concrete structures using Eurocode 2.* How to Design Concrete Structures using Eurocode 2, 2005: p. 9.
42. Salvatore, W., et al., *Effects of corrosion on low-cycle fatigue (seismic) behaviour of high-strength steel reinforcing bars (Rusteel).* 2014.
43. Themelis, S., *Pushover analysis for seismic assessment and design of structures*. 2008, Heriot-Watt University.
44. Meslem, A. *Nonlinear Static (Pushover) Analysis*. in *Nonlinear Analysis and Performance Based Design of Multistorey Buildings*. 2015. New Delhi: NORSAR.
45. Hakim, R.A., M. Alama, and S.A. Ashour, *Seismic Assessment of an RC Building Using Pushover Analysis.* Engineering, Technology & Applied Science Research, 2014. **4**(3): p. 631-635.
46. FEMA, B., *Prestandard and commentary for the seismic rehabilitation of buildings*. 2000, Washington, DC.
47. Engineers, A.S.o.C., *Seismic Evaluation and Retrofi t of Existing Buildings*. 2014, Virginia: www.asce.org/pubs.
48. Craig D. Comartin, R.W.N., Christopher Rojabn, *Seismic evaluation and retrofit of concrete buildings Volume 1*. November 1996, California: APPLIED TECHNOLOGY COUNCIL.
49. Sergio Molina, D.H.L., Abdelghani Meslem and Conrad D. Lindholm, *SELENA v6.5*. June 2015, Kjeller, Norway: NORSAR.
50. Inel, M. and H.B. Ozmen, *Effects of plastic hinge properties in nonlinear analysis of reinforced concrete buildings.* Engineering structures, 2006. **28**(11): p. 1494-1502.

APPENDIX A

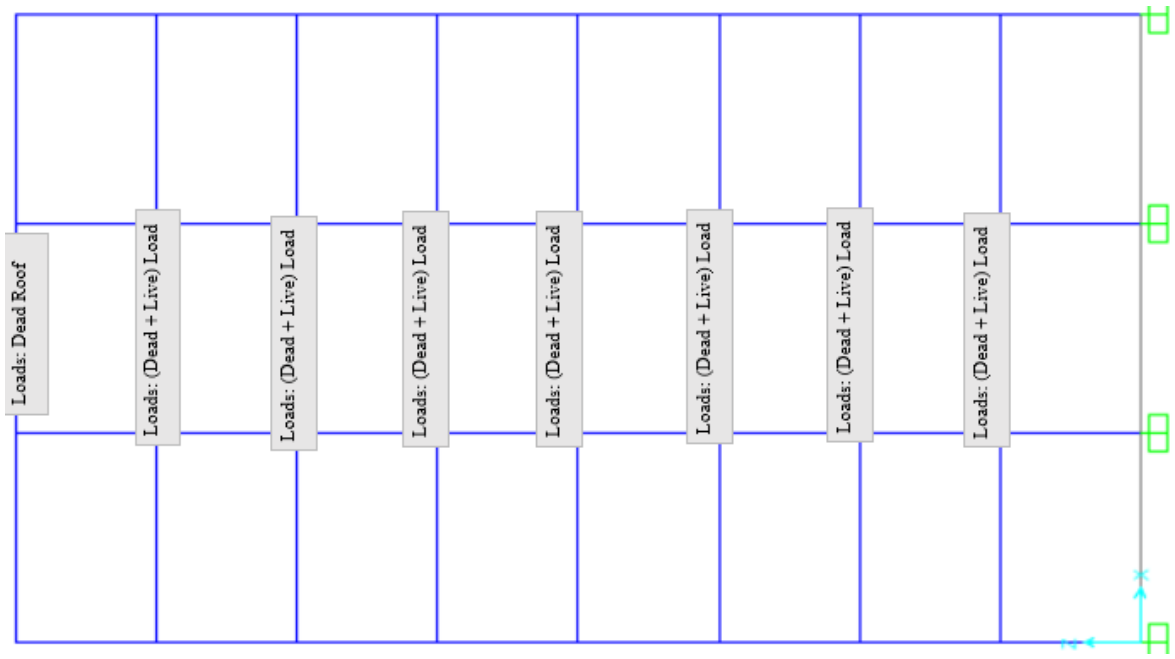

LOADS

Dead Floor		Weight	Thickness: m	Y Dir: m	Load: kN/m
	Slab: kN/m^3	25	0.15	4	15
	Finishing: kN/m^2	2		4	8
				Z Dir: m	
	Walls kN/m^3	9	0.16	3.3	4.752
SUM					27.752

Dead Roof SUM					
					23

Live	kN/m^2	2		4	8

Building A_0

- Response Spectrum Function, Load.

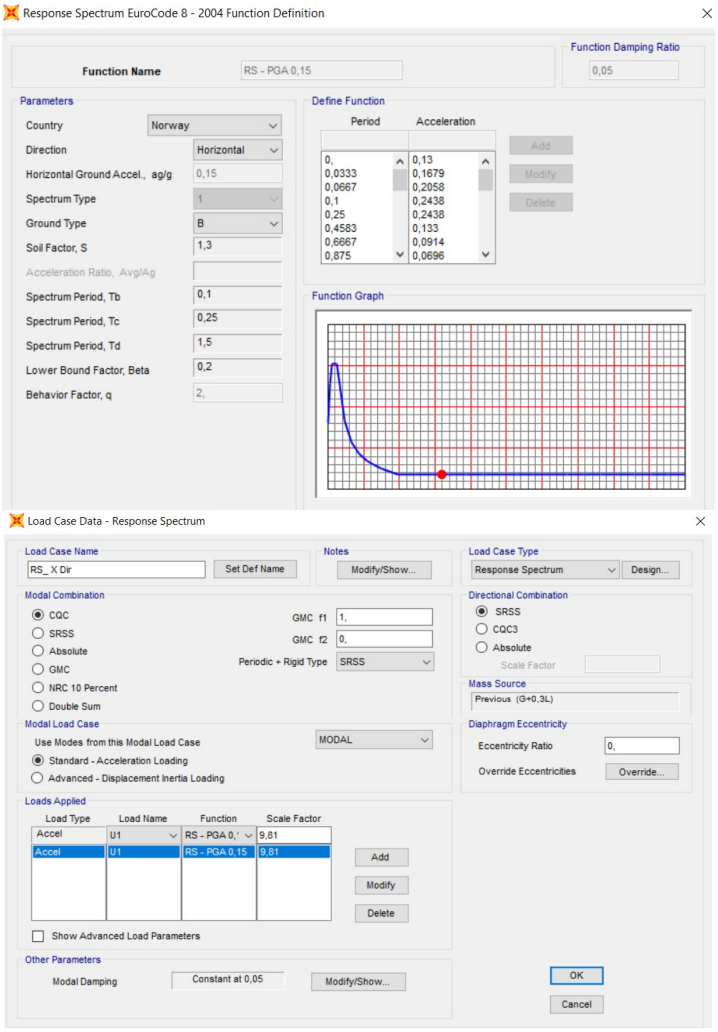

- Structural characteristics.

Beam1						
Concrete		Depth : cm	Width : cm	Material	Area : m2	
	Dimensions	50	30	C25/30	0.15	
Steel		Diameter : mm	number	Material	Area : m2	Cover : cm
	Top	14	4	B450C	0.000616	2.5
	Bottom	14	2	B450C	0.000308	2.5

Beam2

Concrete		Depth: cm	Width: cm	Material	Area: m2	
	Dimensions	30	30	C25/30	0.09	
Steel		Diameter: mm	number	Material	Area: m2	Cover: cm
	Top	14	3	B450C	0.000462	2.5
	Bottom	14	2	B450C	0.000308	2.5

Column 1

Concrete				
	Depth : cm	Width : cm	Material	Area : m2
Dimensions	90	30	C25/30	0.27

Steel				
longitudinal				
	Diameter : mm	number	Material	Cover : cm
Dir 2	20	5	B450C	2.5
Dir 3	20	3	B450C	2.5
Confinement				
	Diameter : mm	number	Material	Spacing : cm
Dir 2	10	2	B450C	10
Dir 3	10	4	B450C	10

Column 2

Concrete				
	Depth : cm	Width : cm	Material	Area : m2
Dimensions	80	30	C25/30	0.24

Steel				
longitudinal				
	Diameter : mm	number	Material	Cover : cm
Dir 2	20	5	B450C	2.5
Dir 3	20	3	B450C	2.5
Confinement				

	Diameter : mm	number	Material	Spacing : cm
Dir 2	10	2	B450C	10
Dir 3	10	4	B450C	10

Column 3

Concrete				
	Depth : cm	Width : cm	Material	Area : m2
Dimensions	70	30	C25/30	0.21

Steel				
longitudinal				
	Diameter : mm	number	Material	Cover : cm
Dir 2	20	5	B450C	2.5
Dir 3	20	3	B450C	2.5

Confinement				
	Diameter : mm	number	Material	Spacing : cm
Dir 2	10	2	B450C	10
Dir 3	10	4	B450C	10

Column4

Concrete				
	Depth : cm	Width : cm	Material	Area : m2
Dimensions	60	30	C25/30	0.18

Steel				
longitudinal				
	Diameter : mm	number	Material	Cover : cm
Dir 2	16	4	B450C	2.5
Dir 3	16	3	B450C	2.5

Confinement				
	Diameter : mm	number	Material	Spacing : cm
Dir 2	8	2	B450C	10
Dir 3	8	2	B450C	10

Column 5

Concrete				
	Depth : cm	Width : cm	Material	Area : m2
Dimensions	50	30	C25/30	0.15

Steel	
longitudinal	

	Diameter : mm	number	Material	Cover : cm
Dir 2	16	4	B450C	2.5
Dir 3	16	3	B450C	2.5

Confinement				
	Diameter : mm	number	Material	Spacing : cm
Dir 2	8	2	B450C	10
Dir 3	8	2	B450C	10

Column 7

Concrete				
	Depth : cm	Width : cm	Material	Area : m2
Dimensions	30	30	C25/30	0.09

Steel				
longitudinal				
	Diameter : mm	number	Material	Cover : cm
Dir 2	14	3	B450C	2.5
Dir 3	14	3	B450C	2.5

Confinement				
	Diameter : mm	number	Material	Spacing : cm
Dir 2	6	2	B450C	10
Dir 3	6	2	B450C	10

Column 8

Concrete				
	Depth : cm	Width : cm	Material	Area : m2
Dimensions	30	30	C25/30	0.09

Steel				
longitudinal				
	Diameter : mm	number	Material	Cover : cm
Dir 2	14	3	B450C	2.5
Dir 3	14	3	B450C	2.5

Confinement				
	Diameter : mm	number	Material	Spacing : cm
Dir 2	6	2	B450C	10
Dir 3	6	2	B450C	10

Building A_{ret}

- Response Spectrum Function, Load.

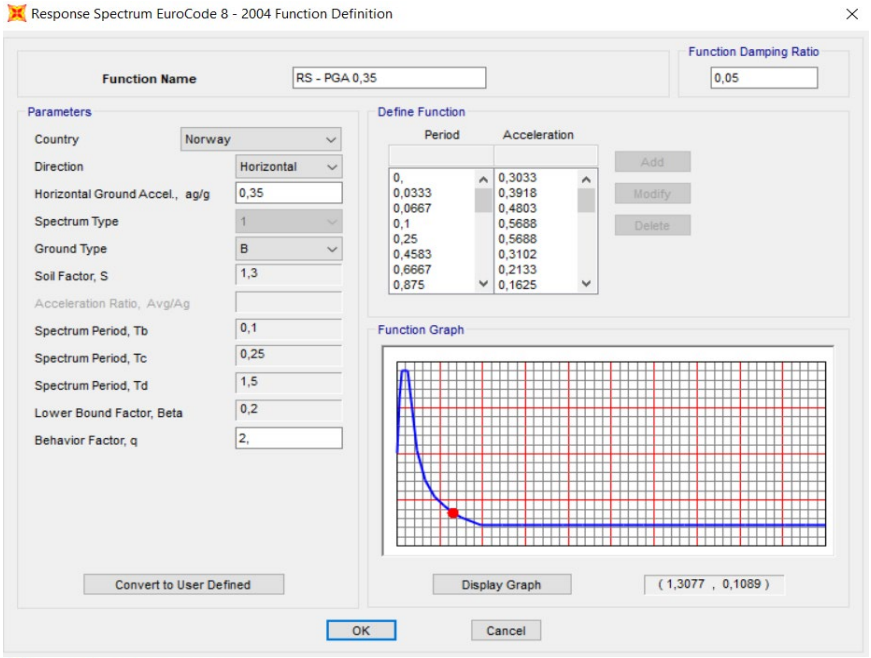

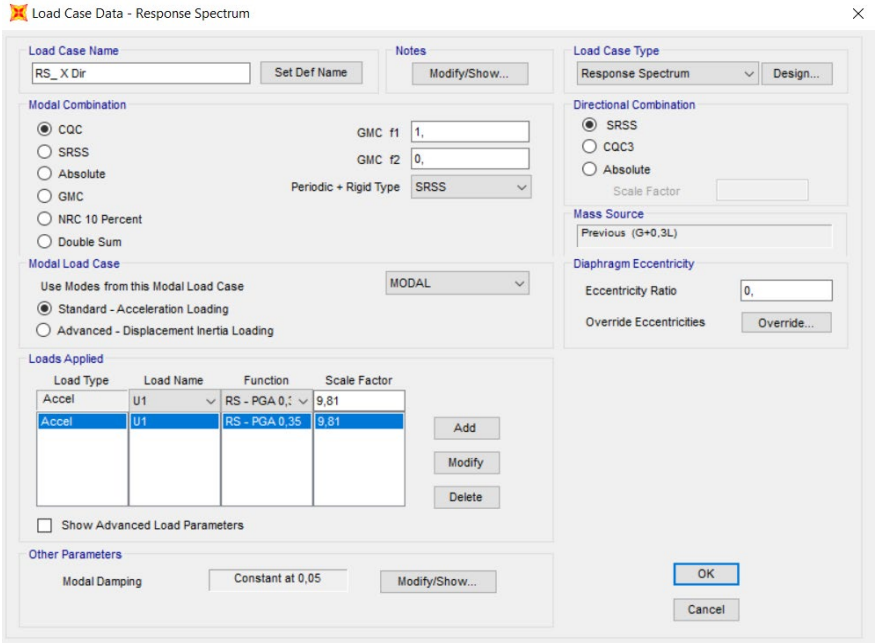

Building B

- Response Spectrum Function, Load

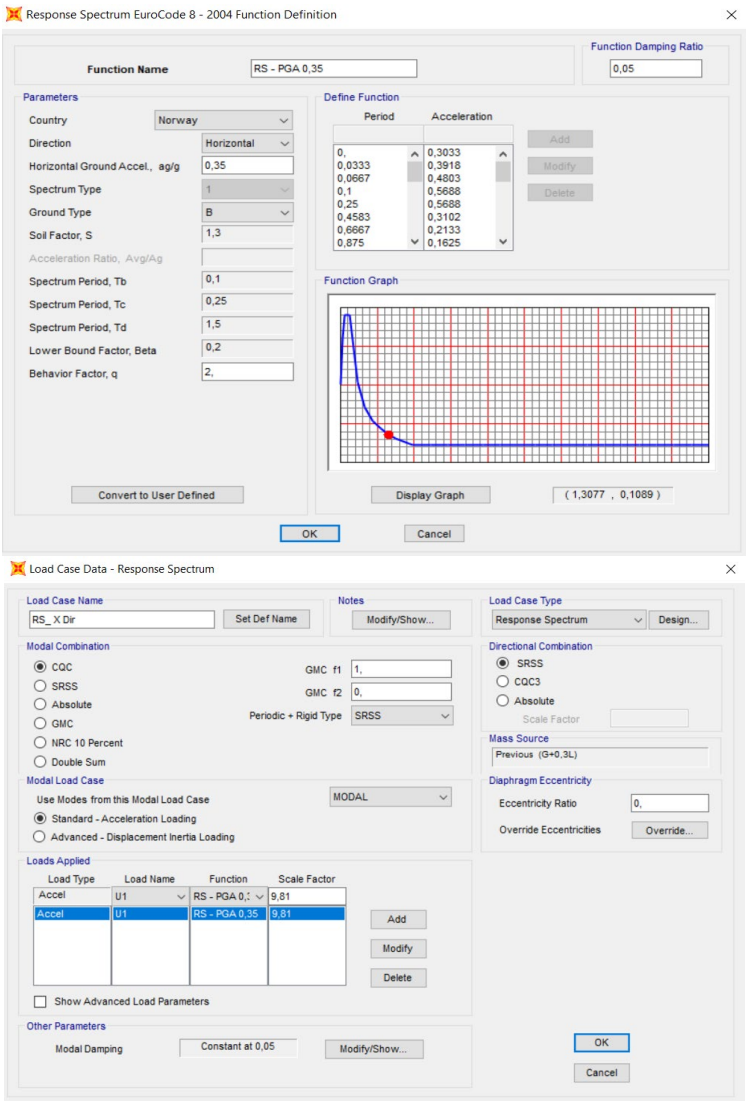

- Step 1: Modify the beams on the 6th ,5th and 4th floor to B3, the rebars in C6 and C5 to 20/10, rebars in C7and C8 to 16/8 not enough!

Building B_Design_Step1

Storey	Beam	Column
1	B1	C1
2	B1	C2
3	B1	C3
4	B3	C4

5	B3	C5/RB
6	B3	C6/RB
7	B2	C7_C6_C6_C7(RB)
8	B2	C8/RB

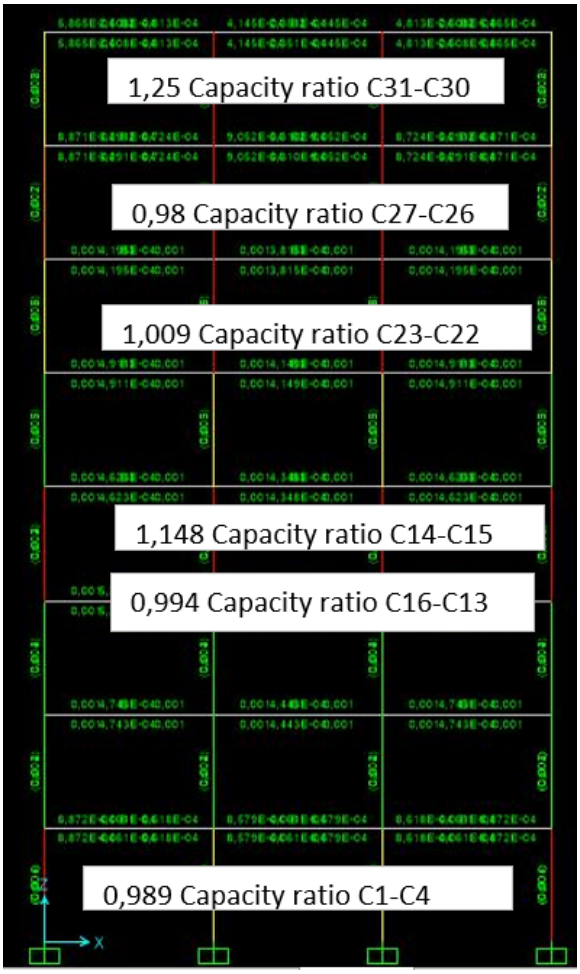

Step (1)

- Step 2: C8 in both middle columns on the 8th floor modified to C6, the are C3& C4 rebars modified to 20/12, and C1 to 25/12 & C2 to20/12, not enough!

Building B_Design_Step2

Storey	Beam	Column
1	B1	C1/RB
2	B1	C2/RB
3	B1	C3/RB

4	B3	C4/RB
5	B3	C5/RB
6	B3	C6/RB
7	B2	C7_C6_C6_C7(RB)
8	B2	C8-C6-C6-C8(RB)

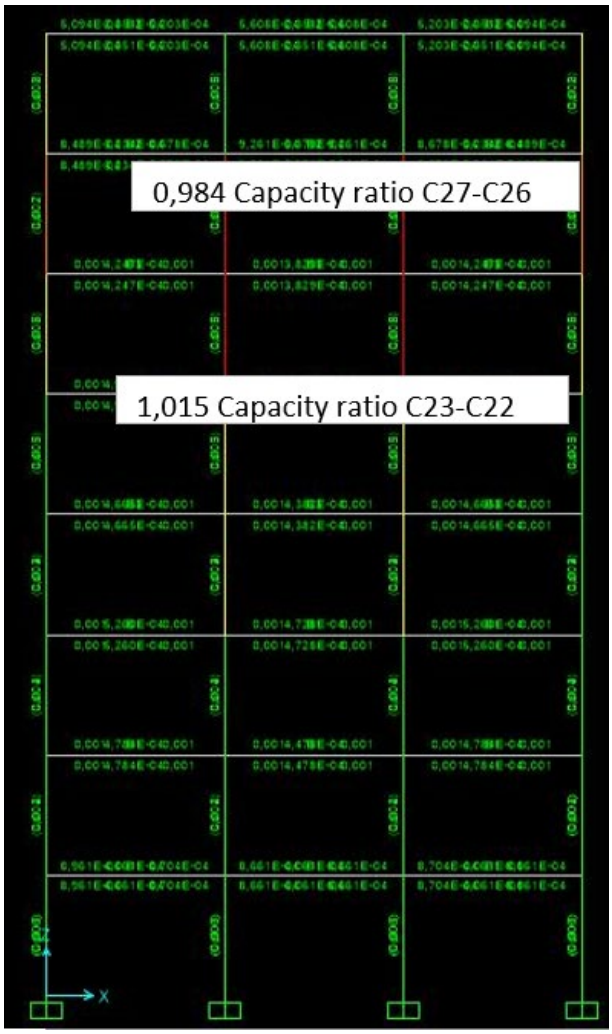

Step (2)

- Step 3: On 7th floor all the columns are modified to C6, on the 6th floor both columns in the middle are modified to C5. And that was enough!

Building B_Design_Step3

Storey	Beam	Column
1	B1	C1/RB
2	B1	C2/RB

3	B1	C3/RB
4	B3	C4/RB
5	B3	C5/RB
6	B3	C6-C5-C5-C6 (RB)
7	B2	C6 (RB)
8	B2	C8-C6-C6-C8(RB)

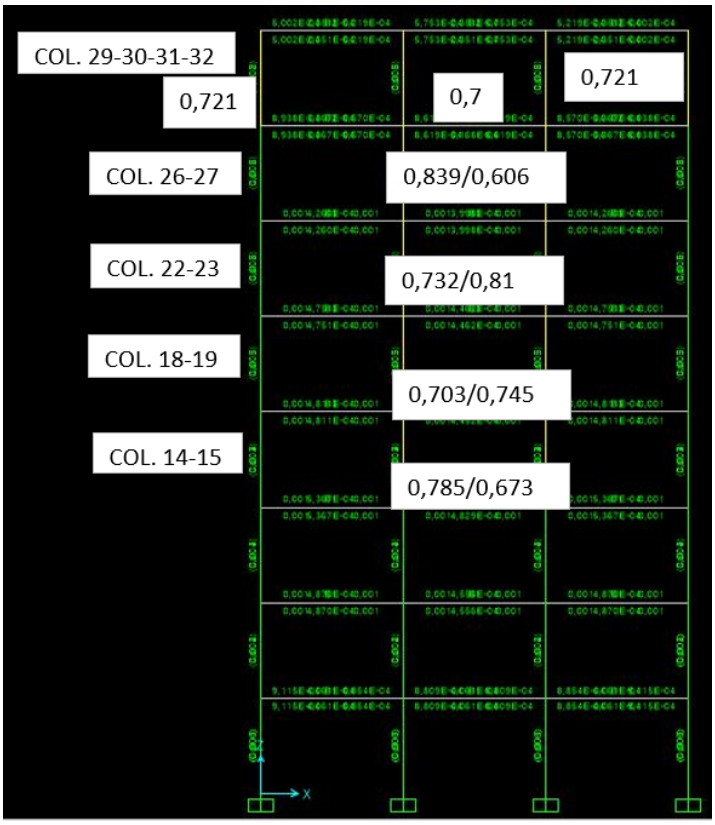

Step (3)

Building B : Δx_Step 3

Point	H : m	Δx : m
9	3.3	0.0649
8	3.3	0.0562
7	3.3	0.0463
6	3.3	0.0365
5	3.3	0.0259
4	3.3	0.017
3	3.3	0.0094
2	3.3	0.0031
1	3.3	0

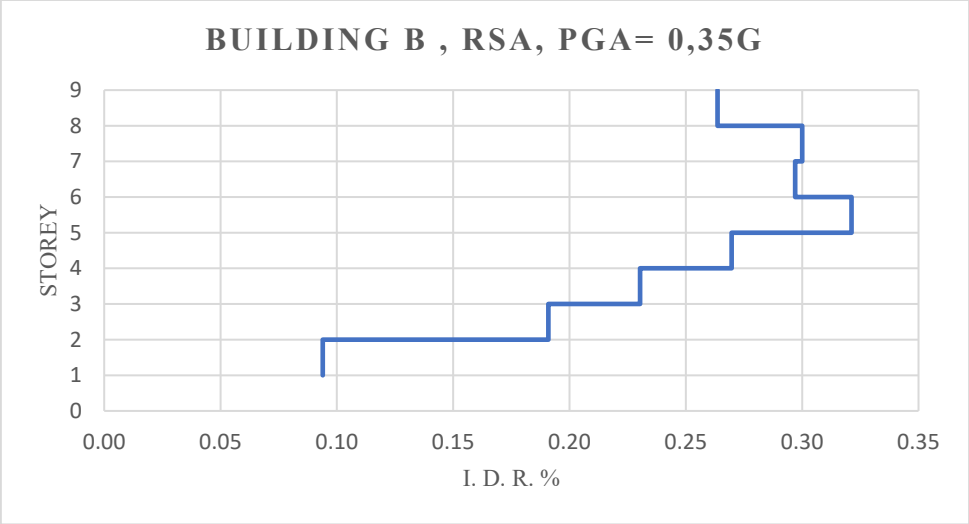

Building B: Interstorey Drift limit Check-Step 3

storey	Δx : mm	qd	ν	*dsi* : mm	dr : mm	dr*ν : mm	Limit =24.75
8	64.9	2	0.5	129.8	17.4	8.7	TRUE
7	56.2	2	0.5	112.4	19.8	9.9	TRUE
6	46.3	2	0.5	92.6	19.6	9.8	TRUE
5	36.5	2	0.5	73.0	21.2	10.6	TRUE
4	25.9	2	0.5	51.8	17.8	8.9	TRUE
3	17	2	0.5	34.0	15.2	7.6	TRUE
2	9.4	2	0.5	18.8	12.6	6.3	TRUE
1	3.1	2	0.5	6.2	6.2	3.1	TRUE

- Step4:
  - the Interstorey drift ratio for the third try is not flowing smoothly between 5^{th} / 6^{th} storey and 7^{th} / 8^{th} storey.
  - Some procedures had to be done to improve the graph flowing.
  - Replace the Steel to ϕ14 for the confinement bars from the base to 4^{th} storey, and ϕ12 to the rest.
  - Replace the Steel to ϕ20 for the longitudinal bars on 7^{th} & 8^{th} storey.
  - He weakness in the middle columns start on the 4^{th} storey and delivers its peak in the 7^{th} storey, the middle columns can be replaced by bigger cross section and the result is satisfying.

Building B_Design_Step4

Storey	Beam	Column
1	B1	C1/RB
2	B1	C2/RB
3	B1	C3/RB
4	B3	C4-C3-C3-C4 (RB)
5	B3	C4-C4-C4-C4 (RB)
6	B3	C6-C5-C5-C6 (RB)
7	B2	C7-C5-C5-C7 (RB)
8	B2	C8(RB)

Building B : Δx_Step 4

Point	H : m	Δx : m
9	3.3	0.0655
8	3.3	0.0553
7	3.3	0.0454
6	3.3	0.0355
5	3.3	0.0258
4	3.3	0.0172
3	3.3	0.0096
2	3.3	0.0031
1	3.3	0

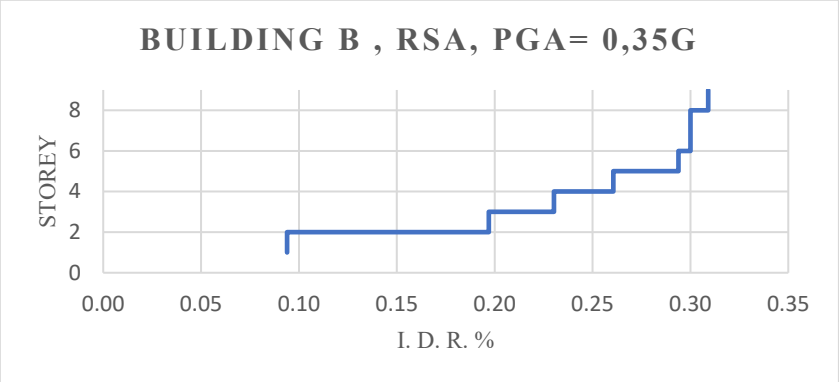

Building B: Interstorey Drift limit Check-Step 4

storey	Δx : mm	qd	ν	*ds*i : mm	dr : mm	dr*ν : mm	Limit =24.75
8	65.5	2	0.5	131.0	20.4	10.2	TRUE
7	55.3	2	0.5	110.6	19.8	9.9	TRUE
6	45.4	2	0.5	90.8	19.8	9.9	TRUE
5	35.5	2	0.5	71.0	19.4	9.7	TRUE
4	25.8	2	0.5	51.6	17.2	8.6	TRUE
3	17.2	2	0.5	34.4	15.2	7.6	TRUE
2	9.6	2	0.5	19.2	13.0	6.5	TRUE
1	3.1	2	0.5	6.2	6.2	3.1	TRUE

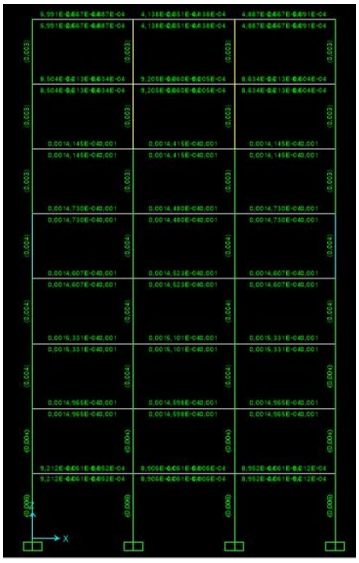

Step (4)

- Structural Characteristics

Beam1						
Concrete		Depth : cm	Width : cm	Material	Area : m2	
	Dimensions	50	30	C25/30	0.15	
Steel		Diameter : mm	number	Material	Area : m2	Cover : cm
	Top	14	4	B450C	0.000616	2.5
	Bottom	14	2	B450C	0.000308	2.5

Beam2					
Concrete		Depth : cm	Width : cm	Material	Area : m2
	Dimensions	30	30	C25/30	0.09

Steel		Diameter : mm	number	Material	Area : m2	Cover : cm
	Top	14	3	B450C	0.000462	2.5
	Bottom	14	2	B450C	0.000308	2.5

Beam3

Concrete		Depth : cm	Width : cm	Material	Area : m2	
	Dimensions	40	30	C25/30	0.12	

Steel		Diameter : mm	number	Material	Area : m2	Cover : cm
	Top	14	3	B450C	0.000462	2.5
	Bottom	14	2	B450C	0.000308	2.5

Column 1

Concrete				
	Depth : cm	Width : cm	Material	Area : m2
Dimensions	90	30	C25/30	0.27

Steel				
longitudinal				
	Diameter : mm	number	Material	Cover : cm
Dir 2	25	5	B450C	2.5
Dir 3	25	3	B450C	2.5

Confinement				
	Diameter : mm	number	Material	Spacing : cm
Dir 2	12	2	B450C	10
Dir 3	12	4	B450C	10

Column 2

Concrete				
	Depth : cm	Width : cm	Material	Area : m2
Dimensions	80	30	C25/30	0.24

Steel				
longitudinal				
	Diameter : mm	number	Material	Cover : cm
Dir 2	20	5	B450C	2.5
Dir 3	20	3	B450C	2.5

Confinement				
	Diameter : mm	number	Material	Spacing : cm
Dir 2	12	2	B450C	10
Dir 3	12	4	B450C	10

Column 3

Concrete				
	Depth : cm	Width : cm	Material	Area : m2
Dimensions	70	30	C25/30	0.21

Steel				
longitudinal				
	Diameter : mm	number	Material	Cover : cm
Dir 2	20	5	B450C	2.5
Dir 3	20	3	B450C	2.5

Confinement				
	Diameter : mm	number	Material	Spacing : cm
Dir 2	12	2	B450C	10
Dir 3	12	4	B450C	10

Column4

Concrete				
	Depth : cm	Width : cm	Material	Area : m2
Dimensions	60	30	C25/30	0.18

Steel				
longitudinal				
	Diameter : mm	number	Material	Cover : cm
Dir 2	20	4	B450C	2.5
Dir 3	20	3	B450C	2.5

Confinement				
	Diameter : mm	number	Material	Spacing : cm
Dir 2	12	2	B450C	10
Dir 3	12	2	B450C	10

Column 5

Concrete				
	Depth : cm	Width : cm	Material	Area : m2
Dimensions	50	30	C25/30	0.15

Steel				
longitudinal				
	Diameter : mm	number	Material	Cover : cm
Dir 2	20	4	B450C	2.5
Dir 3	20	3	B450C	2.5
Confinement				
	Diameter : mm	number	Material	Spacing : cm
Dir 2	10	2	B450C	10
Dir 3	10	2	B450C	10

Column 6

Concrete				
	Depth : cm	Width : cm	Material	Area : m2
Dimensions	40	30	C25/30	0.12

Steel				
longitudinal				
	Diameter : mm	number	Material	Cover : cm
Dir 2	20	3	B450C	2.5
Dir 3	20	3	B450C	2.5
Confinement				
	Diameter : mm	number	Material	Spacing : cm
Dir 2	10	2	B450C	10
Dir 3	10	2	B450C	10

Column 7

Concrete				
	Depth : cm	Width : cm	Material	Area : m2
Dimensions	30	30	C25/30	0.09

Steel				
longitudinal				
	Diameter : mm	number	Material	Cover : cm
Dir 2	16	3	B450C	2.5
Dir 3	16	3	B450C	2.5
Confinement				
	Diameter : mm	number	Material	Spacing : cm
Dir 2	8	2	B450C	10

	Dir 3	8	2	B450C	10

Column 8

Concrete				
	Depth : cm	Width : cm	Material	Area : m2
Dimensions	30	30	C25/30	0.09

Steel				
longitudinal				
	Diameter : mm	number	Material	Cover : cm
Dir 2	16	3	B450C	2.5
Dir 3	16	3	B450C	2.5
Confinement				
	Diameter : mm	number	Material	Spacing : cm
Dir 2	8	2	B450C	10
Dir 3	8	2	B450C	10

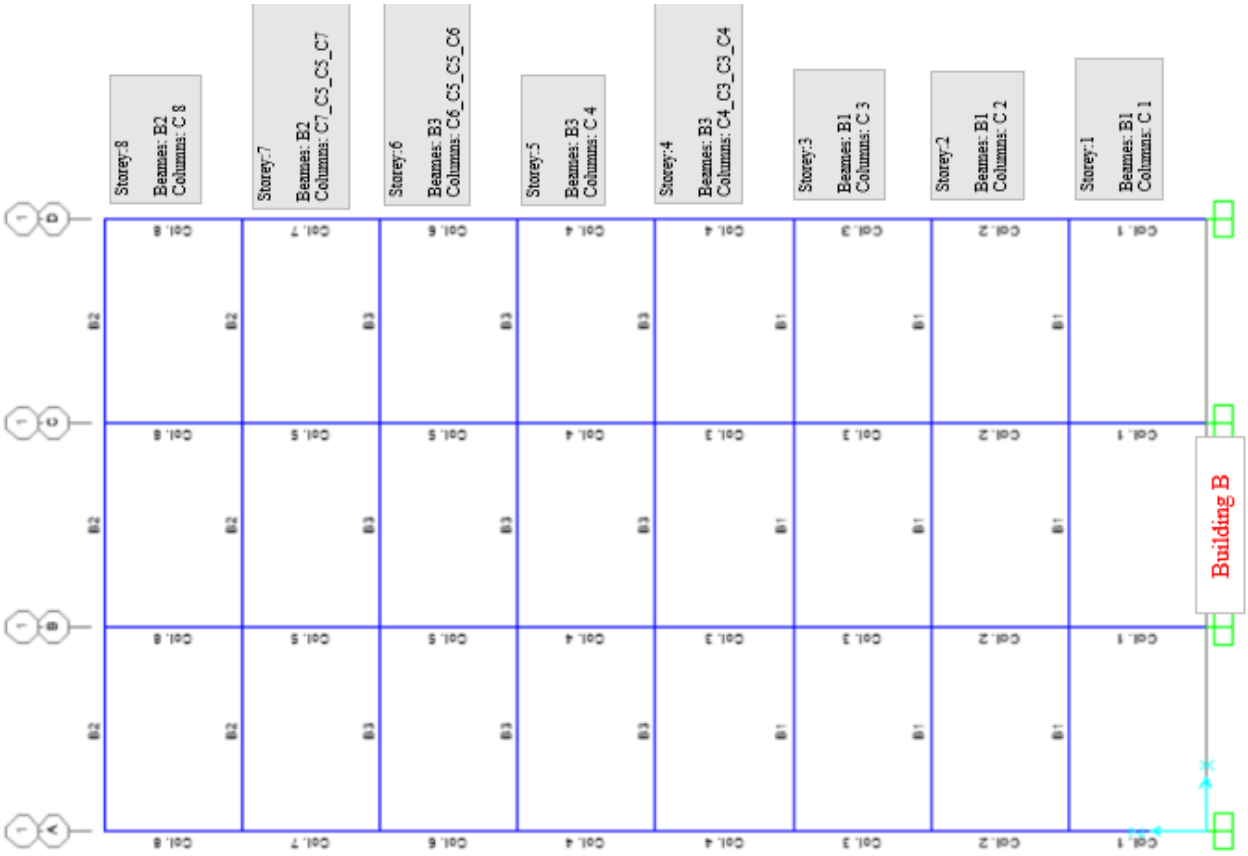

APPENDIX B

Importance classes for buildings according to EC8:

Table 4.3 Importance classes for buildings

Importance class	Buildings
I	Buildings of minor importance for public safety, e.g. agricultural buildings, etc.
II	Ordinary buildings, not belonging in the other categories.
III	Buildings whose seismic resistance is of importance in view of the consequences associated with a collapse, e.g. schools, assembly halls, cultural institutions etc.
IV	Buildings whose integrity during earthquakes is of vital importance for civil protection, e.g. hospitals, fire stations, power plants, etc.

Reduction Factor *ν*

NOTE The values to be ascribed to ν for use in a country may be found in its National Annex. Different values of ν may be defined for the various seismic zones of a country, depending on the seismic hazard conditions and on the protection of property objective. The recommended values of ν are 0,4 for importance classes III and IV and ν = 0,5 for importance classes I and II.

Interstorey Drift Limitation according to EC8:

Table 6.1: Design concepts, structural ductility classes and upper limit reference values of the behaviour factors

Design concept	Structural ductility class	Range of the reference values of the behaviour factor q
Concept a) Low dissipative structural behaviour	DCL (Low)	≤ 1,5 - 2
Concept b) Dissipative structural behaviour	DCM (Medium)	≤ 4 also limited by the values of Table 6.2
	DCH (High)	only limited by the values of Table 6.2

NOTE 1 The value ascribed to the upper limit of q for low dissipative behaviour, within the range of Table 6.1, for use in a country may be found in its National Annex. The recommended value of the upper limit of q for low-dissipative behaviour is 1,5.

NOTE 2 The National Annex of a particular country may give limitations on the choice of the design concept and of the ductility class which are permissible within that country.

Table 6.2: Upper limit of reference values of behaviour factors for systems regular in elevation

STRUCTURAL TYPE	Ductility Class	
	DCM	DCH
a) Moment resisting frames	4	$5\alpha_u/\alpha_1$
b) Frame with concentric bracings Diagonal bracings V-bracings	 4 2	 4 2,5
c) Frame with eccentric bracings	4	$5\alpha_u/\alpha_1$
d) Inverted pendulum	2	$2\alpha_u/\alpha_1$
e) Structures with concrete cores or concrete walls	See section **5**	
f) Moment resisting frame with concentric bracing	4	$4\alpha_u/\alpha_1$
g) Moment resisting frames with infills Unconnected concrete or masonry infills, in contact with the frame	2	2
Connected reinforced concrete infills	See section **7**	
Infills isolated from moment frame (see moment frames)	4	$5\alpha_u/\alpha_1$

(2) If the building is non-regular in elevation (see **4.2.3.3**) the upper limit values of q listed in Table 6.2 should be reduced by 20 % (see **4.2.3.1(7)** and Table 4.1).

4.3.4 Displacement analysis

(1)P If linear analysis is performed the displacements induced by the design seismic action shall be calculated on the basis of the elastic deformations of the structural system by means of the following simplified expression:

$$d_s = q_d \, d_e \tag{4.23}$$

where

d_s is the displacement of a point of the structural system induced by the design seismic action;

q_d is the displacement behaviour factor, assumed equal to q unless otherwise specified;

d_e is the displacement of the same point of the structural system, as determined by a linear analysis based on the design response spectrum in accordance with **3.2.2.5.**

The value of d_s does not need to be larger than the value derived from the elastic spectrum.

NOTE In general q_d is larger than q if the fundamental period of the structure is less than T_C (see Figure B.2).

(2)P When determining the displacements d_e, the torsional effects of the seismic action shall be taken into account.

(3) For both static and dynamic non-linear analysis, the displacements determined are those obtained directly from the analysis without further modification.

4.4.3.2 Limitation of interstorey drift

(1) Unless otherwise specified in Sections **5** to **9**, the following limits shall be observed:

a) for buildings having non-structural elements of brittle materials attached to the structure:

$$d_r \nu \leq 0{,}005\, h\,; \tag{4.31}$$

b) for buildings having ductile non-structural elements:

$$d_r \nu \leq 0{,}0075\, h\,; \tag{4.32}$$

c) for buildings having non-structural elements fixed in a way so as not to interfere with structural deformations, or without non-structural elements:

$$d_r \nu \leq 0{,}010\, h \tag{4.33}$$

where

d_r is the design interstorey drift as defined in **4.4.2.2(2)**;

h is the storey height;

ν is the reduction factor which takes into account the lower return period of the seismic action associated with the damage limitation requirement.

(2) The value of the reduction factor ν may also depend on the importance class of the building. Implicit in its use is the assumption that the elastic response spectrum of the seismic action under which the "damage limitation requirement" should be met (see **3.2.2.1(1)P**). has the same shape as the elastic response spectrum of the design seismic action corresponding to the "ultimate limit state requirement" in accordance with **2.1(1)**P and **3.2.1(3)**

NOTE The values to be ascribed to ν for use in a country may be found in its National Annex. Different values of ν may be defined for the various seismic zones of a country, depending on

the seismic hazard conditions and on the protection of property objective. The recommended values of ν are 0,4 for importance classes III and IV and ν = 0,5 for importance classes I and II.

4.3.3.2.2 Base shear force

(1)P The seismic base shear force F_b, for each horizontal direction in which the building is analysed, shall be determined using the following expression:

$$F_b = S_d(T_1) \cdot m \cdot \lambda \tag{4.5}$$

where

$S_d(T_1)$ is the ordinate of the design spectrum (see **3.2.2.5**) at period T_1;

T_1 is the fundamental period of vibration of the building for lateral motion in the direction considered;

m is the total mass of the building, above the foundation or above the top of a rigid basement, computed in accordance with **3.2.4(2)**;

λ is the correction factor, the value of which is equal to: $\lambda = 0{,}85$ if $T_1 \leq 2\, T_C$ and the building has more than two storeys, or $\lambda = 1{,}0$ otherwise.

NOTE The factor λ accounts for the fact that in buildings with at least three storeys and translational degrees of freedom in each horizontal direction, the effective modal mass of the 1st (fundamental) mode is smaller, on average by 15%, than the total building mass.

(2) For the determination of the fundamental period of vibration period T_1 of the building, expressions based on methods of structural dynamics (for example the Rayleigh method) may be used.

(3) For buildings with heights of up to 40 m the value of T_1 (in s) may be approximated by the following expression:

$$T_1 = C_t \cdot H^{3/4} \tag{4.6}$$

where

C_t is 0,085 for moment resistant space steel frames, 0,075 for moment resistant space concrete frames and for eccentrically braced steel frames and 0,050 for all other structures;

H is the height of the building, in m, from the foundation or from the top of a rigid basement.

(4) Alternatively, for structures with concrete or masonry shear walls the value C_t in expression (4.6) may be taken as being

$$C_t = 0{,}075 / \sqrt{A_c} \tag{4.7}$$

where

$$A_c = \Sigma \left[A_i \cdot (0{,}2 + (l_{wi} / H))^2 \right] \tag{4.8}$$

and

A_c is the total effective area of the shear walls in the first storey of the building, in m^2;

A_i is the effective cross-sectional area of the shear wall i in the first storey of the building, in m^2;

H is as in **(3)** of this subclause;

l_{wi} is the length of the shear wall i in the first storey in the direction parallel to the applied forces, in m, with the restriction that l_{wi}/H should not exceed 0,9.

(5) Alternatively, the estimation of T_1 (in s) may be made by using the following expression:

$$T_1 = 2 \cdot \sqrt{d} \tag{4.9}$$

where

d is the lateral elastic displacement of the top of the building, in m, due to the gravity loads applied in the horizontal direction.

- POA:

EC8:

4.3.3.4.2 Non-linear static (pushover) analysis

4.3.3.4.2.1 General

(1) Pushover analysis is a non-linear static analysis carried out under conditions of constant gravity loads and monotonically increasing horizontal loads. It may be applied to verify the structural performance of newly designed and of existing buildings for the following purposes:

a) to verify or revise the overstrength ratio values α_u/α_1 (see **5.2.2.2**, **6.3.2**, **7.3.2**);

b) to estimate the expected plastic mechanisms and the distribution of damage;

c) to assess the structural performance of existing or retrofitted buildings for the purposes of EN 1998-3;

d) as an alternative to the design based on linear-elastic analysis which uses the behaviour factor *q*. In that case, the target displacement indicated in **4.3.3.4.2.6(1)**P should be used as the basis of the design.

(2)P Buildings not conforming to the regularity criteria of **4.2.3.2** or the criteria of **4.3.3.1(8)**a)-e) shall be analysed using a spatial model. Two independent analyses with lateral loads applied in one direction only may be performed.

(3) For buildings conforming to the regularity criteria of **4.2.3.2** or the criteria of **4.3.3.1(8)**a)-d) the analysis may be performed using two planar models, one for each main horizontal direction.

(4) For low-rise masonry buildings, in which structural wall behaviour is dominated by shear, each storey may be analysed independently.

(5) The requirements in **(4)** are deemed to be satisfied if the number of storeys is 3 or less and if the average aspect (height to width) ratio of structural walls is less than 1,0.

4.3.3.4.2.3 Capacity curve

(1) The relation between base shear force and the control displacement (the "capacity curve") should be determined by pushover analysis for values of the control

displacement ranging between zero and the value corresponding to 150% of the target displacement, defined in **4.3.3.4.2.6**.

(2) The control displacement may be taken at the centre of mass of the roof of the building. The top of a penthouse should not be considered as the roof.

4.3.3.4.2.4 Overstrength factor

(1) When the overstrength ratio (α_u/α_1) is determined by pushover analysis, the lower value of the overstrength factor obtained for the two lateral load distributions should be used.

4.3.3.4.2.5 Plastic mechanism

(1)P The plastic mechanism shall be determined for the two lateral load distributions applied. The plastic mechanisms shall conform to the mechanisms on which the behaviour factor *q* used in the design is based.

4.3.3.4.2.6 Target displacement

(1)P The target displacement shall be defined as the seismic demand derived from the elastic response spectrum of **3.2.2.2** in terms of the displacement of an equivalent single-degree-of-freedom system.

NOTE Informative Annex B gives a procedure for the determination of the target displacement from the elastic response spectrum.

NONLINEAR STATIC (PUSHOVER) ANALYSIS

B.1 General

The target displacement is determined from the elastic response spectrum (see **3.2.2.2**). The capacity curve, which represents the relation between base shear force and control node displacement, is determined in accordance with **4.3.3.4.2.3**.

The following relation between normalized lateral forces $\overline{F}_i$ and normalized displacements Φ_i is assumed:

$$\overline{F}_i = m_i \Phi_i \tag{B.1}$$

where m_i is the mass in the i-th storey.

Displacements are normalized in such a way that $\Phi_n = 1$, where n is the control node (usually, n denotes the roof level). Consequently, $\overline{F}_n = m_n$.

B.2 Transformation to an equivalent Single Degree of Freedom (SDOF) system

The mass of an equivalent SDOF system m^* is determined as:

$$m^* = \sum m_i \Phi_i = \sum \overline{F}_i \tag{B.2}$$

and the transformation factor is given by:

$$\Gamma = \frac{m^*}{\sum m_i \Phi_i^2} = \frac{\sum \overline{F}_i}{\sum \left(\frac{\overline{F}_i^2}{m_i} \right)} \tag{B.3}$$

The force F^* and displacement d^* of the equivalent SDOF system are computed as:

$$F^* = \frac{F_b}{\Gamma} \tag{B.4}$$

$$d^* = \frac{d_n}{\Gamma} \tag{B.5}$$

where F_b and d_n are, respectively, the base shear force and the control node displacement of the Multi Degree of Freedom (MDOF) system.

The mointored displacement according to ASCE

> **3.2.5.1 Building Pounding** Data shall be collected to permit evaluation of the effects of building pounding, wherever a portion of an adjacent structure is located within 4% of the height above grade at the location of potential impact.

Modal A_{ret_1}

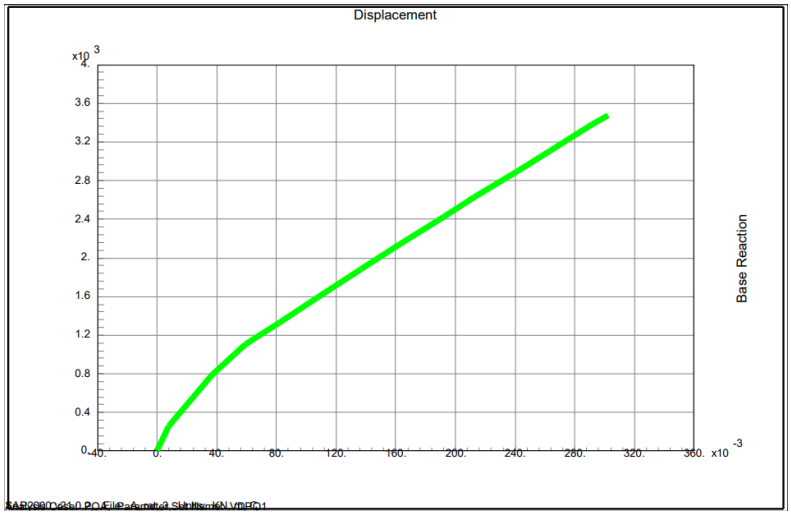

Capacity Curve

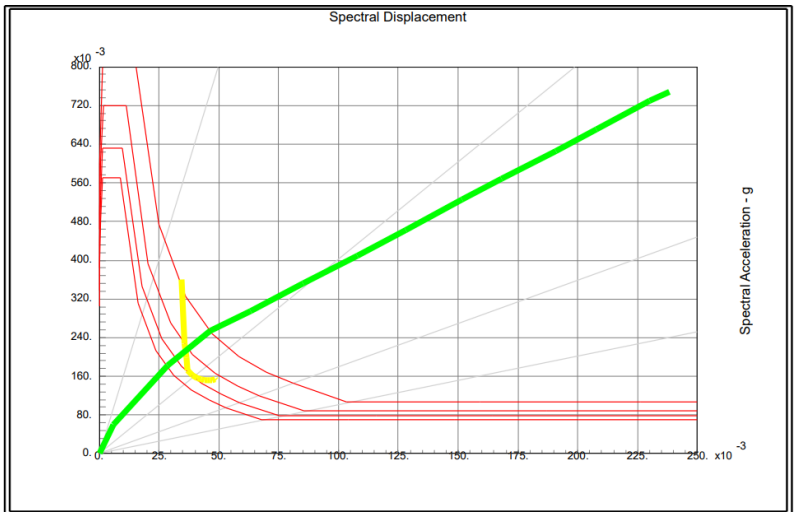

Capacity Spectrum

Modal A_{ret_2}

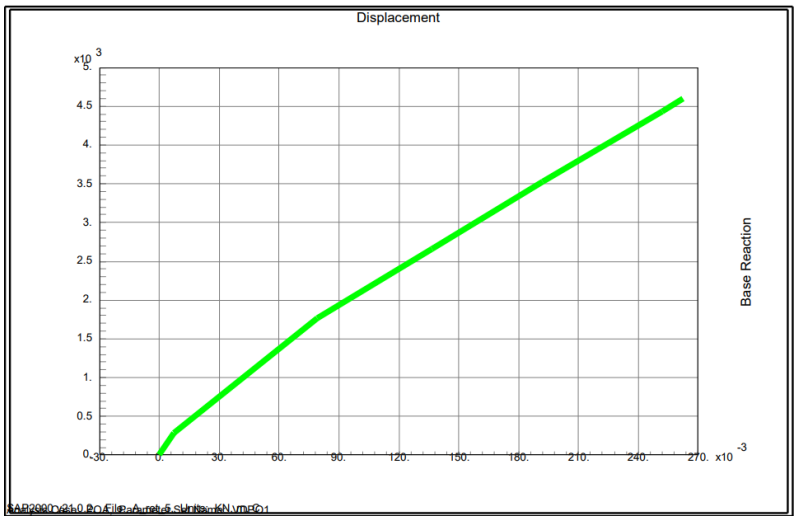

Capacity Curve

Capacity Spectrum

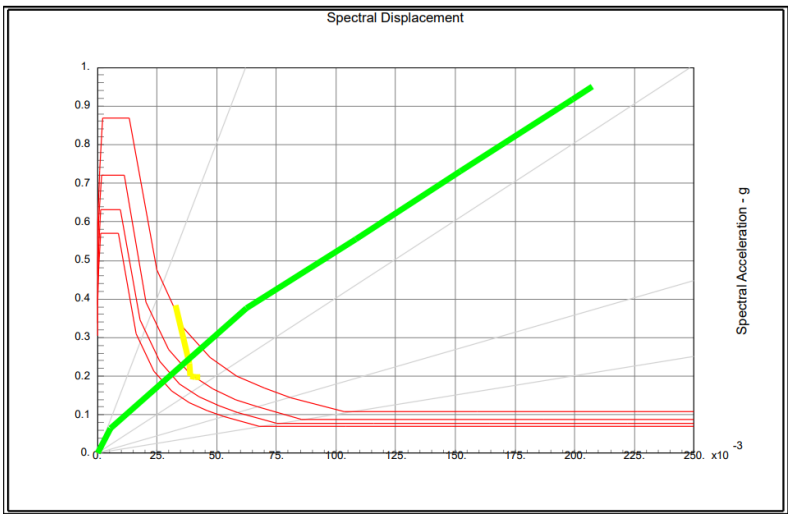

Modal A_{ret_3}

Capacity Curve

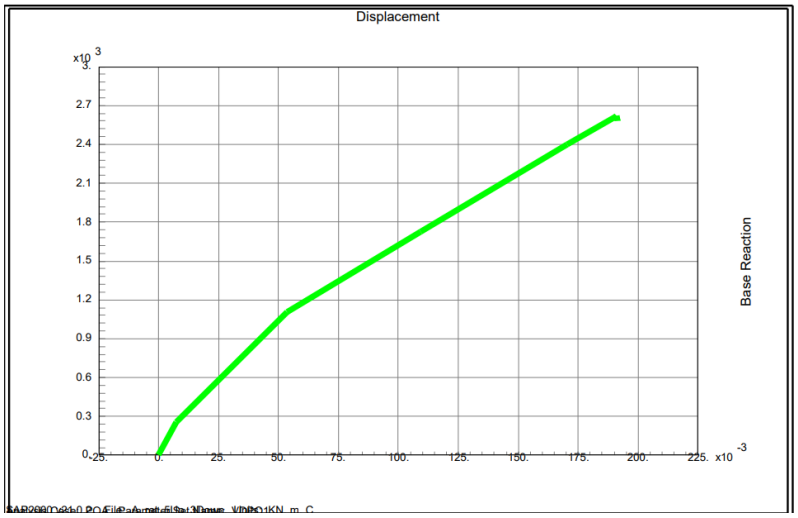

Capacity Spectrum

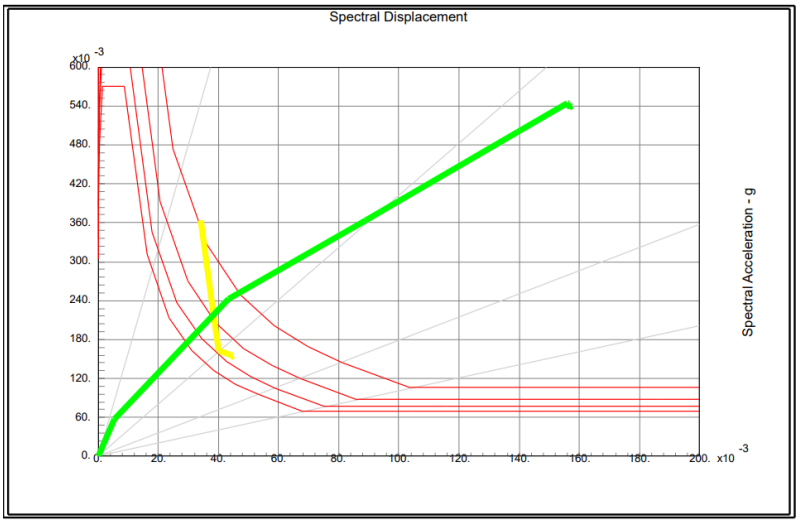

Modal A_{ret_4}

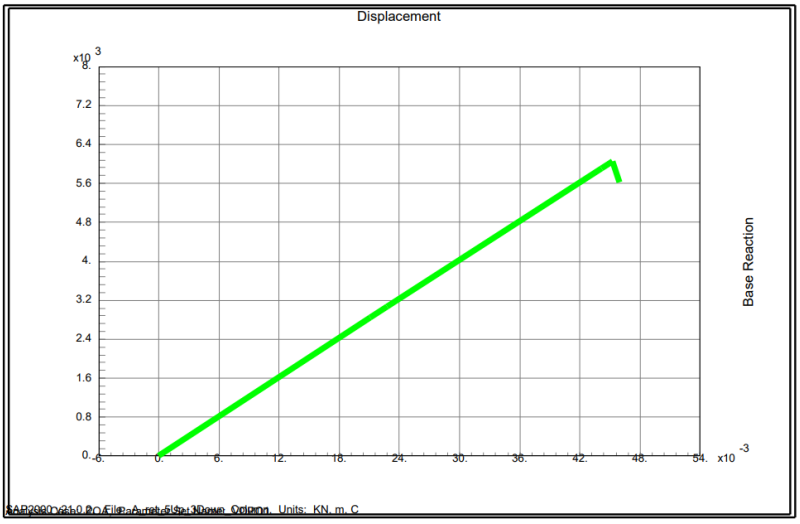

Capacity Curve

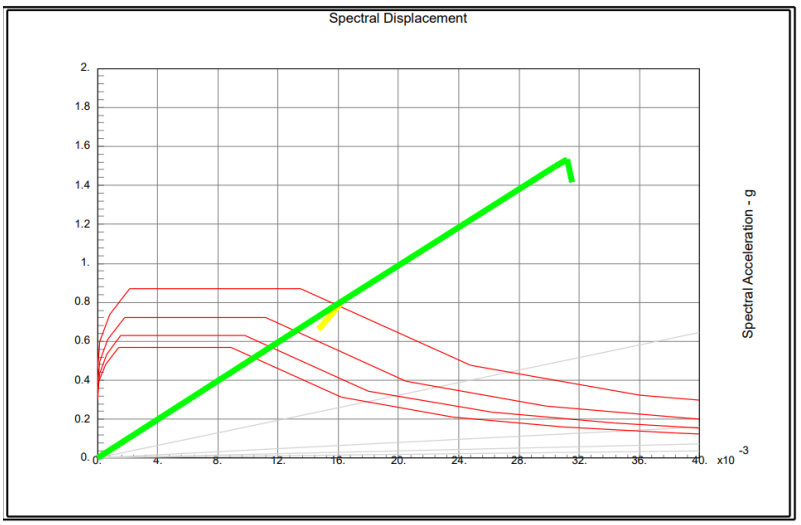

Capacity Spectrum

Modal B

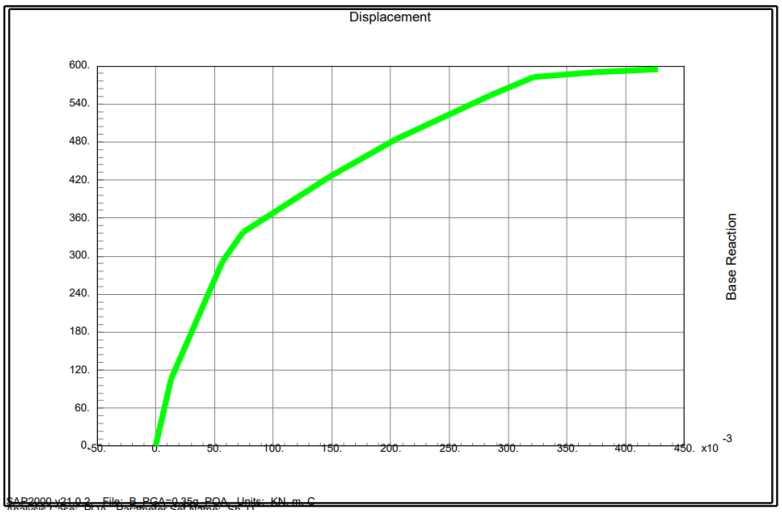

Capacity Curve

Capacity Spectrum

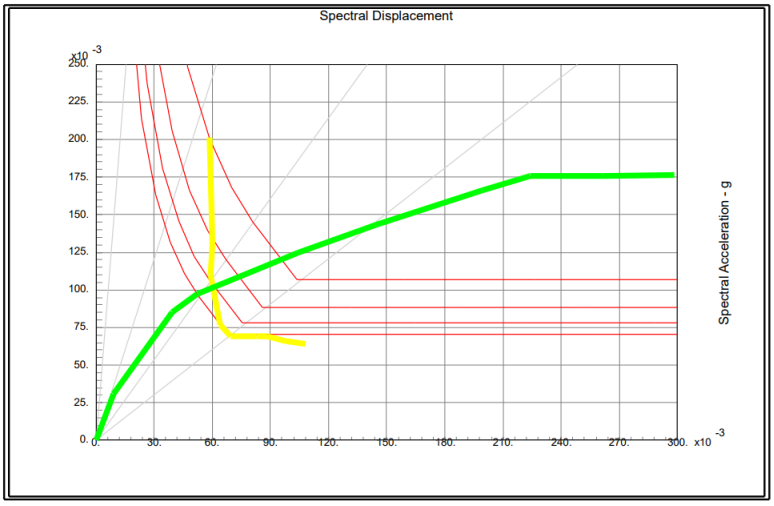

Norges miljø- og biovitenskapelige universitet
Noregs miljø- og biovitskapelege universitet
Norwegian University of Life Sciences

Postboks 5003
NO-1432 Ås
Norway